DEVELOPMENT OF A CONJUGATE HEAT TRANSFER SOLVER

Mansour Al Qubeissi

A Thesis submitted for the degree of Master of Philosophy

School of Engineering and Informatics

University of Sussex, UK

September 2012

DECLARATION

I hereby declare that this thesis has not been submitted, in whole or in part, to another University for the award of any other degree.

Mansour A. Al Qubeissi

September 2012

ACKNOWLEDGEMENTS

I would like to thank my supervisors, Professor Abdulnaser Sayma and Dr. Hao Xia, for their guidance throughout the course of this research. I wish to acknowledge Dr. Christopher Long for his help in clarifying some related heat transfer problems and providing experimental data sheet.

I also thank my colleagues and the technicians at Thermo-Fluid Mechanics Research Centre for their help and useful discussions. I gratefully acknowledge the guidelines given by Professor Erik Burman (Head of Maths Dept., University of Sussex) and Professor Li He (Head of Osney Lab and Director of Rolls-Royce UTC, University of Oxford) in treatment of conjugate heat transfer interface. My sincere thanks go to Mr John Evans for his linguistic comments.

Finally, I would like to thank my family for carrying out so much of my student life load throughout difficult financial situations. I owe deep and special thanks to my brother, Omar, for being always there for me.

UNIVERSITY OF SUSSEX

MANSOUR AL QUBEISSI MASTER OF PHILOSOPHY

DEVELOPMENT OF A CONJUGATE HEAT TRANSFER SOLVER

SUMMARY

The current research study presents a numerical approach in modelling the conjugate heat transfer system of the gas-turbine rotating discs-cavities. The work was undertaken to understand such phenomena and, more specifically, to numerically investigate the thermal interactions in rotating discs-cavities.

The developed solver is capable of dealing with complex heat transfer problems, such as unsteady three-dimensional compressible rotating-flows. The development was based on integrating an in-house computational fluid dynamics code (SURF) with a heat conduction solver internally. Method of interpolation using mapped area was also introduced for treating non-matching meshes at interface, which plays an effective role in exchanging boundary data.

This thesis also documents the development of a numerical finite volume cell-vertex hybrid edge-based heat conduction code by the author using FORTRAN. The heat conduction solver was developed and validated to deal with three dimensional solid-domains using unstructured elements.

The validation process was carried out on several test cases for investigating the temperature distribution. The test results were presented to show good agreement with the analytical, experimental and other commercial numerical solutions where they exist.

CONTENTS

Nomenclatures ..... **VI**

1. Introduction **1**

1.1. Objectives 4

1.2. Rotating Cavities 5

1.3. Thesis Structure 6

2. Literature Review **8**

2.1. Computational Fluid Dynamics 8

2.2. Heat Conduction 10

2.3. Conjugate Heat Transfer 12

2.3.1. Conforming Meshes 15

2.3.1. Non-Conforming Meshes 17

3. Numerical Solution and Methodologies **21**

3.1.Heat Conduction Solver 21

3.1.1. Finite Volume Method 23

3.1.2. Boundary Conditions 26

3.1.2.1. Dirichlet Boundary Condition 27

3.1.2.2. Neumann Boundary Condition 27

3.1.3. Validation Cases 30

3.1.3.1. 1D case 31

3.1.3.2. 2D case 33

3.1.3.3. 3D case 35

3.2. Previously Implemented (1st order) Heat Conduction Solution 37

3.2.1. Validation 39

3.3. Concluding Remarks 40

3.4. Fluid Flow solution 41

4. The Conjugate Heat Transfer Solver **45**

4.1. Interface Treatment 45

4.2. Non-Conforming Meshes 48

4.3. 1D Validation Cases 50

4.3.1. Duct Flow Test Case 50

4.3.2. Pipe Flow Test Case 54

4.4. 2D Validation Cases 56

4.4.1. Analytical Solution 56

4.4.2. Parallel and Counter Flow Double-Pipe Heat Exchangers 59

A. Parallel Flow Heat Exchanger 61

B. Counter Flow Heat Exchanger 63

C. Comparison to a Commercial CHT Solver 65

4.5. Concluding Remarks 68

5. The Gas-Turbine Co-Rotating Discs **70**

5.1. Case Description 70

5.2. Validation 73

5.3. Concluding Remarks 77

6. Discussion & Conclusions **79**

6.1. Discussion 79

6.2. Conclusions 82

Bibliography **85**

Appendices **91**

NOMENCLATURES

Symbol	Definition	Units
a	Conduction area, normal to that edge	m^2
A	Conduction area normal to the edge	m^2
α	Thermal diffusivity ($\frac{heat\ conduction}{heat\ stored}$)	$m^2\ s^{-1}$
C	Specific heat (C_p: at constant pressure; C_v: at constant volume)	$\mathrm{J\ kg^{-1}K^{-1}}$
D_h	Hydraulic diameter	m
δ	Characteristic length	m
$\dot{\boldsymbol{E}}$	Rate of energy	W
$\dot{g}$	Rate of heat generation per volume	$\mathrm{W\ m^{-3}}$
γ	Ratio of specific heat coefficients $\left(\frac{C_p}{C_v}\right)$	-
h	Convection heat transfer coefficient	$\mathrm{W\ m^{-2}K^{-1}}$
i	Index of solid side nodes (in interfacial-cell)	-
j	Index of fluid side nodes (in interfacial-cell)	-
k	Thermal conductivity	$\mathrm{W\ m^{-1}K^{-1}}$
l	Length , or distance between two nodes	m
μ	Dynamic viscosity	$kg\ m^{-1}s^{-1}$
Nu	Nusselt number	-
P	Pressure	$\mathrm{N\ m^{-2}}$
Pr	Prandtl number	-
q	Heat flux	$\mathrm{W\ m^{-2}}$
Q	Rate of heat transfer	W
ρ	Density	$\mathrm{kg\ m^{-3}}$
R	Perfect gas constant	$\mathrm{kJ\ kg^{-1}K^{-1}}$
Re	Reynolds number	-

Rs	Residuals	-
T	Temperature	K
u	Convection speed	$\mathrm{m\ s^{-1}}$
v	Velocity	$\mathrm{m\ s^{-1}}$
V	Volume	m^3

Subscripts

c	cold
h	hot
I	inlet
f	fluid
g	generated
o	outlet
s	solid
st	stored
w	wall

Abbreviations

1D	One Dimension(al)
2D	Two Dimensions
3D	Three Dimensions
CFD	Computational Fluid Dynamics
CHT	Conjugate Heat Transfer
FDM	Finite Difference Method
FEM	Finite Element Method
FSI	Fluid Solid Interface
FVM	Finite Volume Method
HC	Heat Conduction
HE	Heat Exchanger
HTC	Heat Transfer Coefficient

IDI	Interface Data Interaction
LHS	Left Hand Side
PDE	Partial Differential Equation(s)
RHS	Right Hand Side

CHAPTER ONE

INTRODUCTION

The increase in turbine inlet temperature, from approximately 900 K in 1940's Whittles' engines (Owen and Rogers 1989; Illingworth 2006) to about 2000 K in recent combined-cycle power-plant (Hada et al. 2012), is associated with significant improvements in the power outputs and efficiencies. As a result, effective cooling is an essential feature in the design requirements. Internal cavities of rotating discs play an effective role in satisfying the cooling requirements of the system. Providing an accurate temperature distribution profile in a three dimensional (3D) presentation for such domains is essential.

The heat transfer problems in complex geometry domains are very common in industry. Determination of accurate temperature distributions in 3D is a challenge. When heat transfer occurs in complex fluid-solid systems, boundary conditions are continuously interacting between these different domains. The mechanism of continuous fluid-solid interaction is described as Conjugate Heat Transfer (CHT).

CHT operation occurs in a wide range of industrial thermodynamic applications such as Heat Exchangers (HEs), internal cooling in gas-turbine engines, nuclear reactors and computer components cooling system ...etc. The vast development in computer processors, within the last two decades, has offered the opportunity for extensive Computational Fluid Dynamics (CFD) research studies in this field. The applications of CHT are very wide and a further research investigation is needed for this development.

The main challenge in solving CHT problems is the data interaction at interface. The Interface Data Interaction (IDI) means extracting boundary data from each type of domain and sending boundary conditions to the neighbour domains. For fluid domains, the fluid motion equations of Navier-Stokes are solved. For solid domains, Heat Conduction (HC) equation is solved (Al Qubeissi 2012a). At the interface boundaries of these domains, heat flux (temperature gradient) and temperature are exchanged (Al Qubeissi 2012b).

For the 'rotating-discs' system of gas-turbine, discs are represented by the (solid) HC equations; whereas fluid-motion equations are solved to calculate the cooling-air flow profile. In usual cases, heat is transferred from hot blades to the discs through their roots. Also, cooling air feeds the rotating cavity axially and departs throughout the shroud radially. The full scene of the airflow through a typical gas-turbine engine sketch is shown in Figure 1.1.

Different domains usually require different mesh types and sizes. The difference in meshes inside the domains leads to non-conforming, and maybe overlapping, meshes at interface. The treatment of non-matching meshes at interface is performed using linear interpolation. This method was used by Henshaw and Chand (2009) and described as a simpler well working interpolation method. Giles (1997) had previously used this method in treating interface of a Finite Difference Method (FDM) based domain. Both researchers used linear interpolation for structured meshes.

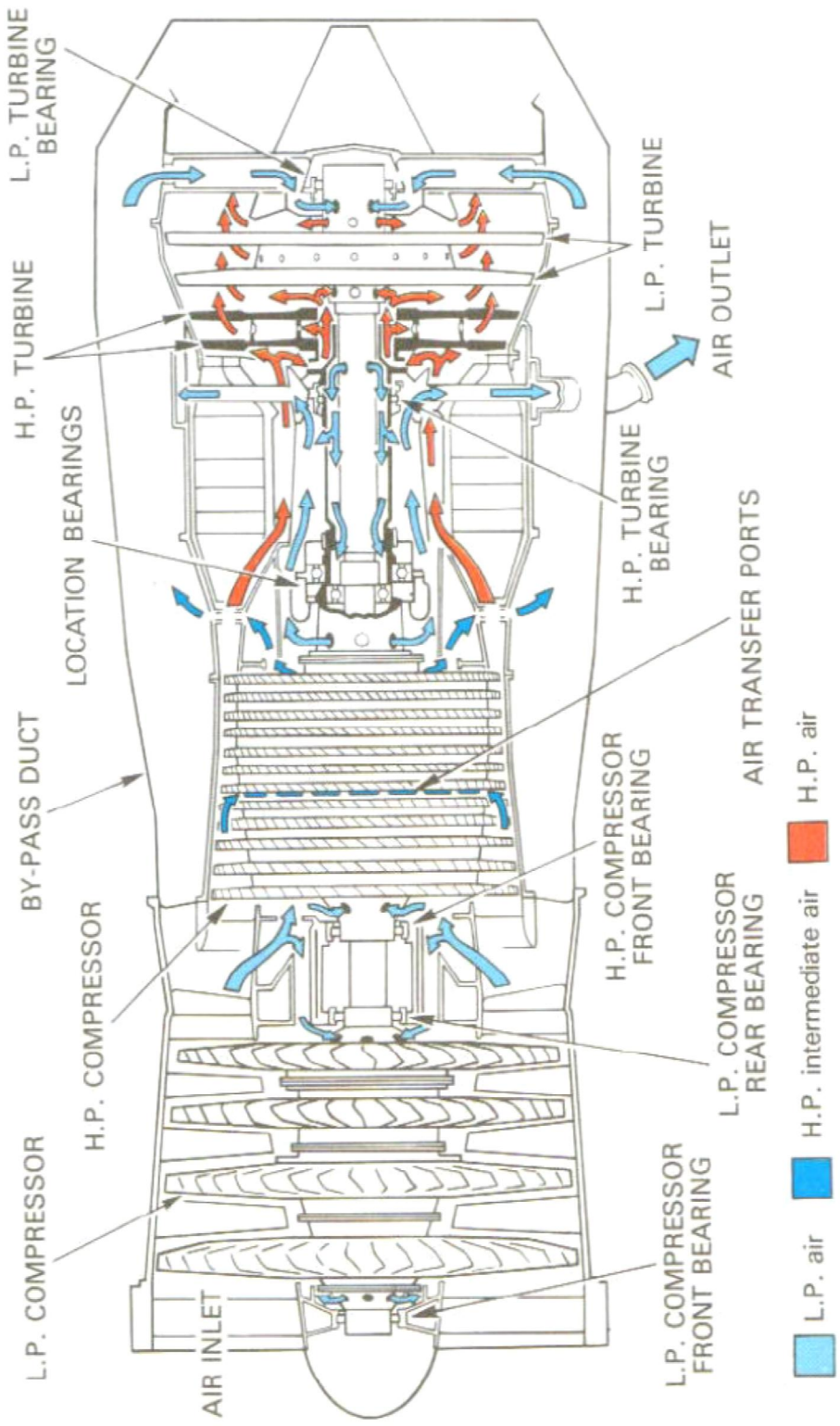

Figure 1.1: Air flow through the components of a typical Gas-Turbine engine (Owen & Rogers 1989)

1.1. Objectives

The current research study was carried out in order to achieve the following main objectives:

1. To simulate and understand the fluid flow and heat transfer profiles in CHT systems.
2. To numerically investigate the complex phenomena of CHT in rotating-discs cavities.
3. To implement a numerical method, in the form of a software development, for solving a wide range of CHT problems.

The process of achieving the above objectives was broken down into the following steps of the research progress:

- Development of a HC code for determining the boundary temperature distribution and heat flux in the solid parts of the system.
- The fluid part of the system is solved using the in-house CFD software, SURF, developed by Sayma et al. (2000).
- IDI treatment. Fluid boundary data at the interfacial areas must align with the HC boundary values of temperature and heat flux. The interface exchange process is performed in internal coupling strategy, i.e. two solvers in one code. Each domain must have consistent transfer of data of its boundaries when boundary grids do not match at interface.

Since the current research interest is in generalising the CHT solver to complex applications, such as rotating flows/cavities. This type of flow is given a special attention and described in the following sub-section:

1.2. Rotating Cavities

The rotating cavity is the flow formed between two co-axial rotating discs. This type of flow contains a range of different configurations depending on type of throughflow of fluid and on temperature of the surrounding walls. The difference in cavity configuration refers to the difference in application. The radial outflow cavity is formed between the turbine co-rotating discs as a coolant flow, which is the topic of the current research interest. It is worth mentioning that the flow regions inside the cavity were classified by Owen and Rogers (1995) into the following categories: source region, Ekman layers, sink region and interior core, as shown in Figure 1.2.

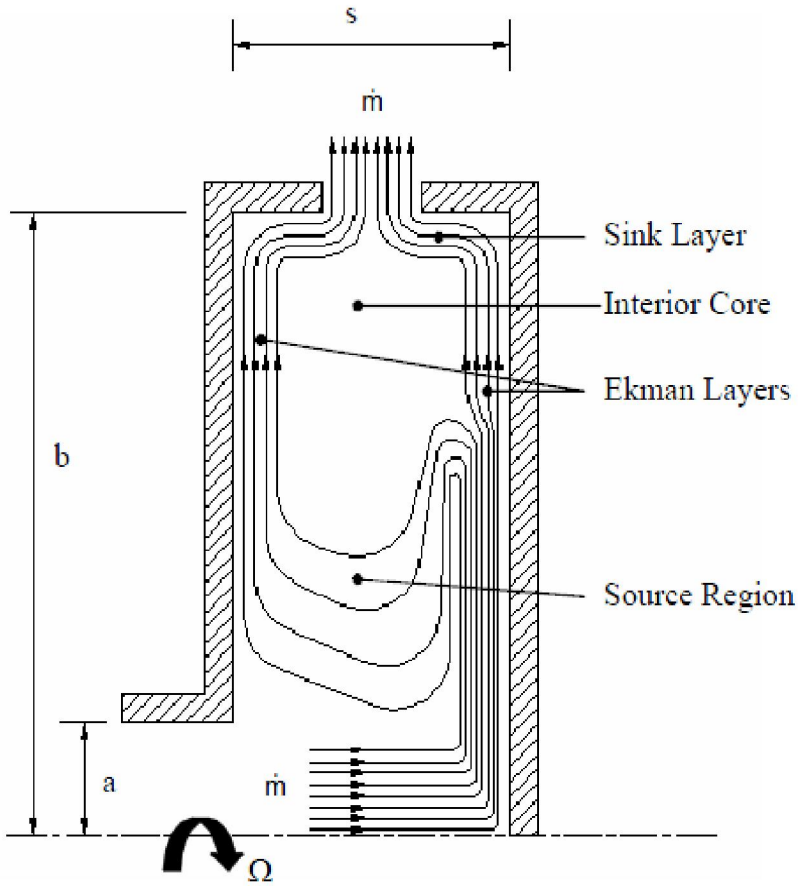

Figure 1.2: The flow structure of an axial-inflow and radial-outflow cavity of co-rotating discs (Owen and Rogers 1995)

From Figure 1.2, source region refers to the flow near the entrance, Ekman layers are flow streams near the wall, sink region refers to flow near the flow exit and interior core is the flow in the middle of the cavity. The name Ekman layer is used to the similarity with Ekman layers where the velocity of fluid outside boundary layer is smaller than the disc speed (Ekman 1905). The primary interest of the current research topic is in the temperature distribution in the radial outflow coolant and rotating discs. As a result, the flow regions are only displayed in this subsection for illustration. However, the reader is referred to some of the early original contributions in the topic for deep understanding of rotating flows such as (Kármán 1921; Daily and Nece 1960; Dorfmann 1963; Owen 1971; Owen and Rogers 1995).

1.3. Thesis Structure

HC code is developed, in the current research study, for solving the heat transfer equation using cell-vertex edge-based FVM. HC code is enhanced with the capability of reading 3D unstructured tetrahedral meshes. Using unstructured grids assists in the flexibility of discretizing complex geometries. The fluid flow equations are solved numerically using SURF (in-house CFD code used at Thermo-Fluid Mechanics Research Centre). SURF is a validated approach in solving unsteady 3D compressible flow problems (Sayma et al. 2000). The code is based on the cell-vertex edge-based Finite Volume discretisation technique, which can read unstructured hybrid grids and deal with a very wide range of complex geometries.

The application of coupling (solid/fluid codes) procedure is performed to exchange the interface thermal boundary conditions. The target (SURF-HC) solver is predicted to

propagate over a wide range of complex CHT applications. Modelling a 3D CHT system of gas-turbine rotating-stationary disc components will be the main validation process of this investigation.

In this thesis, a review of previous work in relation to the topic is presented in Chapter 2. The methodology of developing HC code, the drawbacks in previously used HC solution and fluid solver are presented in Chapter 3. Chapter 4 presents challenges and methodologies of interface treatment with two validation cases of HEs. In Chapter 5, the validation case of gas turbine co-rotating discs is described and modelled. Discussion about obtained results and conclusions are given in Chapter 6. Further analytical descriptions and schematic illustrations are attached at the end of these Chapters in the section of Appendices.

CHAPTER TWO

LITERATURE REVIEW

Advances in numerical methods with the availability of efficient computer hardware have led to widespread simulation of engineering cases on computers. Heat transfer and fluid flow processes are predicted using a numerical solution of the governing partial differential equations (PDE). The development of the numerical technique and modelling strategies used in current research project are concluded from previous research contributions as reviewed in the following historical survey. Since the research project is based on three modelling steps, the literature survey was conducted in three directions, as follows:

2.1. Computational Fluid Dynamics

Computational Fluid Dynamics (CFD) is a computer based numerical simulation, involving fluid flow and heat transfer equations. The CFD technique has become so powerful to span a very wide range of engineering applications, most importantly the gas-turbine systems (Versteeg and Malalasekera 1995). In CHT systems, with the availability of a CFD solver, the most relevant interest is in the fluid behaviour near the wall. In the last two decades, there have been numerous resources of studies and developments in solving CFD problems (Hirsch 1988; Hoffmann 2000a; Hoffmann 2000b; Fletcher 2000; Fletcher 2003; Archameau et al 2004). A selection of the most relevant papers is reviewed below.

Frink and Pirzadeh (1999) presented a review of the algorithmic features and capabilities of an unstructured-grid flow solver “USM3Dns”. This code was developed for solving the Euler and Navier–Stokes equations for domains of complex shapes. Spatial discretization was accomplished by a tetrahedral cell-centred Finite Volume Method (FVM) using Roe’s upwind flux difference splitting. Solution reconstruction within the tetrahedral cells was accomplished with a simple multidimensional analytical formula. Time is advanced by an implicit backward-Euler time-stepping scheme. Flow turbulence effects were modelled by the Spalart–Allmaras one-equation model (Spalart & Allmaras 1991), which is coupled with a wall function to reduce the number of cells in the near-wall region of the boundary layer. Access to the source code of USM3Dns was not available to the current research for testing. As a result, this type of solution did not take part in the current research.

Sayma et al. (2000) introduced an advanced numerical model for the simulation of steady and unsteady viscous 3D compressible flows for modelling a wide range of complex industrial applications including turbomachinery. The compressible Navier-Stokes equations were used together with one-equation turbulence model. The flow domain is discretised using unstructured hybrid grids that can contain a mixture of hexahedral, pentahedral, tetrahedral, and triangular prismatic cells, which adds a benefit of making the solver very flexible to deal with a very wide range of domain complexities. The flow equations were discretised using an edge-based vertex-centred FVM. This work included the development and validation of the CFD software, SURF. The air flow was modelled in the current research using SURF, which solves the fluid flow (Navier-Stokes) set of equations numerically.

Dalal et al. (2008) proposed a FVM formulation for solving unsteady flow cases of 3D complex geometries. The pressure-velocity decoupling was avoided by momentum interpolation. The authors tested the code to have second-order accuracy on unstructured grids. Some Navier-Stokes solutions were presented to verify the method with standard benchmark solutions. However, the drawback of this study was the limitation of the solver applications to incompressible laminar flows only.

2.2. Heat Conduction

The development of the Heat Conduction (HC) code was mainly made for the following purposes: (1) dealing with cases of complex geometries, (2) the capability of customising the boundary conditions and (3) developing a coupled CHT solver in one code. The numerical solution of the HC equation is based on intensive study of the previously developed methods. A selection of the most closely relevant studies is given below:

Lyra et al. (2005) developed a numerical formulation for the 2D HC model. This formulation used a cell-vertex FVM implemented in an edge-based data structure. The author used Laplacian method in calculating the normal vectors for the first order derivatives. The authors claimed that the proposed formulation was an effective and flexible solution of simple model problems as shown in Figure 2.1. However, the validation of this approach on a steady state HC equation, which was carried out at early stages of the current research and shown in Chapter 3, demonstrated an increase in errors and less accuracy with 3D cases.

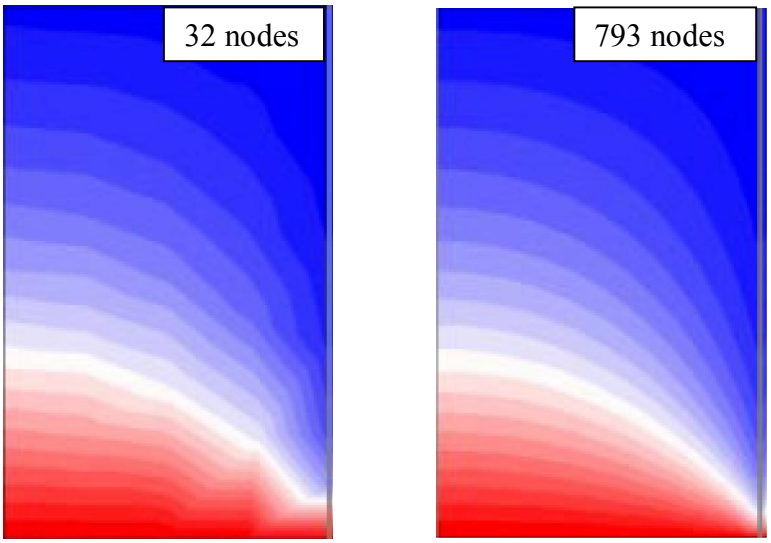

Figure 2.1: A view of temperature contours in the validation of a 2-D heat transfer problem with convection by Lyra et al. (2005)

Asllanaj et al. (2007) has adapted a FVM formulation based on a cell vertex scheme. The method was associated to an interpolation scheme, in which temperature is approximated by linear interpolation using nodal values. The solution was proposed by the authors to solve a typical heat transfer application of a radiative boundary condition.

Xia et al. (2007) proposed a vertex-based FVM using unstructured grids and cell-based data structure for computational analysis of 2D and 3D general problems. The governing equations were spatially discretised with an implicit dual time stepping scheme. The proposed method was applied to calculate 2D and 3D flows. Computational results were described by the authors as of good agreement with the analytical solutions and can be a viable alternative to the traditional finite element method (FEM). This method was implemented in the numerical solution of the Left Hand Side (LHS) of the HC equation.

Wegian and Yazdi (2008) used Gauss's theorem to integrate the unsteady 3D HC equation numerically. The second order accurate discretisation, as described by the authors, was based on the finite volume cell-centred technique. The solution was validated in the current research study for a cell-vertex (or vertex-centred) scheme to prove excellent agreement with the analytical solution where it exists.

2.3. Conjugate Heat Transfer

Montenay et al. (2000) classified solving CHT problems, at the fluid-solid boundaries through the engine cooling cavities, as one of the most important and challenging tasks for the turbo-engine designers. Illingworth (2006) has further defined the reason for its importance as the direct effect of CHT efficiency on life and performance of the engines. This was also seen, by Illingworth (2006), as challenging because the commercial modelling software for fluid domains and their neighbouring solids was only available in separate commercial codes.

In the current research, the main challenge in solving CHT problems is seen to be the IDI. The term IDI means extracting boundary data from each type of domain and sending information to the neighbour domain. Types of governing equations applied and data interacted depend on: type of domain (fluid/solid) and type of application.

Indinger and Shevchuk (2004) considered transient heat transfer in modelling a rotating disc heated to a constant initial temperature. The disc was exposed to unsteady cooling by still air. The study, assisted with analytical solution and experimental tests, showed

that the HTC is independent on transient conditions and that it is equal to its value at steady-state.

The numerical approaches of solving CHT problems can be either of direct or indirect coupling. The direct approach occurs when different fields are solved simultaneously in a large system of equations by a monolithic solver. The direct coupling approach was previously conducted by several researchers (Kao and Liou 1997; Han et al. 2001; Rahman et al. 2005; Luo and Razinsky 2007; Ganesan 2007). The indirect coupling consists of solving each set of field equations separately with interface solvers that exchange boundary conditions. This approach was used by a group of researchers such as (Heselhaus and Vogel 1995; Sondak and Dorney 2000; Papanicolaou et al. 2001; Garg 2002; Bohn et al. 2005). There can be another approach where the coupling strategy lays in between direct and indirect. These approaches can make the coupling codes either strongly or weakly coupled. In addition, a combination can compromise to another middle approach of strong and weak couple. These three coupling approaches are described below:

1. A single (strongly coupled) system approach: fluid equations, of motion and heat balance, are solved for the entire domain with either giving velocities equal to zero in the solid zones. The HC equations for solids can also be solved separately and called within the CFD code. This type is described as the most robust system (Henshaw 2000). This method can also be described by another route as applying energy balance and fluid motion equations on the fluid side and interacting data with the heat balance equation of the solid side. This approach is called, by most researchers in the field, as a CHT approach (Lou & Razinsky 2007).

2. The weakly coupled approach: each side of the system (solid or fluid) is solved separately. The couple exchange data through interfacial equations. The advantage of this approach is the ability to re-use existing physics codes without the need to develop a new single approach. This method is applied, as a shortcut, when no access to one or both of the source codes is provided. This type of coupling does not require deep knowledge in numerical solving techniques and can be used for limited purposes within the limitations of both available codes. An example of a weakly coupled solution was coupling two commercial codes externally as presented by Illingworth (2006).

3. Middle approach: Solving the heat balance equation for the entire system. This method treats walls as very thin, i.e. considering both side-temperatures of the wall while ignoring temperature distribution inside the wall.

The current research interest is in the first type of CHT approach. This is owing to the availability of the CFD solver (SURF). Developing an HC code can widen the opportunity for further research development in the field, such as solving other heat transfer related problems. HC can be used separately for modelling a wide range of heat transfer applications with a flexibility of customizing the boundary conditions. The currently considered choice has the benefit of the weakly coupled and strongly coupled CHT solvers.

At interface, meshes of the coupled domains can either coincide in shape and size or they become non-matching (non-conforming) meshes. The existence of non-conforming meshes is essential in most CHT applications due to the need for different mesh requirements for each domain. The literature review of some of the strongly related

research work, based on these two classifications of interface mesh types, is presented in the following two sub-sections.

2.3.1. Conforming Meshes

Giles (1997) suggested, in his research article, that Dirichlet boundary condition is applied to the fluid side (upon continuity of temperature) and Neumann condition to the solid side (upon continuity of heat flux). The 1D approach has shown viable stability and theoretically applicable to 2D and 3D cases.

A few researchers (Chemin 2006; Radenac, 2006; Roe et al., 2008; Duchaine et al. 2009) suggested applying the Dirichlet boundary condition (fixed temperature from solid boundary) at fluid side and a mixed, Robinson type, boundary condition (temperature and heat flux from fluid boundary) at solid side. This approach is seen to be the most representative to what happens at interface. However, defining the local convection coefficient can result in a set of empirical relationships which may lead to some approximations and errors.

Comini et al. (2007) introduced a modelling of Coupled Conduction-Convection in Moist Air Cooling. The article deals with the numerical simulation of moist air cooling in compact HEs. The energy equation was solved in the whole domain, using the FEM, in one equation. The authors concerns were accuracy, reliability, and capabilities of the methodology. The proposed method was used to solve some problems of HEs with both plate-fin and tube-fin types.

Illingworth (2006) applied an external coupling procedure using the 'two-run' method for the Gas-turbine rotating cavities. The researcher coupled the resulted data of Fluent (a commercial CFD solver) with SC03 (FEM HC code, developed by Rolls Royce) externally. The two run method is based on employing two CFD runs (of the same problem) for extracting the HTC, from the difference of two heat fluxes and two surface-temperatures. Two runs method is using the same solution on the same problem twice in order to verify the thermal convection coefficient from the difference between heat fluxes given in the two runs:

$$h = \frac{q_2 - q_1}{T_{w1} - T_{w2}}$$

Where h is the thermal convection coefficient and q_1 & q_2 are the heat fluxes extracted from the two runs wall temperatures T_{w1} & T_{w2}. Above equation is assumed on the bases that fluid temperatures (T_{f1} & T_{f2}) of both CFD runs are equal, i.e.

$$h = \frac{q_2 - q_1}{(T_{w1} - T_{f1}) - (T_{w2} - T_{f2})}$$

Where T_{f1} & T_{f2} are the fluid temperatures near the wall given by the two runs. Although this method is claimed by the author to be viable, it is time-expensive with strong possibility of input-errors. It is therefore important to address the advantages and disadvantages, in relation to applying this method. The difficulty of this method is in providing the right bulk temperature value when fluid temperature has sharp gradient near the wall. This method may result in defining the wrong thermal boundary layer for the mesh generated. Thus, the two run method is exposed to a high possibility of user-input errors.

He & Oldfield (2010) proposed a conjugate analysis for periodic unsteady flows. The introduced semi-analytical interface condition has enabled the unsteady conjugate coupling to be achieved without simultaneously solving the unsteady temperature field in the solid domain. The study was described by the author as a new approach in introducing a realigning method in the time scale for a periodic coupled, fluid (convection)-solid (conduction), unsteady system. The wall temperature is derived, based on 1D FDM, as:

$$T_w = \frac{T_s\left(\frac{k_s}{\Delta x_s}\right) + T_f\left(\frac{k_f}{\Delta x_f}\right)}{\frac{k_s}{\Delta x_s} + \frac{k_f}{\Delta x_f}}$$

Where T_s & T_f are the solid and fluid temperatures adjacent to their walls, respectively, and Δx_s & Δx_f are the solid and fluid temperature nodes' distances from their walls, respectively. In real life, the transient temperature responds to the time scale much quicker in solid domains than in fluid ones. The study has introduced a time scale ratio, between solid and fluid domains, of 10,000. Assuming that 1D Fluid CFL (Courant–Friedrichs–Lewy) number is less than unity, i.e. $\frac{\Delta y_f\, u}{\Delta x} \leq 1$ and 1D Solid Fourier number is $\frac{\Delta y_s \propto}{\Delta x^2} \leq 0.5$. It is worth mentioning that CFL condition for convergence is that time-step must be less than a certain value in explicit time-marching simulations, otherwise the simulation will produce widely incorrect results. He & Oldfield (2010) has have given an example of CHT system variables as: *u (flow speed)= 300 m/s,* $C_{p(steel)}$*=465 J/kg.K,* ρ*=7800 kg/m*^{3}*, k= 54 W/m.K, both edge sizes (*Δx*)= 0.001 m* will result in time step function of:

$$\frac{\Delta t_s}{\Delta t_f} \approx 10{,}000$$

The time discretisation for solid domain is a factor of 10,000 of the fluid time step, i.e. convection process is about 10,000 times faster than the conduction process of heating in average.

2.3.2. Non-Conforming (Non-Matching) Meshes

Non-matching meshes at interface is the most demanded case when generating the meshes of both domains separately. This is due to the different mesh requirements for each domain. This type of interface develops a complexity in transferring accurate data between both domains. The differences in mesh sizes can raise difficulties in transferring accurate data through interface. This is due to difficulty in passing accurate data between cells of different nodal densities at same interface. Although there has been extensive contribution in this field, there is still some gap in providing a standard method for guaranteeing continuity of temperature and heat flux in such cases.

De Boer et al. (2008) made a comparison of conservative and consistent approaches for the coupling of non-matching meshes. The differences in accuracy and efficiency between conservative and consistent coupling approaches have been investigated by the author. This was done for an analytical test problem as well as a steady quasi-1D FSI problem. The author has proposed a solution for overcoming non-matching meshes by forcing an interface line in the middle of the non-matching/overlapping nodes and redefining the interface meshes and domain-boundaries on both domains according to the line, as shown in Figure 2.2. The success of this approach is limited to 2D applications, but not practical for 3D problems. Also this method is seen to lie in a

complexity of redefining the boundaries and mesh nodes at interface, which leads to the necessity of re-generating the mesh for both domains. Relocating interface-nodes with their domain boundaries and refining the mesh will require a significant memory increase for a reasonably complex geometry.

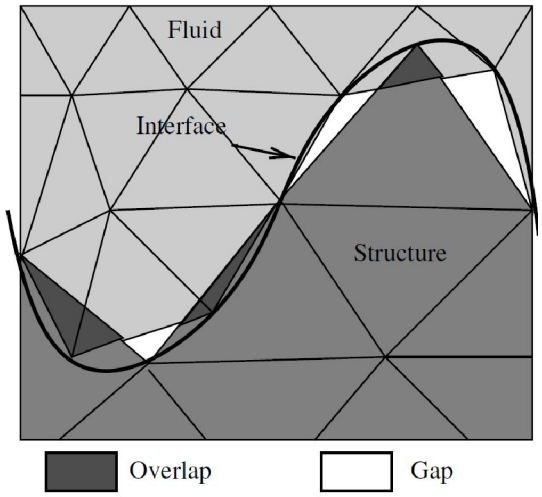

Figure 2.2: A schematic of non-matching and overlapping coarse meshes with a compromising line, as suggested by de Boer et al. (2008)

Mathews et al. (2007) presented a numerical study to analyse 2D conjugate, turbulent mixed convection heat transfer from a vertical channel with four heat sources uniformly flush-mounted to one of the channel walls. The standard k-e turbulence model, modified by including buoyancy effects with customized physical boundary conditions, i.e. without wall functions, was used for the analysis. This method is seen as a limited strategy designed for solving specific CHT problems and will lead to a failure with other applications, such as compressible flow CHT problems.

Jaiman et al. (2006) investigated the accuracy of implementing the interface-mesh refinement method on curved contact boundaries, which is simplified in plane projection, as shown in Figure 2.3.

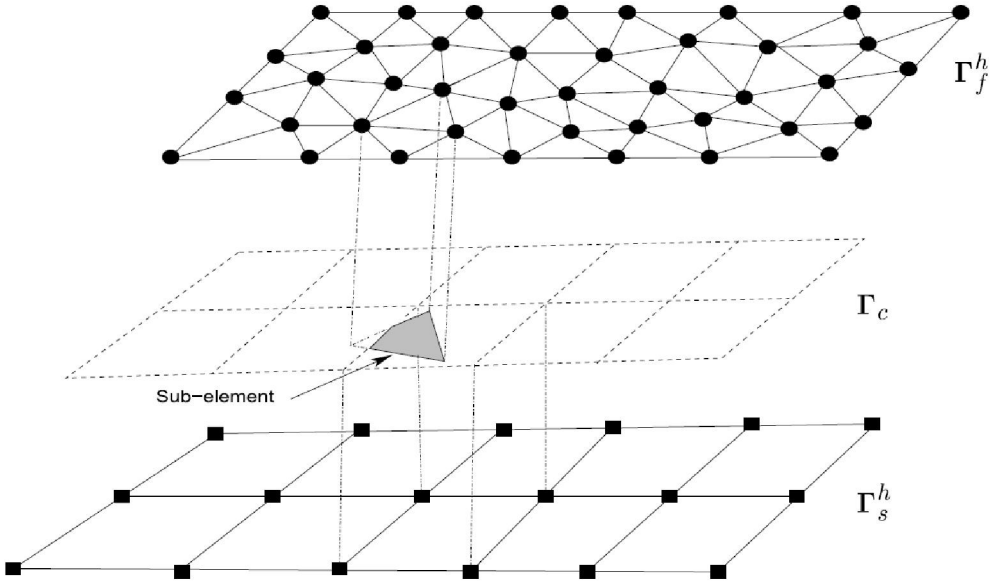

Figure 2.3: A schematic of interface-mesh refined based on projection scheme (Jaiman et al. 2006)

The method introduced by Jaiman et al. (2006) was based on projecting nodes of both domain boundaries on an imaginary interface plane and re-defining the interface mesh. In this method, the author suggested passing the solid temperature at the wall to the fluid domain while the heat flux (load) is delivered from fluid boundary to the solid domain. The authors have proven the success of this proposed method and claimed that this can be generalised on other cases. However, it is seen that the application of interface-mesh refinement ignores the mesh requirements for each domain, which makes the mesh less representative to the domain solution.

Henshaw and Chand (2009) described linear interpolation of non-matching meshes at interface as a simpler well working interpolation method. Giles (1997) had previously suggested the method in treating interface of a structured-mesh based domain using FDM of second order accuracy. Both researchers used linear interpolation for structured meshes. In unstructured meshes, the complexity of transferring accurate data can develop because of the arbitrary shapes of boundary (quadric or triangular) elements. In addition, the sizes of the boundary elements differ from side to another. This view coincides with the current research requirement (Al Qubeissi 2012b). The interest of current research work is providing a solution for treating non-matching interface meshes regardless to the type and size with considering a possibility of overlapping grids.

CHAPTER THREE

NUMERICAL SOLUTIONS AND METHODOLOGIES

The CHT solver, in nature, is a component of HC and fluid flow equations. HC solution is the application of the heat transfer equation in solid domains. The solution of the fluid side is a set of fluid motion, momentum and energy equations. This Chapter presents the numerical techniques in solving these equations including the development of HC code.

3.1. Heat Conduction Solver

Heat conduction can be defined as the mechanism of exchanging internal energy from one part of domain with higher energy (higher temperature) to another of lower energy (lower temperature). A clear understanding of the mechanism of HC is very important for developing a solution of complex problems (McMadams 1942).

The cell-vertex finite volume technique has been implemented using an edge-based data structure for solving the 3D HC problems. This formulation is very flexible and efficient. The implemented strategy of discretisation is flexible to deal with any kind of unstructured meshes and therefore any geometry. The solution methodology presented in this Chapter is also subject to all sorts of boundary conditions (Dirichlet, Neumann, and Cauchy).

HC code is developed to solve the HC equation. The governing equation is solved numerically for a control volume, shown in Figure 3.1, with no internal heat generation as:

$$\rho\, C\, \frac{\partial \mathrm{T}}{\partial \mathrm{t}} + \vec{\nabla} \cdot \vec{q} = 0 \tag{3.1}$$

In equation (3.1), T is the temperature value given in (K) and ρC represent density and heat capacity with units ($\mathrm{kg\,m^{-3}}$) & ($\mathrm{W\,kg^{-1}K^{-1}}$) respectively. $\vec{q}$ is the heat flux in three components, as a vector value, which is given by Fourier's law as:

$$\vec{q} = -k\, \vec{\nabla}\mathrm{T} \tag{3.2}$$

Where, k is the isotropic thermal conductivity.

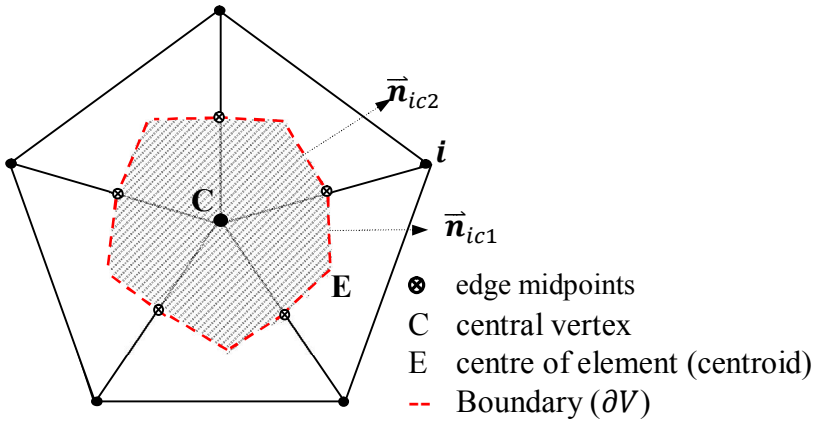

Figure 3.1: 2D view of a vertex centred control volume (the shaded area) from (Al Qubeissi 2012a)

It is worth mentioning that heat fluxes contributing to the central node, in Figure 3.1, must be normal to the boundary weights of that control volume. In cell-vertex scheme the contribution comes from each neighbour node *i* to the central node through the edge

connecting these two nodes. The weights can be represented by the umbrella area at the edge mid-point multiplied by its normal. The numerical solution of equation (3.1) is further described in the following section.

3.1.1. Finite Volume Method

Equation (3.1) over a control volume can be discretised, in Figure (3.1), by the application of the variational method (Younes et al. 2004) and (Wegian and Yazdi 2008):

$$\rho C \int_V \frac{\partial T}{\partial t} dV = \int_V \vec{\nabla} \cdot \left(k \, \vec{\nabla} T\right) dV$$

By considering $k = const.$, HC equation becomes:

$$\frac{\partial T}{\partial t} \int_V dV = \alpha \int_V \vec{\nabla} \cdot \vec{\nabla} T \, dV \tag{3.3}$$

Where the diffusivity $\alpha = \frac{k}{\rho C}$ (with units $m^2 s^{-1}$). Also, $\frac{\partial T}{\partial t}$ can be considered as constant with integration over space, the LHS of equation (3.3) takes the form of:

$$\frac{\partial T}{\partial t} \int_V dV = \frac{\partial T}{\partial t} \, V \tag{3.4}$$

The term $\frac{\partial T}{\partial t}$ can be expressed using the finite difference (forward) explicit scheme:

$$\frac{\partial T}{\partial t} \cong \frac{T^{t+\Delta t} - T^{t}}{\Delta t}$$

It is worth mentioning that in the case of a steady state, $\frac{\partial T}{\partial t}$ will represent the residuals (change of temperature) over the time steps Δt (Wegian and Yazdi 2008). This means in a steady state solution when $t \to \infty, \frac{\partial T}{\partial t} \to 0$ (Hirsch 1988, p. 270). The RHS of equation (3.3) can be solved using Gauss's (divergence) theorem (Chung 2002, p. 231) and (Hirsch 1988, pp. 223-230), as explained in Appendix (A), as:

$$\alpha \int_{V} \vec{\nabla} \cdot \vec{\nabla} T \, dV = \alpha \oint_{\partial V} \vec{\nabla} T \cdot \vec{n} \, \mathrm{dS} \tag{3.5}$$

Where, $\vec{n}$ is the outward normal vector, V is the control volume and ∂V is the control volume boundary surface. By substituting the terms (3.4) and (3.5) into equation (3.3), the HC equation takes the form of:

$$\frac{T^{t+\Delta t} - T^{t}}{\Delta t} = \frac{\alpha}{V} \oint_{\partial V} \vec{\nabla} T \cdot \, d\vec{S} \tag{3.6}$$

Where, the weight at the boundary of the control volume for each edge is $d\vec{S} = \vec{n} \, \mathrm{dS}$ and $\vec{\nabla} T$ is the average temperature gradient at the boundary of the control volume ∂V located at the midpoint based on central differencing scheme, as shown in Figure 3.1, i.e.

$$\vec{\nabla} T = \frac{\vec{\nabla} T_i + \vec{\nabla} T_c}{2} \tag{3.7}$$

Equation (3.7) gives the temperature gradient at the boundary of the control volume, by considering linear distribution of gradient along the edge. Similarly, $\bar{T} = \frac{T_i + T_c}{2}$, as given by Hirsch (1988, p. 255) and Lyra et al. (2004). The gradient temperature components are also calculated using Gauss's (divergence) theorem at the control volume boundary points (midpoints) as:

$$\vec{\nabla} T_c = \frac{1}{V_c} \oint_{\partial V} \bar{T}\, d\vec{S} \tag{3.8}$$

Or in a simplified summation as:

$$\vec{\nabla} T_c = \frac{1}{V_c} \sum_{i=1}^{N} \bar{T}\, \Delta\vec{S}_i$$

Equation (3.6) can be re-written in simplified integration as:

$$\frac{T^{t+\Delta t} - T^t}{\Delta t} = \frac{\alpha}{V} \sum_{i=1}^{N} \left(\vec{\nabla} T \cdot \Delta\vec{S}\right)_i$$

Or further simplified to:

$$T^{t+\Delta t} = T^t + \beta \sum_{i=1}^{N} \left(\vec{\nabla} T \cdot \Delta\vec{S}\right)_i \tag{3.9}$$

Where $\beta = \frac{\Delta t\ \alpha}{V}$, i is the index of neighbour nodes in that cell (around node c) and N is the number of neighbour nodes around that cell central node. The value of β is the control parameter of the equation. Von Neumann condition of stability leads to a restriction over the values of stability factors (Hirsch 1988, pp. 304, 320, 334) as:

$$0 < \alpha \left(\frac{1}{\Delta x^2} + \frac{1}{\Delta y^2} + \frac{1}{\Delta z^2} \right) \Delta t \leq \frac{1}{2} \tag{3.10}$$

Or simplified to:

$$0 < \alpha \left(\frac{\mathrm{A}}{V} \right)^2 \Delta t \leq \frac{1}{2}$$

Where, A represents the boundary area of the control volume V, which is a scalar value given by $A = \sqrt{\Delta x^2 \Delta y^2 + \Delta x^2 \Delta z^2 + \Delta y^2 \Delta z^2}$ and V is the control volume given by $V = \Delta x \Delta y \Delta z$, with the units m^2 and m^3 respectively. Low values of β within the range given in equation (3.10) will keep a bound to the amplified errors between initial and updated values. The range of time steps can be expressed by:

$$0 < \Delta t \leq \frac{1}{2\alpha} \left(\frac{\mathrm{V}}{A} \right)^2 \tag{3.11}$$

Test over the value Δt was carried out within the range (3.11). The test was applied on a simple geometry, given in Appendix B, with the following grid densities: $\sim 390, \sim 13000, \sim 91000$ and $\sim 500{,}000$ nodes. With finer grids Δt was found to be smaller to a minimum of $\sim 0.5\ s$. Δt becomes bigger with coarser meshes to $\sim 6\ \mathrm{s}$. Higher values of Δt in the tests resulted in unstable solutions. Hence, it is essensial to assume a fixed small value of Δt in order to avoid developing unstable solutions with coarse grids, e.g. assuming $\Delta t = 0.5\ s$ regardless to the grid sizes.

Also, in equation (3.9) the temperature is updated from the given initial value and boundary conditions. Hence, it is necessary to choose the appropriate initial guess. This

can be set within the given range of boundary conditions. Equation (3.9) is applied at each cell central node (indexed c in Figure 1) for solving 2D and 3D problems.

3.1.2. Boundary conditions

There are two major types of boundary conditions applied, either given boundary temperature (Dirichlet) or given heat flux (Neumann) boundary conditions. There can be a case of a mix of these two types of boundary conditions. Further details about the solution of these types are given in the following sections.

a) **Dirichlet boundary condition**

When the temperature is imposed at the boundary, a Dirichlet boundary condition is applied. Hence the temperature values at the boundary nodes will be replaced by the prescribed values of temperature $\bar{T}$ over that boundary, i.e.

$$T = \bar{T}$$

However, the temperature gradient is still needed in equation (3.7) and thereafter equation (3.9) is used in order to find the temperatures at the adjacent nodes.

b) **Neumann boundary conditions**

In this type of boundary conditions, the normal temperature gradient (as a function of heat flux) is imposed at the boundary. The HC flux is given by Fourier's law as: $\vec{q}_c = -k\,\vec{\nabla}T$. At the boundary, the normal heat flux from both sides is balanced as:

$$\vec{q}_c \cdot \vec{n} = q_b$$

Where, $\vec{n}$ is the normal vector components at that boundary node, $\vec{q}_c$ is the heat flux components that conducted from internal nodes towards the centre of the boundary cell and q_b is the prescribed heat flux from outside the domain normal to the boundary, which can be convection ($q_b = h(T_f - T_b)$), fixed heat flux ($q_b = const.$), or adiabatic ($q_b = 0$). Therefore,

$$k\,\vec{\nabla}T \cdot \vec{n} + q_b = 0 \qquad (3.12)$$

The boundary temperature gradient has two components: (1) normal $\vec{F}_n$ and (2) tangential $\vec{F}_t$ vectors, as shown in Figure 3.2.

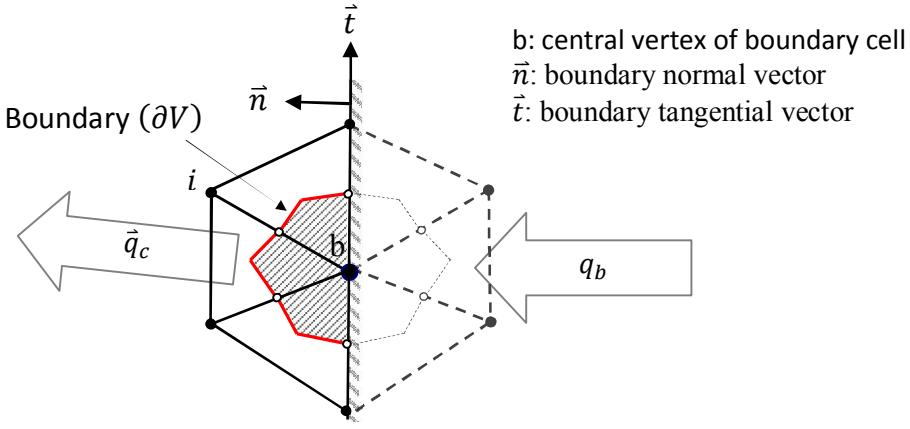

Figure 3.2: A 2D view of a boundary cell showing the normal and tangential vectors, from (Al Qubeissi 2012a)

Equation (3.12) is subject to the normal boundary fluxes only. The tangential portion of the flux is not taken into account in equation (3.12). It is therefore important to calculate the tangential temperature gradient. Since the tangential gradient is unknown, it can be decomposed from the tangent gradient of neighbour nodes (Wegian and Yazdi 2008). At the boundary, the temperature gradient can be decomposed as:

$$\vec{\nabla}T = \vec{F}_n + \vec{F}_t \tag{3.13}$$

To overcome the complexity of determining the tangential vectors, the tangential temperature gradient is decomposed from the estimated gradient as,

$$\vec{F}_t = \vec{\nabla}T_e - \left(\vec{\nabla}T_e \cdot \vec{n}\right)\vec{n} \tag{3.14}$$

Where: $\vec{\nabla}T_e$ represents the estimated value of $\vec{\nabla}T$, which is defined as the rate of heat exchange (divided by k) per unit volume of the surface (Wegian and Yazdi 2008). It is important to distinguish between $\vec{n}$, given in (3.5) and (3.14), which is the average inward normal vector at the boundary.

The estimated gradient $\vec{\nabla}T_e$ is calculated from the assumed control volume at the boundary by creating a mirror cell to close that control volume, as shown in Figure 3.2. When the weights and the volume are doubled for that control volume, equation (3.8) will be called again, with adding the boundary temperature distribution effect for computing $\vec{\nabla}T_e$ as:

$$\vec{\nabla}T_{\mathrm{e}} = \frac{1}{V_b}\left(\int_{\bar{\partial}\bar{V}} \bar{T}\, d\vec{S} - \sum_{i}^{N} \bar{T}_i\, \vec{n}_i\, \Delta a_i\right) \tag{3.15}$$

Where, Δa is the boundary area of that node within the connected boundary elements and N refers to the total number of segments around that boundary node. From above assumption, the gradient in equation (3.15) takes into account tangential derivatives accurately but not the normal ones. However, with Neumann boundary type, it is only important to get the right tangential component because the normal one is already specified by the imposed normal heat flux, in (3.12), as:

$$\vec{F}_n = -\frac{q_b}{k}\,\vec{n} \tag{3.16}$$

By substituting (3.14) and (3.16) into (3.13), the (corrected) temperature gradient at the surface is:

$$\vec{\nabla}T = -\frac{q_b}{k}\,\vec{n} + \vec{\nabla}T_{\mathrm{e}} + \left(\vec{\nabla}T_{\mathrm{e}} \cdot \vec{n}\right)\vec{n} \tag{3.17}$$

In order to find the temperature at the boundary, the heat flux term is added to equation (3.9) for closing the boundary control volume. Equation (3.9) at the boundary will become:

$$T^{t+\Delta t} = T^{t} + \beta \sum_{i=1}^{N} \left(\vec{\nabla}T \cdot \Delta\vec{S}\right)_i + \frac{\beta}{k} \sum_{\mathrm{j}=1}^{K} (q_b\,\Delta \mathrm{a})_{\mathrm{j}} \tag{3.18}$$

Where j is index of boundary elements and K is the number of boundary elements of that control volume. Δa is the boundary area of each boundary element. The temperature gradient $\vec{\nabla}T$, given in (3.17), can be substituted into (3.18) in order to find the temperature at the boundary. Although Figures 3.1 and 3.2 of the control volume show

2D views for simplifications, the discretised HC equations (3.9) and (3.18) are straightforwardly applicable to 3D problems.

3.2. Validation Cases

The solution, derived in previous sections, has been validated against the available exact solution for 1D and 2D cases. It is worth mentioning that the geometries used for these tests are 3D, however, the dimensions of the heat transfer will vary depending on the case applied. The mesh generated for this case is unstructured tetrahedral element type. In 3D case, the validation was carried out against Fluent (commercial CFD code). A grid independence check was carried out for a wide range of node numbers: $\sim 390, 13{,}000$ & $91{,}000$ nodes, as shown in Figure 3.3. In round and spherical shapes, the solution becomes much simpler because there is no difficulty in treating edges between surfaces of different boundary conditions. This shape sample is for showing the validation for sharp angles.

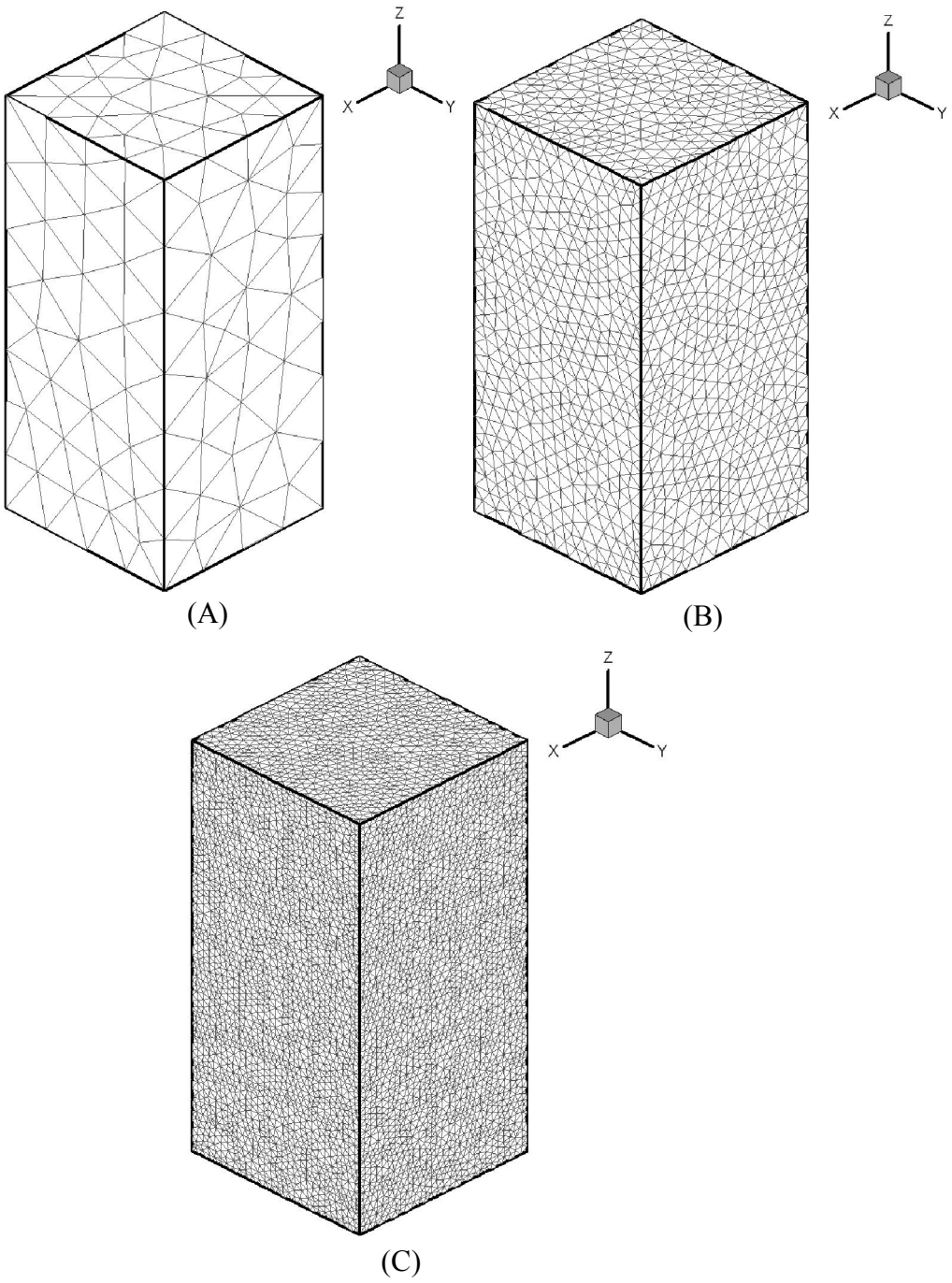

Figure 3.3: 3D view of the tetrahedral meshes used in testing HC code for the 3D case (A) nodes (B) nodes (C) nodes

a) **1D Test Case**

In 1D case, the temperature is specified at both ends of the domain as: at z= 0, *T*= 400 *K* and at z= 1, *T*= 300 *K*. The other sides of the domain were assumed perfectly adiabatic. In this case, the coarse mesh was enough to produce excellent approach against the exact solution, as shown in Figure 3.5. The given solution of this case compared to the analytical solution and Fluent (ANSYS, version 12.0) in Figure 3.4 was made for the coarse mesh, shown in Figure 3.3(A), of 390 nodes of the 3D geometry, which makes an equal to 90 nodes in 1D cut. The middle cut is shown in Figure 3.4 for illustration. Grid independence check was carried out for a wide range of node densities, as shown in Figure 3.6. Further details about visual comparisons and validations are displayed in Appendix B. The solution was converged after about 250 iterations.

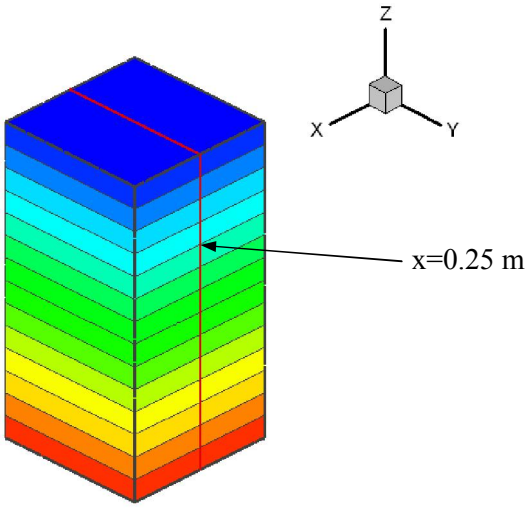

Figure 3.4: 3D view of the geometry showing the 1D temperature profile

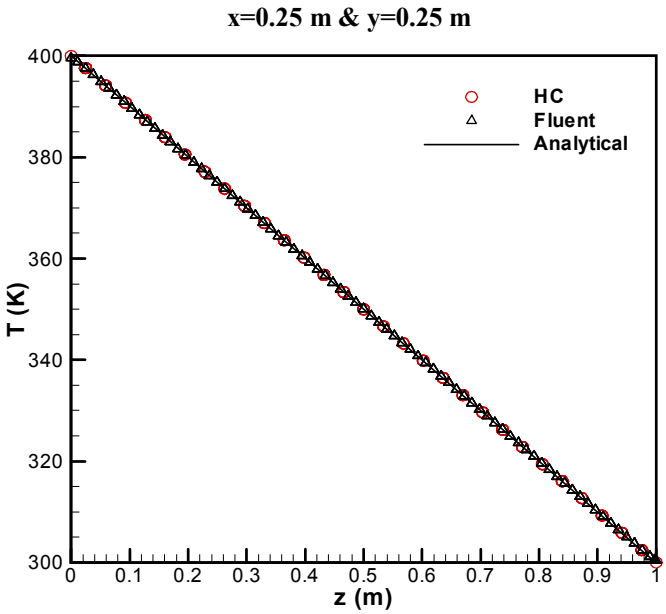

Figure 3.5: Comparison of HC results vs. Fluent & Analytical solutions for 1D case, on 1D mesh of about 90 nodes

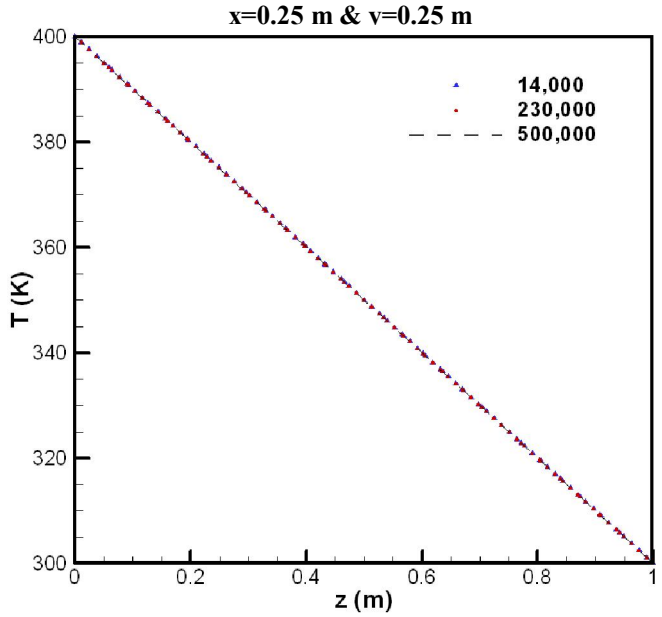

Figure 3.6: Grid independence check for the 1D case, over a range of node numbers from nodes in 3D (equivalent to 9-100 in 1D)

b) 2D Test Case

In 2D case, a geometry of a plate, with dimensions $(1 \times 1 \times 0.2)m^3$, was used for validation. It is worth mentioning that, since the geometry is 3D, the 2D case is based on the 2D heat transfer. The following types of boundary conditions have been prescribed: at x=0 and x=1, T = 0; at y=0, T = 0; at y=0.5, $T = \sin(\pi x/L)$; at z=0 and z=1, adiabatic surfaces $(q = 0)$. This case has been introduced because of the availability of the exact solution (Karlekar & Desmond 1982, p. 161) and (White 1984, p. 113), as:

$$T(x, y) = \frac{\sinh(\pi\, y/L)}{\sinh(\pi\, H/L)} \sin(\pi\, x/L)$$

Where, L is the length of that cross section $(L = 1\, m)$ and H is the hight $(H = 1\, m)$. The validation results, in comparison between temperature distribution given by numerical and analytical solutions in different directions, are shown in Figures 3.7 and 3.9, respectively. Figures 3.8 and 3.10 show the grid independence check in y and x directions respectively. More diagrams about visual validations of this case are attached in Appendix B.

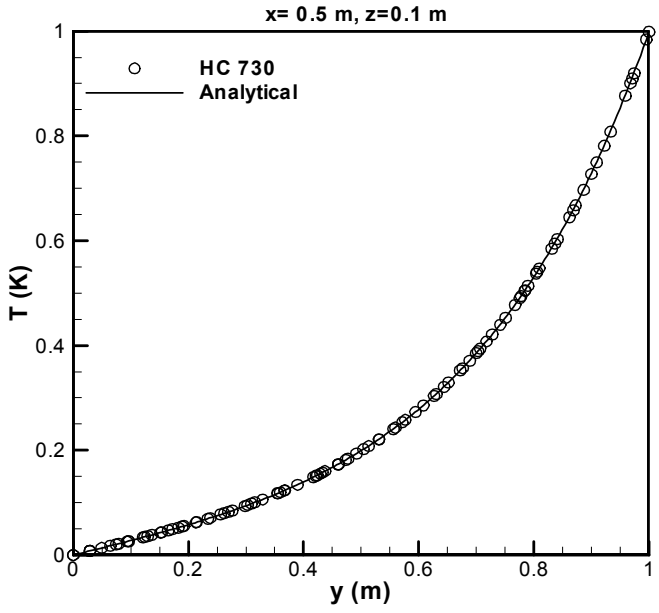

Figure 3.7: Temperature distribution in y-direction at z=0.1 and x=0.5 of HC (with ~740 nodes) vs. the analytical solution

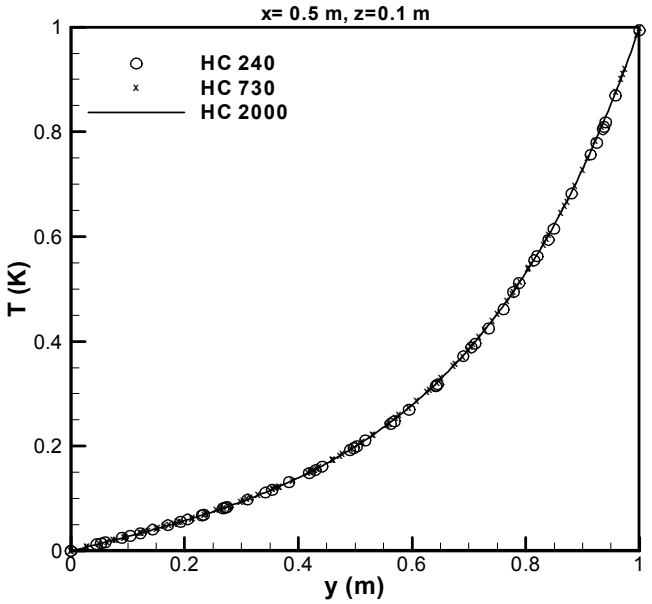

Figure 3.8: Grid independence check for the 2D case, over a range of node numbers from ~240 to ~2,000 nodes at the section z=0.1, in y-direction

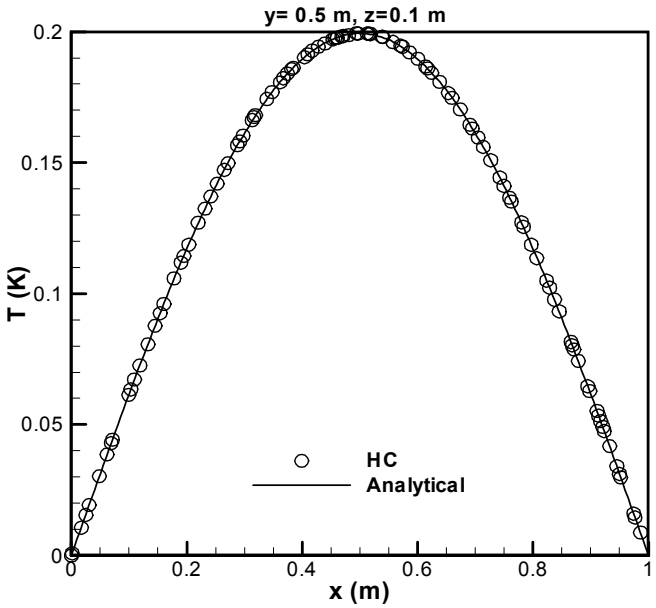

Figure 3.9: Temperature distribution in x-direction at z=0.1 and y=0.5 of HC (with ~740 nodes) vs. the analytical solution

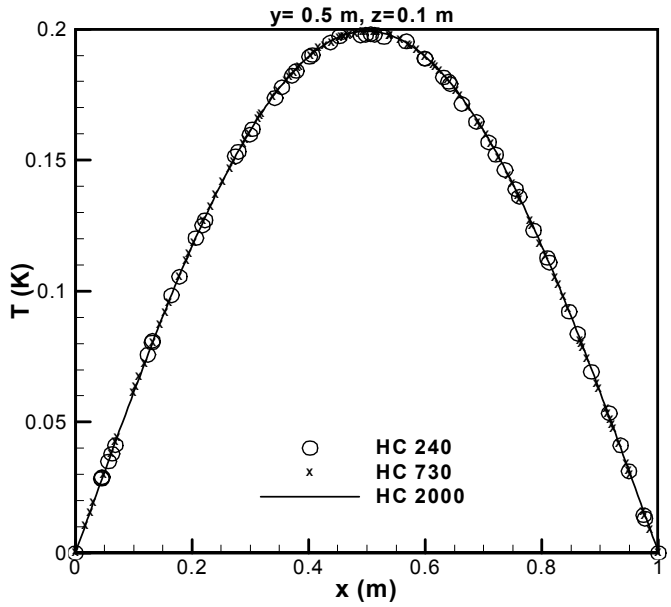

Figure 3.10: Grid independence check for the 2D case, over a range of node numbers from ~240 to ~2,000 nodes, at section z=0.1, in x-direction

It should be emphasised that the steady state solution, shown in above Figures (3.5 to 3.10), was obtained at large time value when the transient temperature values become functions of space only. This strategy was similarly applied to the following 3D case.

c) 3D Test Case

The validation is made in 3D for the geometry of a rectangular stainless steel rod of the dimensions $(0.5 \times 0.5 \times 1)\ m^3$, which is used for 1D case, with thermal conductivity $k = 15.1\ W\ m^{-1}\ K^{-1}$, as shown in Figure 3.3. The boundary conditions applied on this case are: at x= 0.25 m, y= 0.25 m & z= 0, T = 300 K; at x= 0, y= 0 & z= 1 m, fixed heat flux ($q = 800\ W\ m^{-2}$). The temperature distribution given by HC in z and y directions is compared to Fluent results in Figures 3.11 and 3.12, respectively. The visual comparisons of HC with FLUENT solver are illustrated in Appendix B.

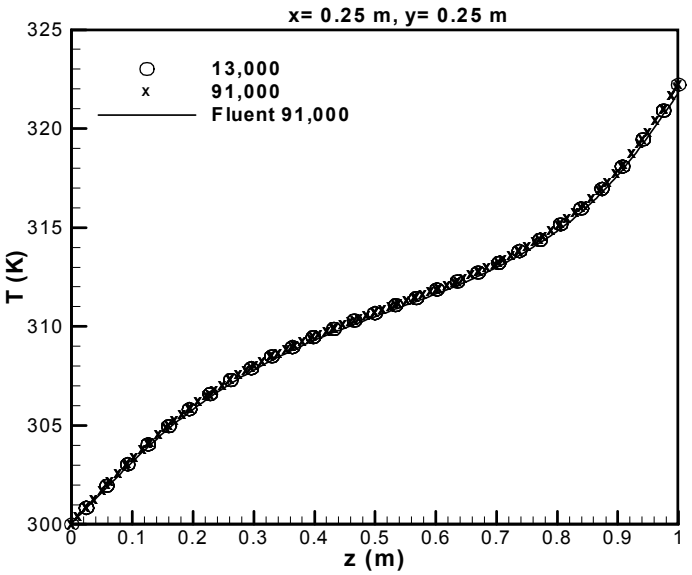

Figure 3.11: Temperature distribution in z-direction of the 3D case for HC (with different grid densities) vs. Fluent, at x=0.25 m, y= 0.25 m

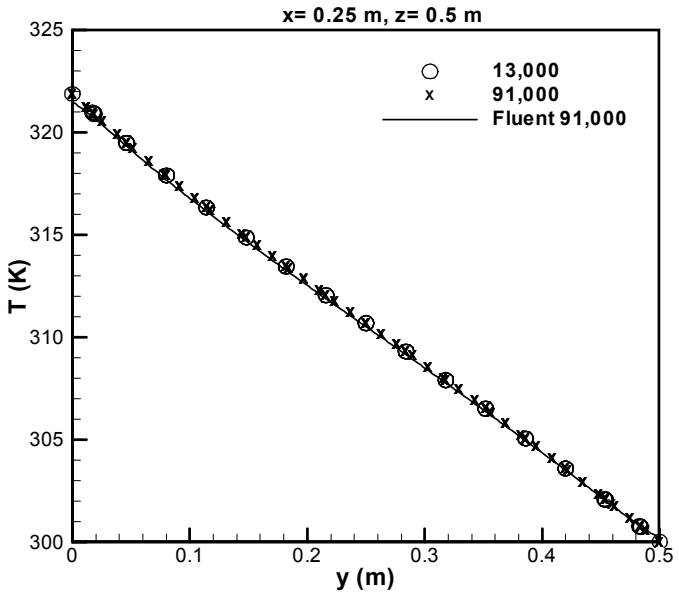

Figure 3.12: Temperature distribution in y-direction of the 3D case for HC (with two grid densities) vs. Fluent at x=0.25 m, z= 0.5 m

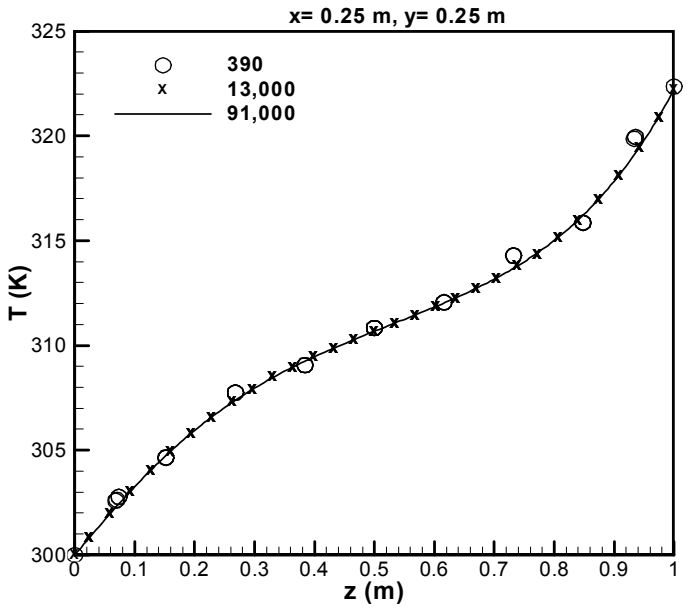

Figure 3.13: Grid independence check for the 3D case, over a range of node numbers from ~390 to ~91,000 nodes in z-direction

The above profiles of temperature were extracted at central locations in x-, y- and z-axes.

3.3. First Order Solution

The numerical solution of the HC was initially solved using Laplace equation, as suggested by Lyra et al. (2005). The purpose of this Chapter is to provide an evidence of the accuracy of this solution in comparison to the HC solution implemented in the current research. The 3D steady state HC equation was solved directly without using the LHS term of time interval. The steady state HC equation is:

$$\frac{\partial}{\partial x}\left(k\frac{\partial T}{\partial x}\right)+\frac{\partial}{\partial y}\left(k\frac{\partial T}{\partial y}\right)+\frac{\partial}{\partial z}\left(k\frac{\partial T}{\partial z}\right)=0$$

This equation is solved numerically in a FVM cell-vertex scheme. Heat fluxes around central node are delivered through the edges that share the central node, which are normal to the conduction areas, as shown in Figure (3.1). The steady state form, for a homogenous domain with no heat generation, can be re-written as:

$$\nabla^2 T = 0 \tag{3.19}$$

Laplace derivative, with second order accuracy, can be represented in the following format:

$$\nabla T = \sum_{i=1}^{N} \frac{T_c - T_i}{l_i}\vec{n} \tag{3.20}$$

Where i is index of neighbour nodes, l_i is the absolute distance between c & i and $\vec{n}$ is the normal vector as: $\vec{n} = \frac{x_c - x_i}{l_i}$. For $\Delta x_i = x_c - x_i$, The first order derivates can be written as:

$$\frac{\partial T}{\partial x} = \sum_{i=1}^{N} \frac{T_c - T_i}{{l_i}^2} \Delta x$$

And so on for $\frac{\partial T}{\partial y}$ and $\frac{\partial T}{\partial z}$. Using divergence theorem, the second order derivative can be written as:

$$\nabla^2 T = \frac{1}{V} \sum_{i=1}^{N} \nabla T \cdot \vec{n}\, A_i \tag{3.21}$$

Where A is the cell boundary boundary area and V is the volume of that cell. By substituting (3.20) into (3.21), equation (3.19) will be:

$$\frac{1}{V} \sum_{i=1}^{N} \frac{T_c - T_i}{l_i} (\vec{n} \cdot \vec{n})\, A_i = 0$$

$$\sum_{i=1}^{N} \frac{T_c - T_i}{l_i} \left[\left(\frac{\Delta x_i}{l_i} \right)^2 + \left(\frac{\Delta y_i}{l_i} \right)^2 + \left(\frac{\Delta z_i}{l_i} \right)^2 \right] A_i$$

Since ${l_i}^2 = {\Delta x_i}^2 + {\Delta y_i}^2 + {\Delta z_i}^2 \rightarrow (\vec{n} \cdot \vec{n}) = 1$ and the discrete form of the equation can be written as:

$$\sum_{i=1}^{N} \frac{T_c - T_i}{l_i} A_i = 0 \tag{3.22}$$

Equation (3.22) is applied to the whole domain. For example when considering a simple domain shown in Figure 3.14, the relationship (3.22) can used considering the central nodes: 6, 7, 10 and 11.

$$(T_6 - T_5)\frac{A_{56}}{l_{56}} + (T_6 - T_7)\frac{A_{76}}{l_{76}} + (T_6 - T_2)\frac{A_{26}}{l_{26}} + (T_6 - T_{10})\frac{A_{106}}{l_{106}} = 0$$

$$(T_7 - T_6)\frac{A_{76}}{l_{76}} + (T_7 - T_8)\frac{A_{87}}{l_{87}} + (T_7 - T_3)\frac{A_{37}}{l_{117}} + (T_7 - T_{11})\frac{A_{117}}{l_{117}} = 0$$

$$(T_{10} - T_9)\frac{A_{910}}{l_{910}} + (T_{10} - T_{11})\frac{A_{1110}}{l_{1110}} + (T_{10} - T_6)\frac{A_{610}}{l_{610}} + (T_{10} - T_{14})\frac{A_{1410}}{l_{1410}} = 0$$

$$(T_{11} - T_{10})\frac{A_{1011}}{l_{1011}} + (T_{11} - T_{12})\frac{A_{1211}}{l_{1211}} + (T_{11} - T_7)\frac{A_{711}}{l_{711}} + (T_{11} - T_{15})\frac{A_{1511}}{l_{1511}} = 0$$

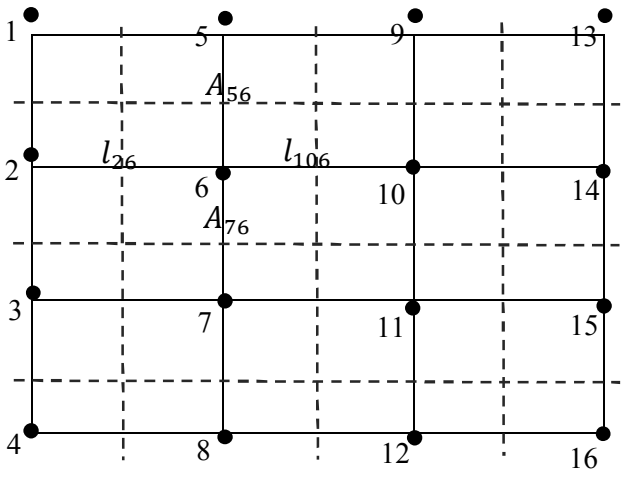

Figure 3.14: Simple domain with uniform grid

The temperature value at each central node can be derived from (3.22) as:

$$T_c = \frac{\sum_{i=1}^{N} \frac{T_i}{l_i} A_i}{\sum_{i=1}^{N} \frac{A_i}{l_i}} \tag{3.23}$$

The solution given by Laplacian derivative, shown in equation 3.23, is proved by tests to be of first order accuracy. The validation cases of this solution are explained in the

next section. It should be emphasised that this solution is not used as part of the currently developed CHT solver.

3.3.1. Validation of the First Order Solution

The validation is made on a simple case of rectangular box, $(0.5 \times 0.5 \times 1)$ m^3, with various boundary conditions. The validations, made in comparison to Fluent solver, are shown in Appendices C. In 1D heat transfer, a rectangular bar of insulated side surfaces with two ends fixed with temperatures of 273 K and 373 K respectively. The Figures in Appendix C show temperature distribution along z-direction for 1D heat transfer. In the 2D case, the body is insulated from two side surfaces and the other sides are exposed to convection of 300 K and thermal convection coefficient of 300 $\frac{\mathrm{W}}{\mathrm{m}^2.\mathrm{K}}$ apart from the bottom face which is fixed with a temperature of 400 K. Temperature distribution in y-direction, at x=0.25 m & z=0.5 m, and in z-direction, at x=0.25 m & y=0.25 m, are shown through Appendix C In 3D, two types of boundary conditions, Dirichlet and Neumann, were applied on the opposite corners. One corner including its three faces were exposed to heal flux of $800\, W\, m^{-1}$ and the opposite ones were of fixed temperature $300\, K$..

3.3. Concluding Remarks

In 1D and 2D test cases of the FVM solution, Figures 3.5 to 3.10, the results are of excellent agreement with the exact solution. The grid independence check has also shown the code validation of running the code for a wide range of mesh densities. In 3D test case, the analytical solution does not exist. A comparison to another commercial numerical solver (Fluent) was made, as shown in Figures 3.11 and 3.13. The results of HC were of good agreement with Fluent in the 3D test case. It is worth mentioning that the temperature variation in y-direction (Figure 3.12) looks linear due to the short distance with some negligible effect of heat transfer in the other two directions.

The results of discretisation scheme used by Lyra et al. (2005), given in Appendix B, show that the accuracy of the solution deceases for more complicated, for instance higher dimensional, problems. The results of 1D case show good agreement of the numerical simulation with the exact solution. However, the solution becomes less accurate in the 2D problem and shows significant errors with the 3D problem, in comparison to the second order accurate commercial solver. On the other hand, this solution is faster than the FVM solution, with about double speed of convergence. This technique can still be used for solving 1D problems and 2D applications with careful attention for the type of application. For the matter of accuracy, the FVM proposed in this thesis can be generalised for almost all HC applications within the specified three types of boundary conditions.

3.4. Fluid Flow

In CHT systems, when the CFD solver is coupled to a heat transfer solver, the accuracy of the coupled tool is mainly controlled by the fluid solver (Duchaine et al. 2009). In previous section, primary attention was given to the HC problems in solid domains. In this section, a brief review about what happens in the fluid domain and the representative equations used is given.

The industrial development in turbomachinary is performed by dealing with very complicated systems of heat transfer and fluid flow. It is therefore essential to understand the behaviour of the flow in order to derive or use the most appropriate solution. The fluid flow equations based on the laws of conservation, conservation of mass, conservation of momentum (Newton's Second law of fluid motion) and conservation of energy (First law of Thermodynamics), are defined as continuity, Navier-Stokes and energy equations, respectively (Blažek 2001). Since the current research interest is in the thermal behaviour of fluid near the walls, it is important to view the general form of the energy equation. The energy equation is explained in this Chapter in order to understand the importance of HC in fluid domain, as given below:

$$\frac{\partial}{\partial t}\int_{\Omega} \rho\, E\, d\Omega + \oint_{\partial\Omega} \rho\, E\, \vec{v}\cdot d\vec{S} = \oint_{\partial\Omega} k\, \vec{\nabla}T\cdot d\vec{S} + \int_{\Omega} \left(\rho\, \vec{f}_e\cdot\vec{v} + q_h\right) d\Omega + \oint_{\partial\Omega} (\bar{\bar{\sigma}}\cdot\vec{v}) d\vec{S} \qquad (3.23)$$

Where ρ is the density with units $(kg\, m^{-3})$, E is the total (internal and kinetic) energy per unit mass of units $(J\, kg^{-1})$, v is the velocity of units $(m\, s^{-1})$, k is the thermal conductivity coefficient of units $(W\, m^{-1}\, K^{-1})$, T is the absolute temperature in (K), $\vec{f}_e$

represents the acceleration caused by any external volume forces with units $(m\ s^{-2})$, q_h is the generated energy per unit volume of any heat sources other than HC with units $(W\ m^{-3})$ and $\bar{\bar{\sigma}}$ is the shear stress tensor caused by any internal forces with units $(N\ m^{-2})$. The form, given in equation (3.23), represents the balance of the following types of energy: rate of change in energy inside the fluid element equals the net heat flux into the element added to the rate of work done on the element due to body and surface forces (Blažek 2001). For further details about the fluid motion equations and their numerical solutions applied in SURF, the reader is referred to (Sayma et al 2000).

The heat transfer between the solid-interface surface and the fluid layer adjacent to that interface can be assumed of pure conduction when considering the fluid in that region as motionless (Çengel and Turner 2001). The thermal boundary layer thickness δ_T can be obtained in a relationship with the velocity boundary layer thickness and Prandtl number (Owen and Rogers 1989) as:

$$\delta_T = \mathrm{Pr}\ \delta_v \tag{3.24}$$

Where, δ_v is the velocity boundary layer thickness and Pr is Prandtl number, which is assumed, for approximation, as $\mathrm{Pr} \cong 0.697$ (when air flow in a pipe of higher temperature than the surface) and $\mathrm{Pr} \cong 0.707$ (when the flow is of lower temperature than the surface). The formula of the velocity boundary layer thickness δ_v can be approximated for laminar and turbulent flows (Kay and Nedderman 1979) and (Schlichting and Gresten 2000). In laminar flow over flat surfaces, the estimated boundary layer thickness can be determined as:

$$\delta_v = 5.83\ (Re)^{-\frac{1}{2}} \tag{3.25}$$

Where, Reynolds number $Re \leq 2000$. Whereas in turbulent flow, the estimated maximum boundary layer thickness can be written in the following approximation formula:

$$\delta_v = 0.379\, x\, (Re)^{-\frac{1}{5}} \tag{3.26}$$

Where, x is the length of channel and $Re \gg 2000$. In fully developed laminar flows through pipes, the boundary layer thickness can be approximated to:

$$\delta_v = \frac{1}{2} D_h \tag{3.27}$$

Where, D_h is the characteristic length measurement (the hydraulic diameter in channel flow) with unit (m). In channel flows, the Reynolds number (defined as the ratio of inertia to viscous forces) can be determined as:

$$Re = \frac{\rho\ \nu D_h}{\mu} \tag{3.28}$$

Where, μ is the dynamic viscosity with units $(kg\, m^{-1} s^{-1})$. The convection mode of heat transfer is treated by the solid domain as a boundary condition. This can either occur due to external forces (Forced convection) or freely (Natural convection) due to temperature gradient and buoyancy. The current research interest is in forced convection. A detailed review of treating the boundary of fluid-solid interface is given in Chapter four.

CHAPTER FOUR

CONJUGATE HEAT TRANSFER SOLVER

Present study proposes a methodology of treating heat transfer interaction between solid and fluid domains. At interface, the exchange of boundary conditions means replacing the fluid adiabatic walls with HC domains. This Chapter presents the technique of dealing with interface boundary conditions. The CHT coupling code was tested with selective examples of the most common cases of CHT in industry. The code was also validated on a double-pipe HE with parallel and counter flows in comparison to the analytical and other commercial CHT solutions (Al Qubeissi 2012b).

4.1. Interface Treatment

The main benefit of coupling solid/fluid domains is data transfer (interaction) at the interface. The data interaction accuracy becomes more complicated when dealing with non-conforming meshes, which is a common case in coupled solid/fluid solutions. Some of the most extensive research studies in the field (Giles 1997; Luo & Razinsky 2007; Henshaw & Chand 2009; He & Oldfield 2010 ...etc.) described the physical requirements for a heat transfer interface interaction as (first) energy conservation (the continuity of heat flux) across interface and (second) temperature continuity across interface.

The application of the two conditions, continuity of temperature and heat flux, on both (fluid/solid) domains in one solution can be difficult when dealing with unstructured grids. However, the condition of energy and temperature continuities at interface can be applied on each domain differently. This method was previously introduced by Kassab et al. (2003) and proved by Henshaw and Chand (2009) as a successful approach of coupling. The method is described as below.

First (Fluid side): Continuity of temperature along interface, applied to the fluid part (Dirichlet boundary condition).

$$T_f = T_w \tag{4.1}$$

Second (Solid side): Continuity of heat flux, applied to the solid part, i.e.:

$$q_s = q_f \tag{4.2}$$

Heat fluxes, normal to the interfacial surface, are balanced from both sides at each interfacial solid node. On the other side, temperature continuity (from solid to fluid boundaries) is applied at each interfacial fluid node. When the wall temperature is prescribed, as given in equation (4.1), both density and the energy can be directly specified (Blažek 2001) when there is no pressure gradient normal to the wall, as:

$$\rho = \frac{P}{T_w R} \tag{4.3}$$

Where ρ is density (at the wall), P is pressure (near the wall) and R is the ideal gas constant. Also:

$$\rho\, E = \frac{P}{\gamma} \tag{4.4}$$

Where, E is the energy per unit mass, γ is the ratio of specific heat coefficients at constant pressure and volume. In most applications, boundary elements sizes, shapes and therefore numbers of nodes from both sides may differ, as shown in Figure 4.1. The case of non-conforming meshes at interface is very common. The gross heat flux from one boundary cell to its neighbour will therefore be different.

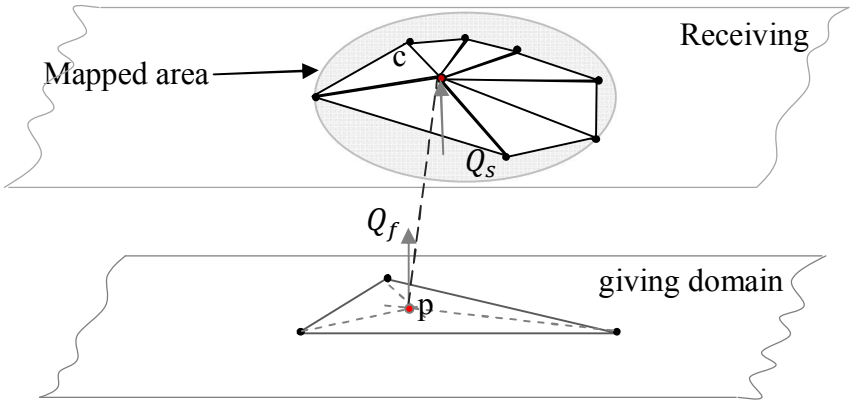

Figure 4.1: Interpolation between a cell-centred-node and nearest opposite group of boundary elements (Al Qubeissi 2012b)

When boundary meshes are non-conforming at interface, interpolation of heat flux and temperature values is applied. The nodes included in the interpolation are found by mapping the opposite boundary within a radius of the largest element size as shown in Figure 4.1. Heat flux leaving the fluid boundary towards solid domain can by determined within the boundary layer by Fourier's law (equation 3.2) when zeroing the velocity terms of the fluid energy equation (3.23) (He & Oldfield 2010) as:

$$\vec{q}_f = -k_f\, \nabla T_f \tag{4.5}$$

Heat rate arriving at the solid boundary is the product of surface area weights and the heat flux received from fluid domain (Li & Kong 2011) as: $Q_s = \vec{q}_f \cdot \vec{A}_s$. The operation of giving and receiving boundary data (data interaction) is repeated with iterations. The solution convergence is been checked by assuring that the difference between the total integrated heat rates of both interface boundaries is within an acceptable tolerance as:

$$\sum_{i=1}^{N_s} Q_s - \sum_{i=1}^{N_f} Q_f \approx 0 \tag{4.6}$$

The tolerance was made according to the number of iterations performed by the code and the minimum reach value with no change in this value with time. The initial set of tolerance is $\frac{2|Q_s - Q_f|}{(Q_s + Q_f)} \leq 0.1$ when iterations exceed 600 steps with stabilized residuals within this error. In most cases, the code approaches this tolerance beyond 200 iterations. Therefore, the other condition of ending the iterations will be the stabilised values of tolerance, i.e. no change with time steps.

4.2. Non-Conforming Meshes

Non-Conforming (or non-matching) solid-fluid meshes at interface are common cases in CHT modelling. Exchanging accurate data between solid and fluid zones at the interfacial line is very important. The interfacial 2D line (or 3D surface) is made of connecting nearest nodes from both sides, as illustrated in Figure 4.2. Heat fluxes, normal to the interfacial surface, are balanced from both sides at each interfacial solid node. On the other side, temperature continuity (from solid to fluid boundaries) is applied at each interfacial fluid node. The operation is carried out through inverse distance weighted interpolation of enclosing triangle technique. The selection of the

opposite side nodes, included in this interpolation, is based on nearest triangle or square. However, if the node is conforming to another node on the opposite side, the temperature and heat flux continuities will apply at those nodes without interpolation.

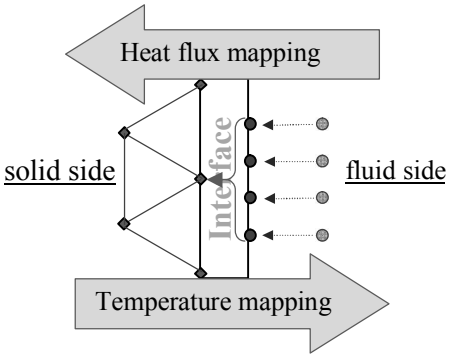

Figure 4.2: Side-view of heat flux and temperature interaction between fluid and solid boundary elements

For interaction between fluid and structure heat flux, the following two-side (1D) equations are proposed:

$$q_s = \vec{A}_{solid-cell} \frac{\sum_{i=1}^{K} \vec{q}_{interp} \cdot \vec{n}}{\sum |A_{mapped}|} \tag{4.7}$$

Where, $\vec{A}_{solid-cell}$ is the boundary-cell area, i.e. the sum of the shared elements multiplied by their normal vectors, i is the index of the fluid node that falls within the mapped area, $\vec{q}_{interp}$ is the heat flux interpolated from the fluid boundary, $\vec{n}$ is the vector normal to the fluid boundary node (cell) and A_{mapped} is the sum of the fluid boundary areas covered within the radius of mapped area. In terms of finding the temperature as a scalar value at the fluid side, the solution will become more straightforward. In scalar interpolation, a direct linear interpolation between elements is applied as:

$$T_f = (T_s)_{interp} \tag{4.8}$$

Where, T_f is the fluid temperature at the boundary and $(T_s)_{interp}$ is the interpolated temperature from the opposite solid-side boundary element, as shown in Appendix A.

From equations (4.7) & (4.8), heat flux and temperature at boundary nodes of both sides can be determined. It is important to avoid using these interface equations for cases with oscillation of heat flux along interface line (in 2D) or surface (in 3D). This kind of problem is very rear and is not common with rotating discs. Temperature gradient oscillation does not occur in gas-turbine rotating discs because cooling flow passes from centre of rotation towards the shroud orifice. In order to check if the interface solution is converged, the maximum difference between old and updated data is measured until it reaches a reasonable and stable tolerance. The following cases show examples of CHT systems of non-conforming interface-meshes.

4.3. 1D Validation Cases

In this section, 2 arbitrary cases were selected carefully to meet real life industrial applications based on resources of (Incropera & DeWitt 1996); Incropera. and DeWitt 2002; Çengel & Turner 2001). The selection of these cases was also based on the existence of their analytical solutions. The test cases were air flow problems associated with HC boundary types as given in the following sections.

4.3.1. Duct Flow Test Case

A 1D fluid flow and HC case of a CHT system is generated to test the currently developed method of coupling. The solid part is a stainless steel plate, with a cross

section area of $(0.2 \times 0.1)m^2$, attached to the base of the channel flow. The hot air, at atmospheric pressure and 353 K temperature enters a channel of $(0.2 \times 0.2)m^2$ cross sectional area and 8 m long, with flow rate $(\dot{m}) = 0.15\ m^3\ s^{-1}$. The solid domain has a fixed wall temperature 333 K on the downstream surface and receives heat flux from the upstream surface, which is in contact with the fluid domain, as shown in Appendix D. The fluid domain is meshed with structured grids of about 35000 nodes, whereas unstructured tetrahedral mesh is used for the solid domain with about 14500 nodes. This ensures non-conforming grids at the interface of both domains, as shown in Figure 4.3.

The solid thermal properties of stainless steel tables can be found in literature (Çengel & Turner 2001), at the specified average temperature as: thermal conductivity $(k) = 15.6\ W\ m^{-1}\ K^{-1}$. Fluid properties can also be found from the tables of dry air thermal properties (attached to this thesis in Appendix H) as: $\rho = 1.043\ kg\ m^{-3}$, Pr $\cong 0.707$, thermal conductivity of air $k_f = 0.029\ W\ m^{-1}\ K^{-1}$, specific heat at constant pressure $(C_p) = 1007\ J\ kg^{-1}K^{-1}$ and $\mu = 2.03 \times 10^{-5}\ kg\ m^{-1}s^{-1}$. The analytical solution of this case can be determined as follows below. Substituting equations (3.2 & 4.5) into (4.2) gives:

$$-k_s\ \frac{\partial T_{sw}}{\partial y} = -k_f\ \frac{\partial T_{fw}}{\delta_T} \tag{4.9}$$

Where, $\frac{\partial T_{sw}}{\partial y}$ is the temperature gradient of solid domain near the convection boundary and $\frac{\partial T_{fw}}{\delta_T}$ is the temperature gradient of fluid domain near the wall.

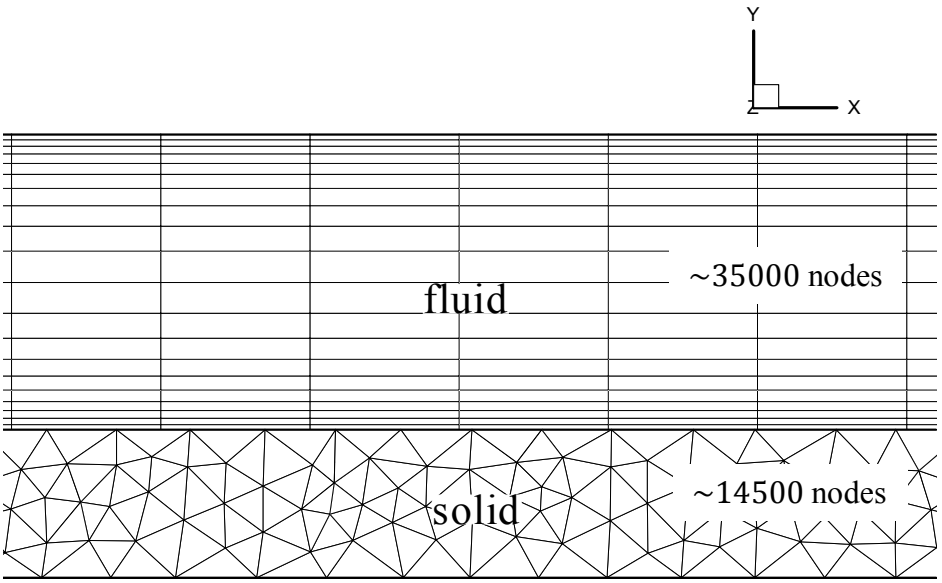

Figure 4.3: Mesh types and densities used in both domains of the 1D CHT problem

Since the fluid temperature near wall is unavailable in the analytical solution, it is important to replace the RHS term, in equation (4.9), with a heat convection term as:

$$-k_s \frac{\partial T_{sw}}{\partial y} = h\left(T_f - T_w\right) \tag{4.10}$$

Where, the thermal convection coefficient (h) is a function of the thermal conductivity and Nusselt number as:

$$h = \frac{Nu\, k_f}{D} \tag{4.11}$$

The type of flow can be known by calculating the Reynolds number (Re) from equation (3.28), where $D_h = 0.2$ m and velocity $(u) = 3.75\ m\ s^{-1}$, giving Re $\cong 3.82653 \times 10^4$ (turbulent flow). The Nusselt number can also be approximated by the empirical expression for turbulent flow (Kay and Nedderman 1979) as:

$$Nu = 0.023\, Re^{0.8} Pr^{0.3} \cong 96.12 \tag{4.12}$$

And from (4.11), $h = 14.273\ W\ m^{-2}\ K^{-1}$. Substituting h in (4.10) gives:

$$15.6\frac{T_w - 333}{0.1} = 14.273\ \left(T_{f_{av}} - T_w\right) \tag{4.13}$$

Where, $T_{f_{av}}$ is the average bulk temperature $\left(\frac{T_{in}+T_{out}}{2}\right)$, which cannot be determined without knowing the fluid exit temperature. Hence, the stored energy equation (due to temperature difference) is used as:

$$q = \dot{m}\ C_p\ (T_{in} - T_{out}) \tag{4.14}$$

Substituting equation (4.14) into (4.10) gives the bulk temperature value of about $T_{f_{av}} \cong 343.1\ K$. Hence, the average interface temperature can be found as $T_w \cong 334.2$ K and the heat flux as $q_f = 187.2$ W m^{-2}. The results given by HC-SURF couple gives average interface temperature (T_w) $\cong 334.15$ K and the heat flux $q_f \cong 179.5$ W m^{-2}, as displayed in Figure 4.4.

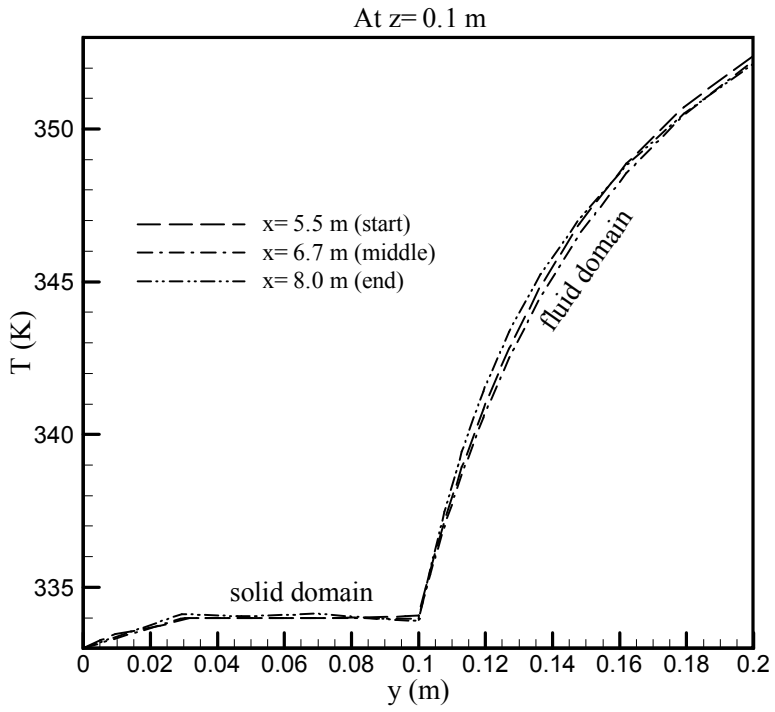

Figure 4.4: The temperature profile at three locations, in the fully developed flow region, of the 1D case solved by the CHT code

These results give good agreement between numerical and analytical solutions, with maximum errors of 0.02% in temperature and about 4% in heat flux. It is worth mentioning that the entry channel length of turbulent flow was tested to ensure the fully developed flow, upon which initial calculation was made (Çengel and Turner 2001) as:

$$L = 4.4\ D\ Re^{\frac{1}{6}} = 5.1\ m \tag{4.15}$$

However, the chosen length of the duct was above this value for guaranteeing fully developed flow. The temperature profile, in Figure 4.4, refers to no considerable change in temperature at three main locations of the fully developed flow region.

4.3.2. Pipe Flow Test Case

Another 2D CHT case is a numerical test on hot air flow, of $440\ K$ temperature, in a pipe of $0.4\ m$ diameter. The pipe is buried in the centre of a squared section domain of construction material with dimensions of $(2 \times 2)\ m^2$, as shown in Figure 4.5. The cube material is of thermal conductivity $k_s = 10\ W\ m^{-1}\ K^{-1}$ and fixed outside boundary temperatures of $400\ K$. The internal air thermal conductivity is $k_f = 0.04\ W\ m^{-1}\ K^{-1}$. The depth of the solid domain and the pipe are of $2\ m$ length. This flow gives Reynolds number (Re)=9.81×10^5 (turbulent flow).

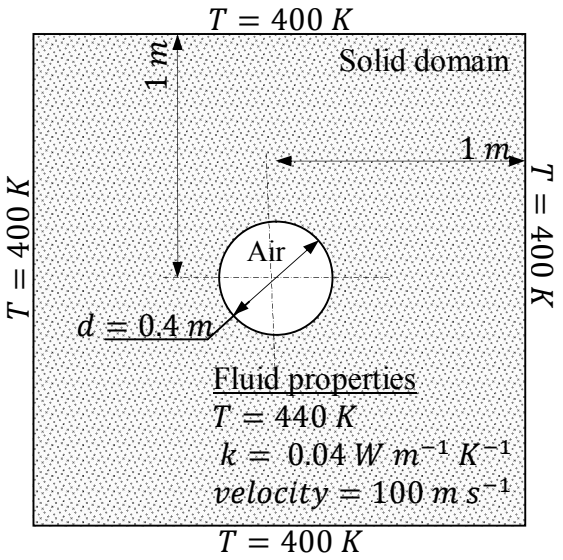

Figure 4.5: A schematic of the 2D conjugate heat transfer problem

The velocity boundary layer thickness of the pipe flow is given, in equation (3.27), as $\delta_v \cong 0.006\ m$, shown in Figure 4.6. This gives the thermal boundary layer thickness of $\delta_T \cong 0.0042\ m$ as given in equation (3.24). Also from equation (4.6), $\vec{q}_s = \vec{q}_f$, the interface temperature (seen from both domains) can be found as given in equation (4.10) of the 1D test case. Similarly to the previous 1D case, the Nusselt number of this case was found as: $Nu \cong 92.4$. In pipe flow the thermal convection coefficient can be found as: $h = \frac{Nu\ k_f}{D}$, leading to: $h = 9.24\ W\ m^{-2}\ K^{-1}$, which gives:

$$10\frac{T_w - 400}{0.8} = 9.24\ (440 - T_w)$$

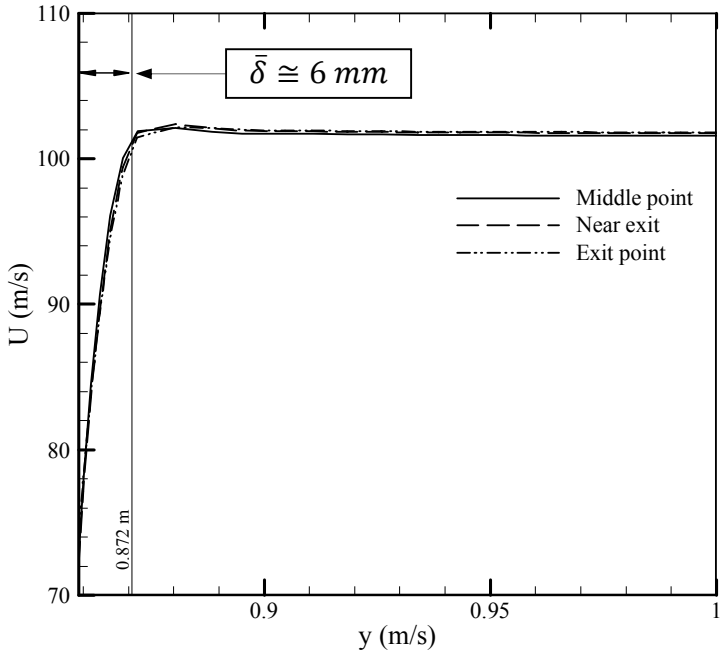

Figure 4.6: Velocity profile of the air flow in a quarter of the pipe, showing the estimated average boundary layer thickness ($\bar{\delta}$) of turbulent flow

This analytical solution, above, gives interface temperature of $T_w \cong 417\,K$ and $\vec{q}_f \cong 215\,W\,m^{-2}$. The numerical solution given by the CHT solver (HC-SURF couple) resulted in $T_w \cong 416.5\,K$ and $\vec{q}_f \cong 212.3\,W\,m^{-2}$, which gives $\sim 0.12\%$ error in temperature and $\sim 1.3\%$ error in heat flux, according to the given analytical solution. The boundary layer thickness given by the analytical solution is an approximate average value because this is local and will vary at different locations. Hence, the heat flux is also an approximated average value of the local ones. It is worth mentioning that a coarse grid is used for the 3D solid domain of 4450 nodes and a relatively average density structured grid is employed for the 3D fluid domain with about 7700 nodes. The numerical solution results provided by SURF-HC couple are illustrated in diagrams of Appendix D.

4.4. 2D Validation Cases

At current stage of the research progress, the validations of the couple CHT solver on HE cases are presented as in the following sections. The analytical solution is also given, in the following section, to be applied for comparison with the currently implemented numerical solver. It is worth mentioning that the Nusselt number in round pipe-flows, for Reynolds≤ 2000, can be approximated to $Nu \cong 4.36$ according to the calculations presented by Çengel and Turner (2001) and tests of Abraham et al. (2009).

4.4.1. Analytical Solution

The local heat flux from fluid side, given in equation (3.2), is determined from the temperature distribution near wall. These temperatures are computed using the gas law of states: $= \frac{P}{\rho \cdot R}$, where ideal gas constant (R) for dry air = 286.9 $\frac{J}{kg.K}$. The heat balance in HEs requires exchanging the exact amount of heat rate between domains, i.e. the received amount equal to the lost amount. This is to ensure that there is no leakage of heat outside the system, as illustrated in Figure 4.7.

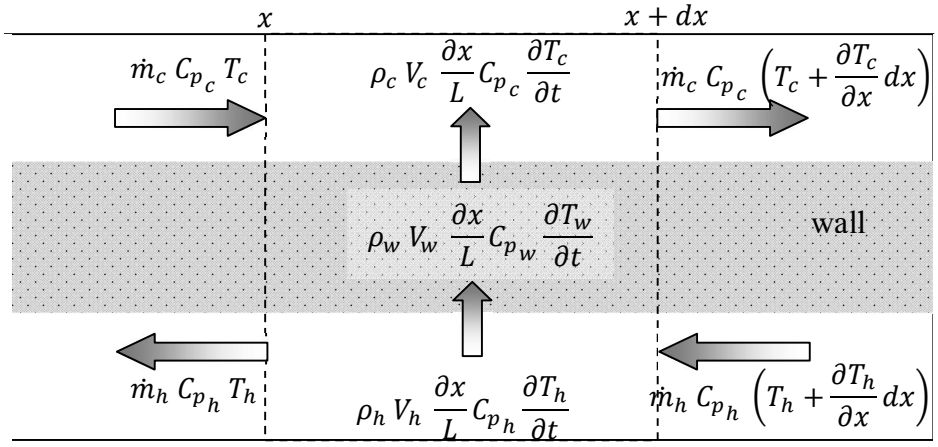

Figure 4.7: A schematic element of a conjugate heat transfer system showing the heat balance requirement

In double pipe HEs, for example, the heat absorbed by the cold fluid-flow side equals the heat loss from the hot fluid-flow side. In a control volume element of the system, the heat losses, or gains, by fluid equal to the change in energy through the solid medium. These relationships can be written in equations as follows:

$$Q_{cold} = Q_{hot} = UA\ \Delta T \tag{4.16}$$

Also:

$$UA\ \Delta T = U_{cold}A_{cold}\ \Delta T = U_{hot}A_{hot}\ \Delta T \tag{4.17}$$

Where, U is the total HTC with units (W m^{-2}), A is the surface area through which heat exchange occurs and ΔT is the average temperature difference between hot and cold sides. Selecting the element size for performing the control volume calculation, of equation (4.16), can affect the accuracy of the solution significantly. This is because of ignoring the temperature gradient along the pipe when performing the calculation, i.e. the analytical solution is more accurate for smaller size (smaller temperature gradient) elements. In this typical example of CHT system, shown in Figure 4.7, the thermal resistance $\left(\frac{1}{UA}\right)$ involves two convection mediums and one conduction medium of heat transfer. This can be determined by the following relationship (Çengel and Turner 2001):

$$\frac{1}{UA} = \frac{1}{h_c A_c} + \frac{\left|ln\left(\frac{D_h}{D_c}\right)\right|}{2\pi kL} + \frac{1}{h_h A_h} \tag{4.17}$$

Where, h_c& h_h are the cold and hot sides thermal convections, A_c & $A_h$are the cold and hot sides surface areas and D_c& D_h are the cold and hot sides (interface) diameters. The thermal convection in fully developed laminar flow can be found from:

$$h = \frac{Nu\ k}{D} \tag{4.18}$$

Where, Nu is the Nusselt number and D is the hydraulic diameter (m). In laminar flow, the Nusselt number can be approximated in a uniform heat flux from surface of pipe flow as: $Nu = 4.36$ and for a uniform temperature at surface of pipe flow as: $Nu = 3.66$ (Incropera & DeWitt 2002). As illustrated in Figure 4.7, the gained or lost heat rate through fluid flow is:

$$Q = \dot{m}\ C\ (T_o - T_i) \tag{4.19}$$

Where, $\dot{m}$ is the mass flow rate $(kg\ s^{-1})$, C is the heat capacity $(J\ kg^{-1}K^{-1})$ and T_i & T_o are the inlet and outlet flow temperatures respectively. The mass flow rate is a function of velocity (v), density (ρ) and fluid-flow cross sectional area (A_x). Hence, equation (4.18) can be re-written accordingly as:

$$Q = \rho v A_x\ C\ (T_o - T_i) \tag{4.20}$$

By substituting (4.16) into (4.20), the outlet temperature of one side of the flow is:

$$T_o = T_i + \frac{UA\ \Delta T}{\rho v A_x\ C} \tag{4.21}$$

The sign in the RHS of (4.21) can be either positive in heating or negative in cooling operations, i.e. heating for the cold flow side $(\Delta T > 0)$ or cooling for the hot flow side $(\Delta T < 0)$.

4.4.2. Parallel and Counter Flow Double-Pipe Heat Exchangers

The current test cases are the parallel and counter flows HEs using the same geometry. The tested geometry is a high pressure double-pipe of inner-pipe and outer-pipe diameters of 0.3 mm and0.64 mm, respectively. The inner pipe thickness is 0.07 mm, i.e. 0.44 mm in outer-diameter, as shown in Figure 4.8, and of $80\,mm$ in length to ensure a fully developed laminar flow. This system represents a double pipe HE wrapped with a perfect insulation. The flow direction in the double pipe system is tested for both parallel and counter flows.

It is worth mentioning that coarse meshes, structured and unstructured, are used in order to test the code with worse conditions of non-matching meshes. This will also ensure gaps between the two domains and overlaps of the two different meshes, as shown in Figure 4.9, in order to test the code with these features.

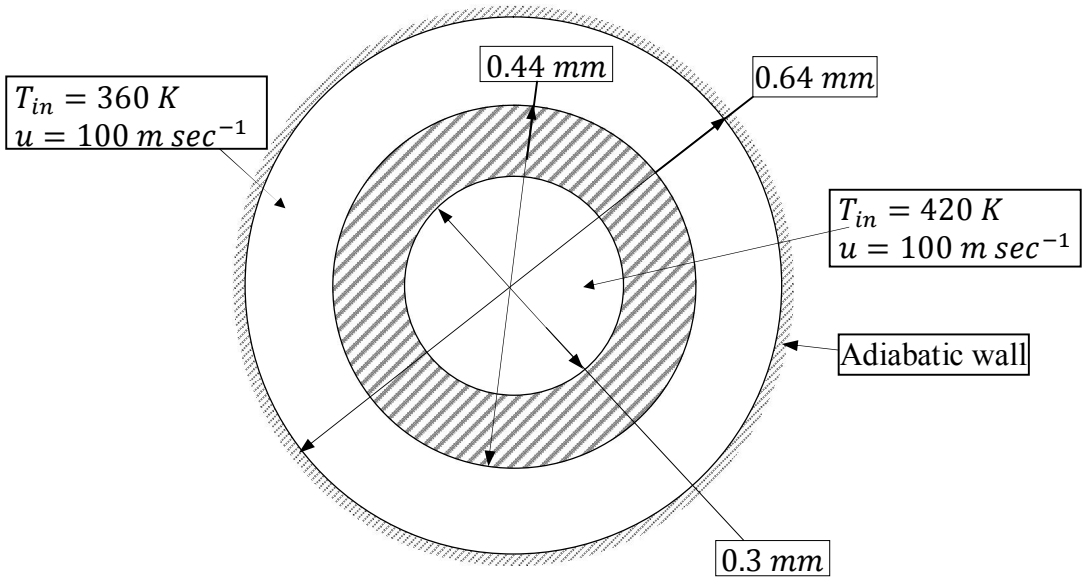

Figure 4.8: Cross-section of the double-pipe heat exchanger

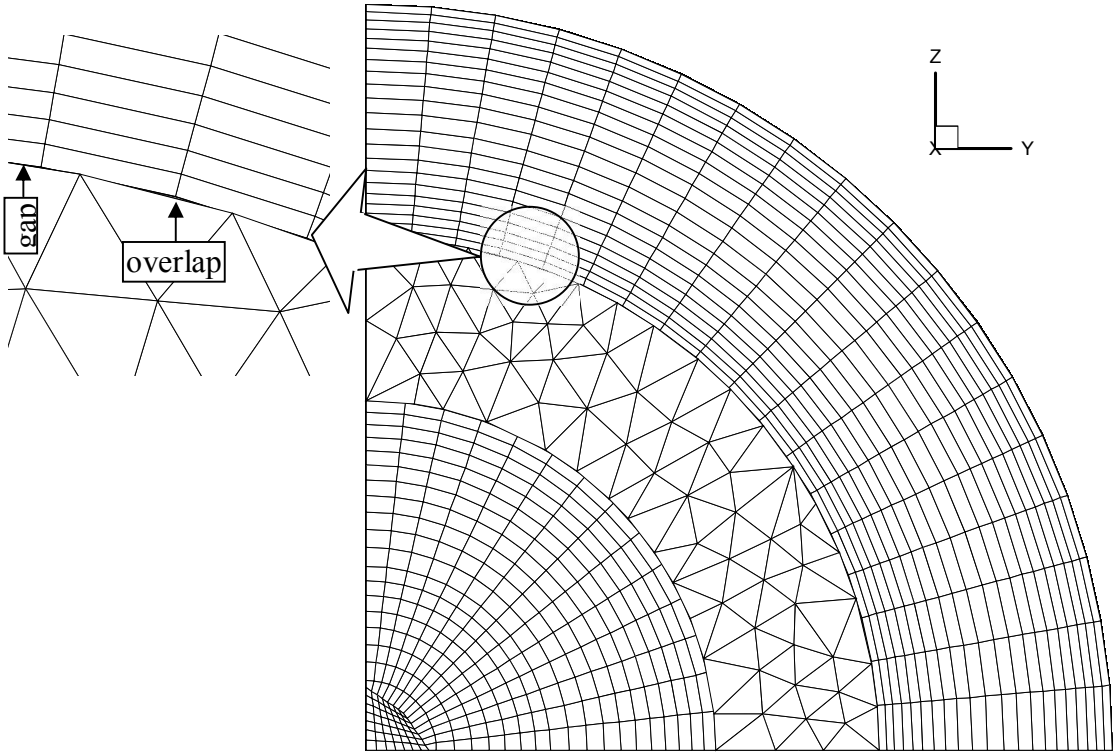

Figure 4.9: A 2D side-view of the meshes used in different domains

The length of the pipe was chosen carefully, in accordance with the minimum length requirement for a fully developed (hydrodynamically developed) flow. The hydrodynamic entry lengths in laminar and turbulent flows inside pipe are given by Çengel and Turner (2001) as:

$$L_{laminar} \cong 0.06\, D\, Re \tag{4.22}$$

$$L_{turbulent} \cong 4.4\, D\, (Re)^{\frac{1}{6}} \tag{4.23}$$

Where, L is the minimum length requirement for a fully developed flow region, D is the diameter and Re is Reynolds number. It should be emphasised that in counter-flow HE the minimum length requirement is doubled. This is to ensure that fully developed flow is achieved in both, inner-pipe and outer-pipe, flows. Çengel and Turner (2001) also

clarified the importance of Reynolds number (Re) in recognising the types of flow in pipes as: Laminar flow when $Re < 2300$, Turbulent flow when $Re > 4000$ and Transitional flow in the remaining range when $2300 \leq Re \leq 4000$.

A. Parallel Flow Heat Exchanger

The air velocity inside both pipes, in Figure 4.8, are of the same values, $u \approx 100\, m\, sec^{-1}$; while inlet temperatures at entrance are: in the inner pipe $T_{in} = 376\, K$ and in the outer pipe $T_{in} = 424\, K$. The thermal conductivity of the inner pipe (Steel/Nickel Ni40%), between both micro-channel flows, is $k = 10\, W\, m^{-1}\, K^{-1}$. The element of test is a 45 degrees angle deducted from the cylindrical shape, as shown in Appendix D. The case was validated against the solution of section 4.3, as shown in Figure 4.10.

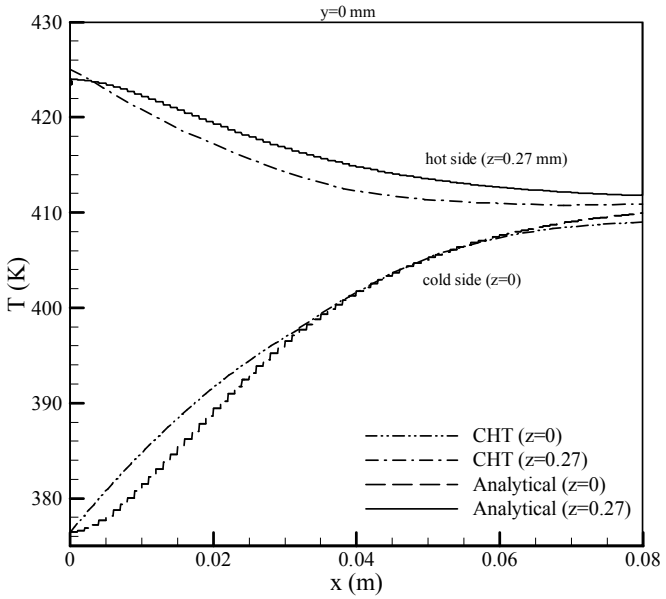

Figure 4.10: The temperature profile along the double-pipe in comparison to the analytical solution

From Figure 4.10, it was found that the results were of poor agreement with the analytical solution. This will be further investigated in section C when a comparison to a commercial CHT solver is made. It should be emphasised that it is so difficult to control the temperature at (at least) one input and opposite output at the same time in the analytical solution. In the given analytical solution, the exit boundary condition in each flow is calculated from next point and opposite flow point, i.e. only inlet boundary conditions were applied in equation (4.21). This error caused divergence between both (numerical and analytical) solutions.

The velocity profile was checked across the pipe section at three axial locations in order to ensure a fully developed flow. The comparison between axial velocities at three points near the pipe mid-length was displayed in Figure 4.11.

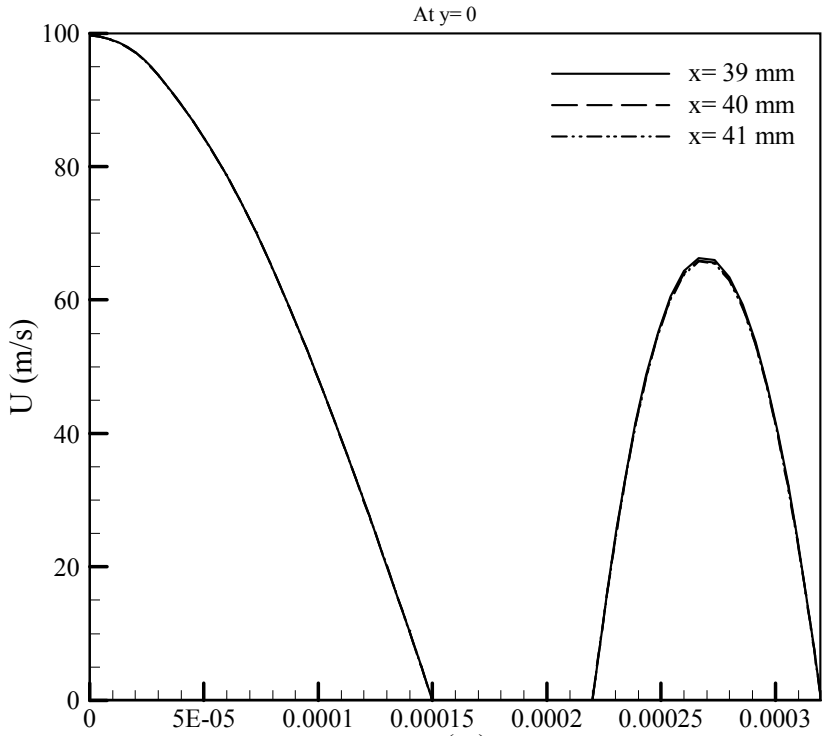

Figure 4.11: The velocity profile across the parallel-flow double-pipe in three axial locations

B. Counter Flow Heat Exchanger

The system given in case A is used again with the same flow properties and opposite velocity direction in the hot side (outer-pipe) flow. The schematic of the flow characteristics in counter-flow double-pipe HE is given in Figure 4.12, by Demko and Chow (1984), for illustrating a typical CHT case of a turbulent counter-flow HE. In comparison and similarity, the laminar counter-flow velocity vectors for the current test case are shown in Figure 4.13.

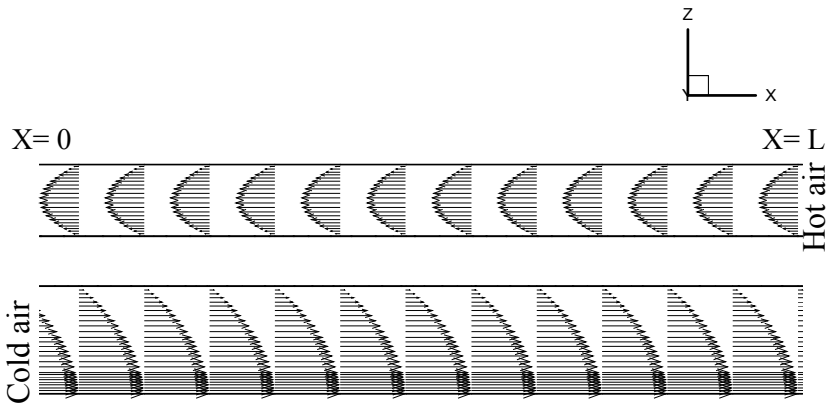

Figure 4.12: Element of the fully developed laminar-compressible flow of the counter-flow double-pipe system showing velocity along the pipe

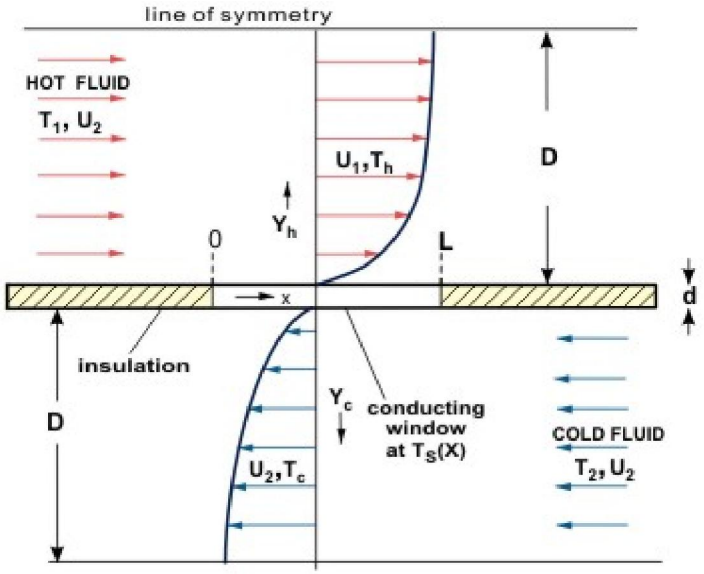

Figure 4.13: sketch of the counter-flow HE showing the general heat 2 m transfer and fluid flow profiles, from (Demko and Chow 1984)

The velocity profile of this problem was checked to ensure a fully developed flow. The axial velocity is plotted at three regions in the middle of the flow, as shown in Figure 4.12. It is worth mentioning that the available analytical solution is not the exact solution for this case, where some approximations were performed. As a result, it is difficult to judge the solution in comparison to the available analytical solution. The results shown in Figure 4.14 show a significant difference between both results.

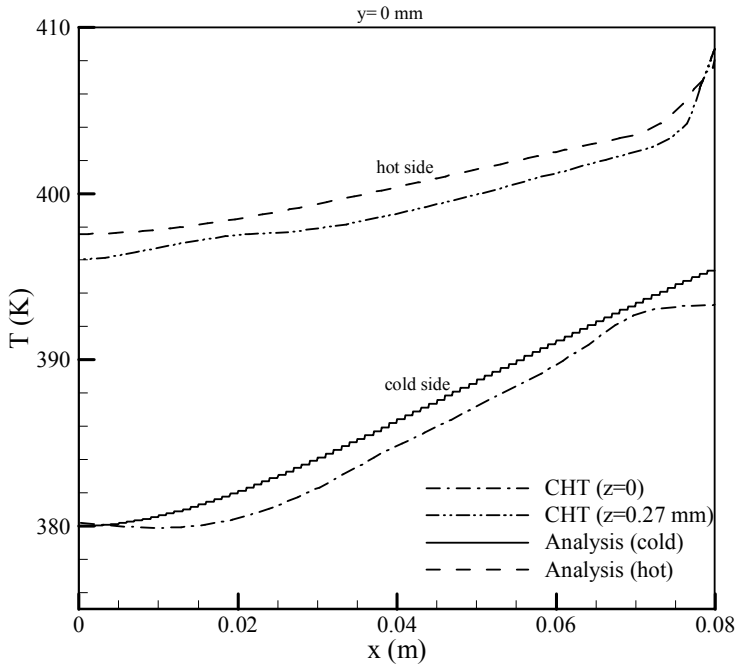

Figure 4.14: Temperature profile of the counter-flow CHT double-pipe system in comparison to the analytical solution

Therefore, the solution carried out in SURF-HC couple resulted in a poor agreement with the analytical solution. More diagrams of the solution are illustrated in Appendix D. This case gives a good example for the necessity of CFD where no exact solution exists for solving such a problem. Hence, a comparison to another commercial CFD solver is given in the next section.

C. Validation with Commercial CHT Solver

In previous section, the validation was performed in comparison to the analytical solution. The derived analytical solution, of equations (4.16) to (4.21), is approximated in 1D for each small element of the domain. The approximation of the analytical solution led to uncertainty about the results. Hence, the comparison between temperature profiles given by numerical and analytical solutions, shown in Figures 4.10 and 4.14, does not confirm the validation of the code. It was therefore essential to make further investigation about how accurate the current numerical solution can be in comparison to another commercial CHT solver, ANSYS CFX software (version 12.0). CFX is a high-performance general purpose fluid dynamics program that has been commercially used to solve a wide-range of combined fluid flow and heat transfer problems. The comparison was performed using same geometry, grid shape and node densities. The results are displayed in Figures 4.15 and 4.16 as temperature profiles in the middle of the flow along the pipes.

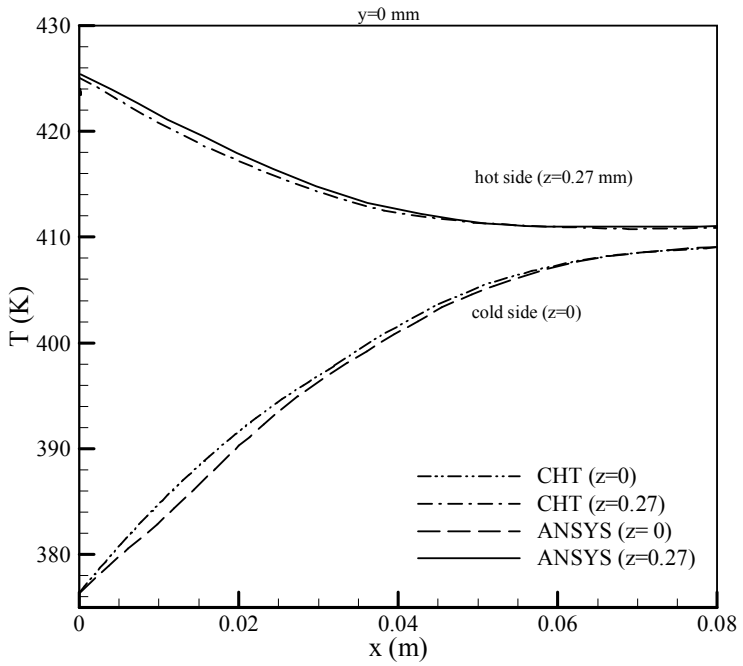

Figure 4.15: Temperature profile of the double-pipe parallel-flow by CHT solver in comparison with CFX (ANSYS)

It is worth mentioning that results obtained, for this numerical solution illustrated in Figures 4.15 and 4.16, were based on mesh densities of 7700 nodes (outer pipe) and 4450 nodes (inner pipe). The same boundary conditions were applied on both, CHT and ANSYS, solvers. It is also known that both solver used FVM of discretisation with careful consideration of mesh refinement near fluid boundaries.

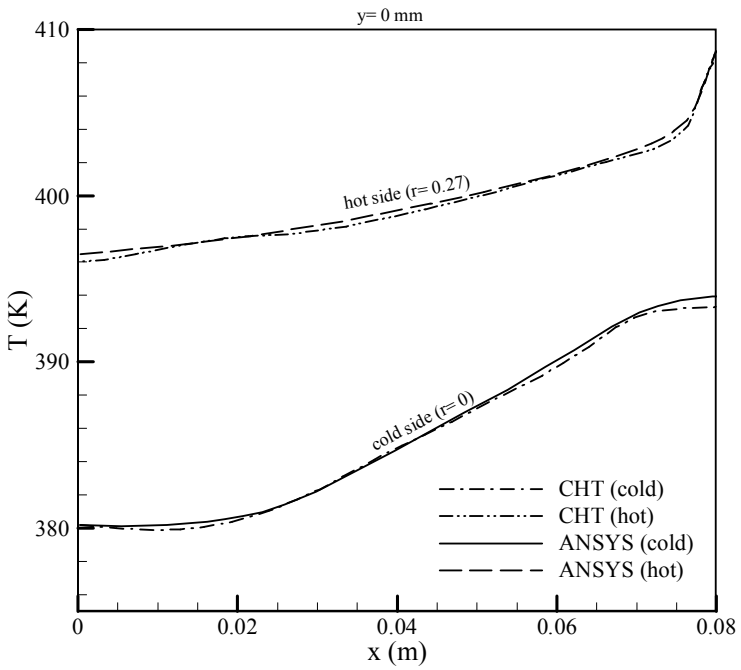

Figure 4.16: Temperature profile of the double-pipe parallel-flow by CHT solver in comparison with CFX (ANSYS)

The temperature profile of the parallel-flow types, shown in Figure 4.15, gives a better vision about the accuracy of the developed CHT solver. The results are of good agreement, with maximum error between both solutions of ~ 1%. The counter-flow double-pipe problem was also solved in CFX (ANSYS version 12.0) for validating the CHT solver. The temperature profile of the counter-flow problem was checked by the developed CHT in comparison to ANSYS, as shown in Figure 4.16. The solution given by CHT is of a very good agreement with ANSYS with a maximum error of about ~ 0.5%.

4.5. Concluding Remarks

The numerical solution implemented in the CHT was tested on 1D and 2D problems. The results were visualized to test and validate the code. In 1D problems, the analytical solution exists, which can represent the exact solution in most applications. It was therefore essential to validate the code in comparison to the analytical solution for such problems. Tests on 1D problems have shown excellent agreement of the developed CHT solver with the available analytical solutions. The test on duct flow has shown maximum errors of 0.02% in temperature and about 4% in heat flux in comparison to the exact solution. Also, the test on the pipe flow, buried in concrete, has given $\sim 0.12\%$ error in temperature and $\sim 1.3\%$ error in heat flux. These Figures prove the validation of the developed CHT solver (SURF-HC code) in solving 1D CHT problems.

Further tests were carried on the code for validation in 2D problems. The double pipe HEs are very common CHT cases in industry. It should be noticed that the analytical solution given for 2D CHT problems may not represent the exact solution due to many approximations. Also the given analytical solution, in section 4.4.1, was based on the estimating the second dimensional variation in temperature from the 1D calculation. However, the comparison to the analytical solution, in 2D, did not show a valid solution. It was therefore essential to perform further tests on the code in comparison to a commercial CHT solver (ANSYS 12.0/ CFX). The comparison to the ANSYS solver, has given good agreement between both solvers with about 1% difference in parallel flow and about 0.5% difference in counter flow. These results prove the validation of the developed CHT solver on 2D problems.

Since the CHT solver was mainly developed for the purpose of solving complicated problems, it is essential to perform further test on a 3D case. This validation was given a special attention in the thesis, which will be provided in next Chapter.

CHAPTER FIVE

THE ROTATING CAVITY AND DISCS

This Chapter presents fluid flow and heat transfer visualisations of the CHT cavity and two co-rotating discs. Rotating cavities are the most common cases for testing the cooling flow profile in turbomachinery. The test is carried out to validate the developed CHT solver. The selection of a typical rotating cavity is based on the availability of the experimental data. Since the code has been validated in comparison to the analytical and other commercial CFD solutions, in Chapter 4, it is most important to show the validity of the code in solving real industrial problems. The following sections give a description of the test case and results, assisted with diagrams.

5.1. Case Description

The rotating cavity of air with radial outflow is a common case for studying the cooling flow between two co-rotating turbine discs. The test case is a component of two axisymmetric co-rotating discs with a shroud. The shroud is punched with 32 holes of 9 mm diameter each, as shown in Figure 5.1. The current modelling prediction is examined against the experimental results, provided by Northrop (1984), for validation. The cavity model was simplified in order to be consistent with the mesh type shown in Figure 5.3. The necessity of simplifying the mesh shape lies in the difficulty of dealing with the sharp edges of round holes. The mesh in the fluid domain, inside the holes, becomes so difficult to refine to level of dealing with high speeds when the mesh is

unstructured. Hence, first, the mesh in the fluid domain needs to be structured for a better mesh refinement near the wall. Also, the structured mesh will need straight line edges rather than round holes to keep the mesh shape and size increase in the groove smooth with the rest of the mesh.

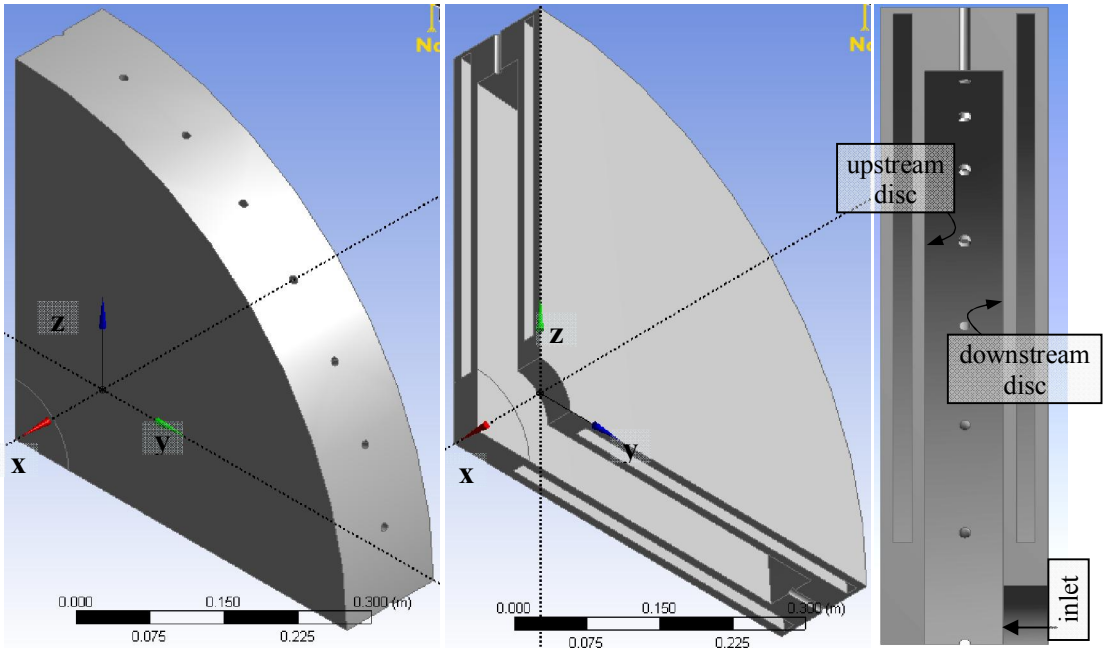

Figure 5.1: 3D views of the test-element of the rotating-discs and shroud showing the original shape with 9 mm holes

The meshes of the rotating-discs and the modified cavity are shown in Figures 5.2 and 5.3, respectively. The 32 holes of 9 mm diameter were replaced with a circumferential groove for the exit of the radial outflow. The simple conversion calculation is attached in Appendix A.

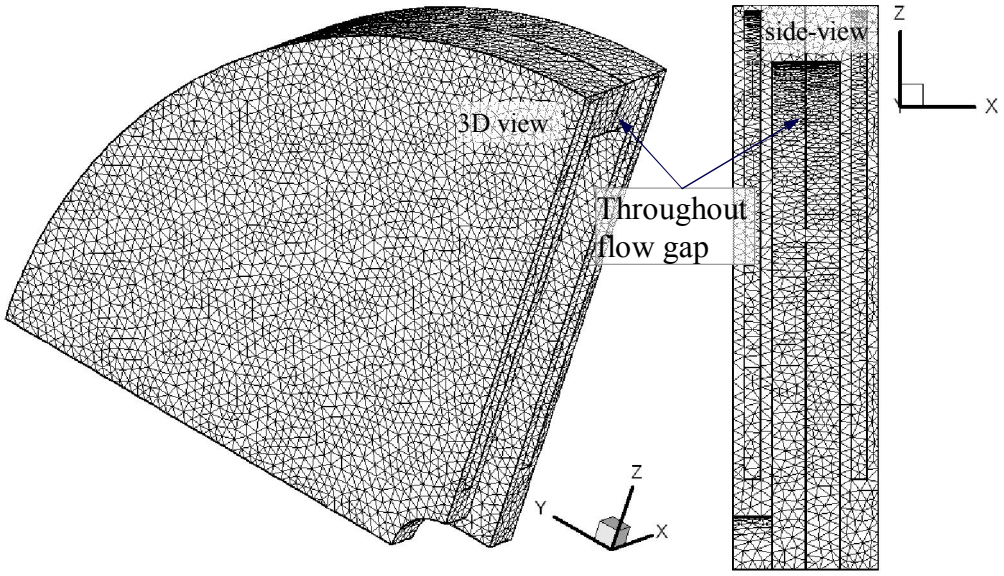

Figure 5.2: 3D and 2D-side views of the rotating-discs tetrahedral mesh, showing the groove replacing the 32 holes in solid side

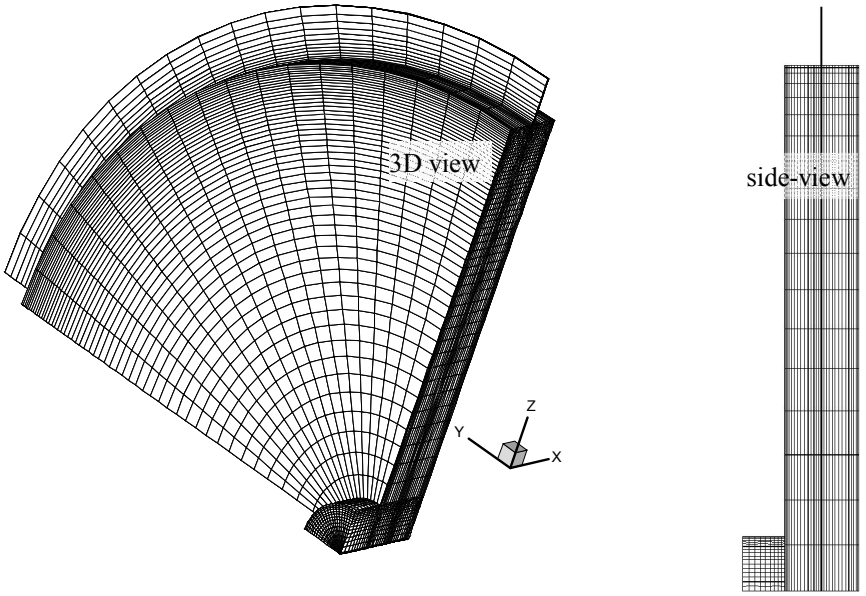

Figure 5.3: 3D and 2D-side views of the cavity quadrilateral mesh, showing the groove replacing the 32 holes in fluid side

It is very important to know that SURF is capable of dealing with unstructured meshes with the same performance when solving fluid flow problems. However, a structured mesh has been used in the fluid domain for the following important purposes: structured meshes are preferred in the CFD solver because an unstructured mesh needs higher

processing memory, which leads to lower code running speed. The uniform structured mesh was tested in comparison to the unstructured mesh, in fluid domain, to show more accurate results with a faster solution. This is due to the fact that, with structured grids, the temperature gradient is obtained directly from a uniformly distributed temperature at neighbouring points; whereas in an unstructured grid, neighbouring nodes at the edge are integrated with approximation, which can cause significant errors when dealing with a high normal temperature gradient near the walls. This is also convenient to ensure non-matching meshes at the interface, which can further test the CHT solver with this feature.

5.2. Validation

CFD predictions presented in this Chapter show the influence of the non-dimensional parameter, rotational Reynolds number, Re_θ, on the cavity structure. The test on SURF-HC code has shown a valid agreement with the results of temperature distribution given by Northrop (1984) for different input parameters, mainly rotational speed as shown in Figures 5.4, 5.5 and 5.6. The plot is made according to the experimental data displayed in Tables (E.1 to E.3) of Appendix E.

It is worth mentioning that the experimental test presented by Northrop (1984) did not represent a perfect symmetric cavity due to the difficulty in controlling some input parameters, such as heat flux. The unbalanced heat flux distribution led to some deviation, which was neglected by the author, in what the symmetric cavity should look like. This is further discussed in Chapter 6. More Figures illustrating the temperature

contours in rotating discs, assisted with tables of input/output readings, are displayed in Appendix E.

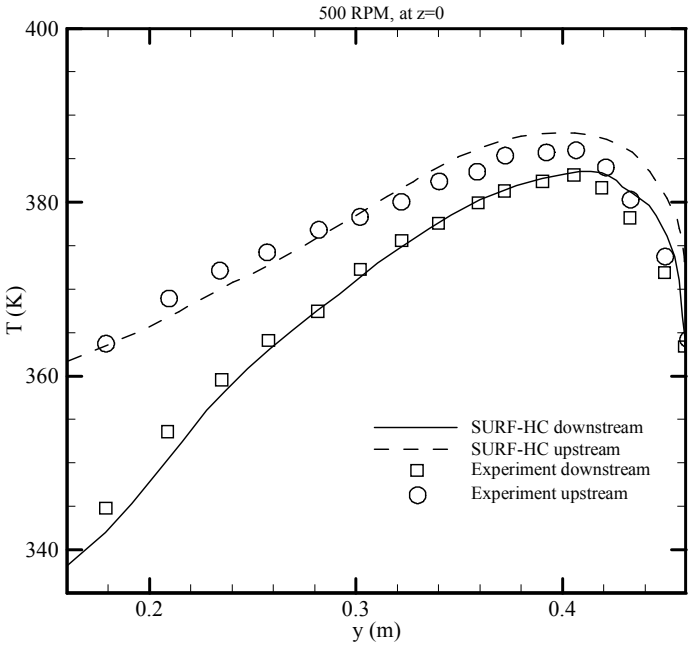

Figure 5.4: Temperature distribution radially at discs-cavity interface line for 500 RPM speed & $q = 3200\ W\ m^{-2}$, from numerical CHT solution (SURF-HC) vs Northrop experiment

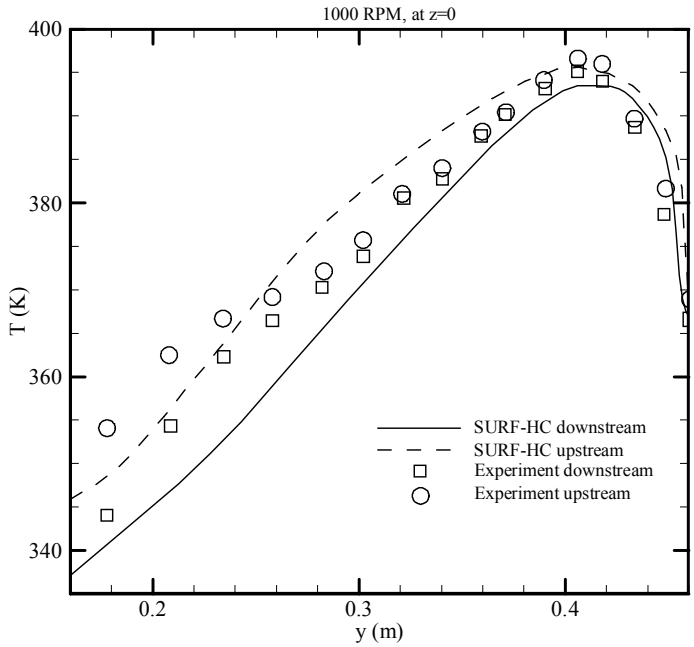

Figure 5.5: Temperature distribution radially at discs-cavity interface line for 1000 RPM speed & $q = 4300\ W\ m^{-2}$, from numerical CHT solution (SURF-HC) vs Northrop experiment

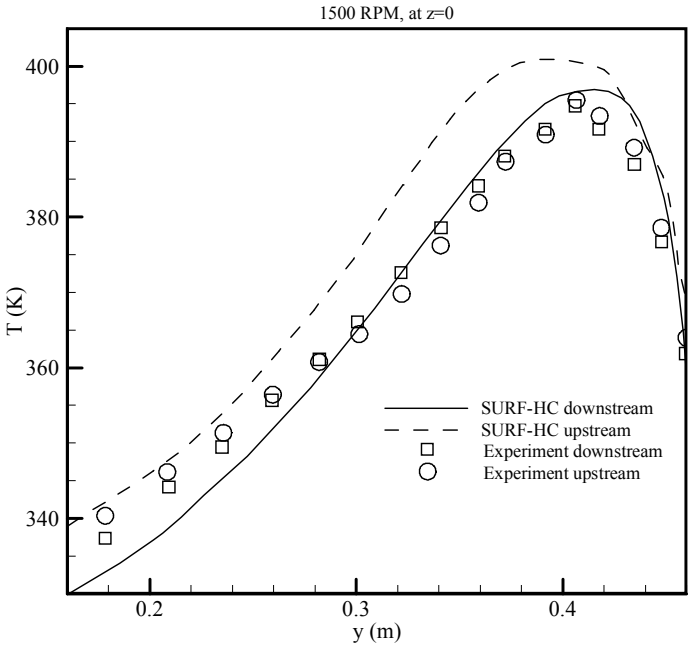

Figure 5.6: Temperature distribution radially at discs-cavity interface line for 1500 RPM speed & $q = 4600\ W\ m^{-2}$, from the numerical CHT solution (SURF-HC) vs Northrop experiment

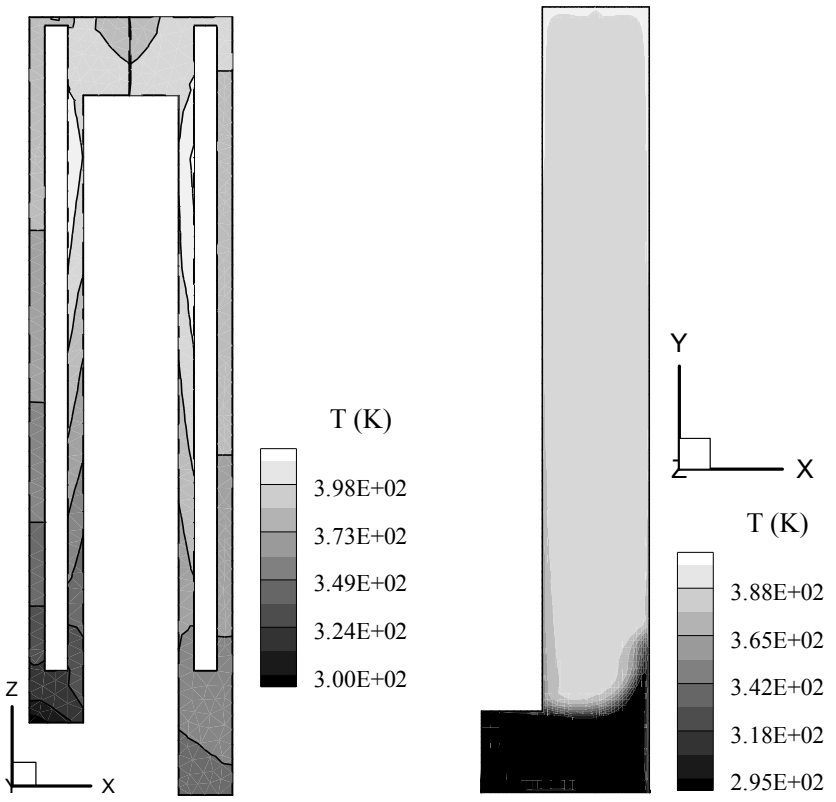

(A) Solid domain (B) Fluid domain

Figure 5.7: 2D view of the temperature contours in (A) solid and (B) fluid domains

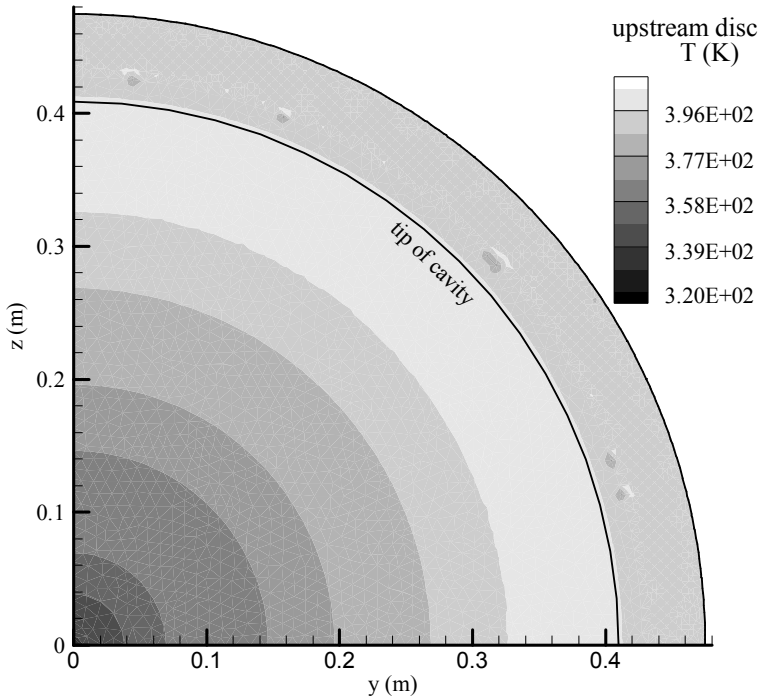

Figure 5.8: Typical 2D view of Temperature contours at upstream disc at 1000 RPM rotational speed

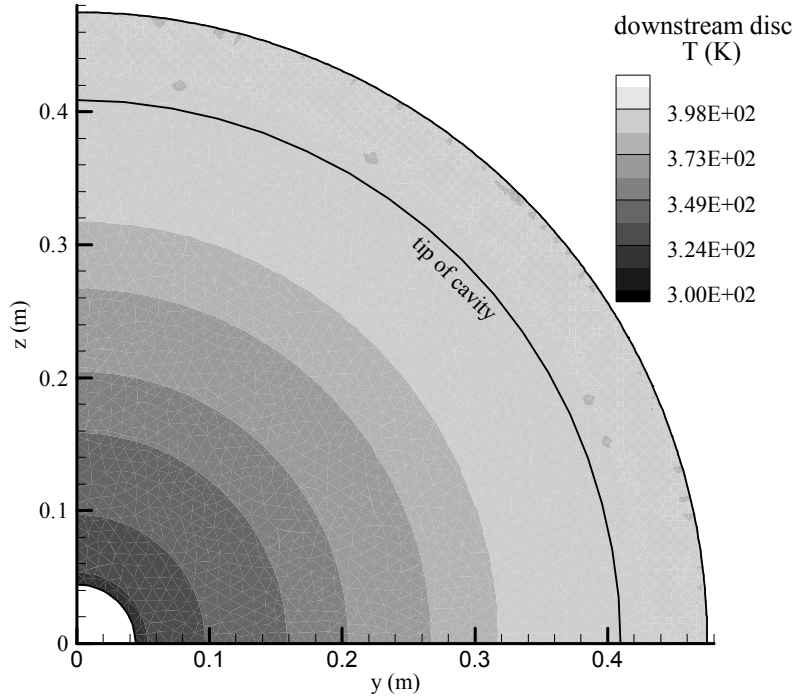

Figure 5.9: Typical 2D view of temperature contours at downstream disc at 1000 RPM rotational speed

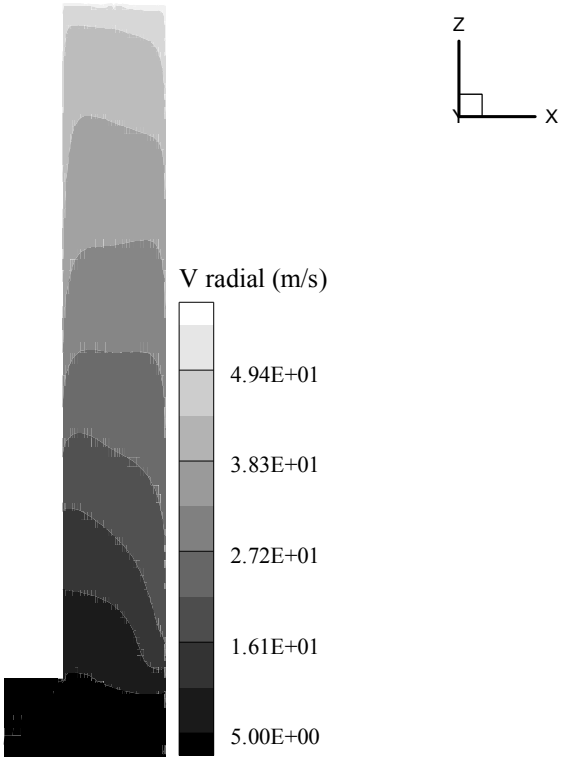

Figure 5.10: Typical 2D view of absolute velocity contours in axial-radial section at 1000 RPM rotational speed

5.3. Concluding Remarks

In the previous section, three selective test cases were made on the CHT solver for a cavity of co-axial co-rotating discs. The test cases were made with a relatively wide range of rotational speeds, $500, 1000$ & 1500 RPM. The results were validated in comparison to the available experimental data, for these particular transitional and turbulent flow CHT examples.

The temperature distribution radially, at upstream and downstream interface, shown in Figures 5.4 to 5.6, is of acceptable agreement with Northrop's experimental results. However, the accuracy of the numerical solution (given by CHT solver) reduces with

the increase of rotational speed. This error is caused by the assumption of no movement near the wall, made in CHT solver. This assumption becomes less accurate when the flow turbulence increases, i.e. $Re \gg 10^5$.

Also, the temperature profile near the exit at the downstream disc becomes similar to the one at the upstream disc for the wide range of rotational velocities. This similarity in temperature distribution is due to the increase in HTC. This means that the temperature profile in the higher velocity test shows closer agreement between temperature profile at downstream disc and upstream disc. This is due to the fact that the increase in HTC is associated with the increase in velocities.

In Figures 5.8 and 5.9, the temperature distribution at, upstream and downstream, interfaces is viewed in contours. In Figure 5.7, the temperature contours are viewed inside the rotating cavity to show the full view of temperature distribution radially. Also, the absolute velocity inside the cavity is viewed in axial-radial section, as shown in Figure 5.10. It should be emphasised that these visual diagrams of temperature and velocity were not provided by Northrop (1984). However, these Figures are of close similarity with the prediction of the flow profile given by Owen and Rogers (1995) for such type of rotating cavity.

CHAPTER SIX

DISCUSSION AND CONCLUSIONS

The main findings of the current research study are summarized in this Chapter. The major tasks carried out in the current research investigation were proposing numerical solving techniques for HC and CHT problems. The strategy was integrating a CFD solver with the developed HC solver by the author. At interface, a linear interpolation of mapped area technique was implemented to deal with non-matching (non-conforming) meshes. In this Chapter, the results are discussed and conclusions of the work are given in detail.

6.1. Discussion

The time steps in fluid domain vary from 200 to 10,000 iterations for each time-step in solid domain. The choice of the exact number from this range depends on the time interval needed for each domain. Initially, 500 time steps are achieved in fluid domains for each one time-step in solid domains. HC solver starts taking the boundary data when CFD solver reaches convergence within the specified range given in Chapters 3 and 4.

The variation of time-step ratio can reflect a better vision of what happens in real life, when the time needed for variation in each domain changes accordingly with the change of other physical properties (He and Oldfield 2010). This process is carried out until the CHT solution is converged.

Other criteria of the CHT solver are the conditions of convergence and temperature continuity. In convergence, the heat transfer rates across the interface between both domains must remain close. The difference between lost and gained heat fluxes must not exceed the set tolerance. This operation is made as the criterion of convergence. The convergence criterion assures no leakage of heat from the system. The temperature continuity is applied automatically inside the code when the first condition of convergence is approached. The temperature is passed from the solid surface to fluid as a Dirichlet boundary condition.

In the tests on parallel and counter flow HEs, the analytical solution has shown corrugated lines as shown in Figures 4.11 and 4.14. This error in fact is due to the assumption of average temperature in each segment (element) of the analytical calculation, given in equation (4.21). This result will therefore not refer to the exact predicted profile of temperature, but an approximate Figure of the estimated temperature distribution. The numerical CHT solver has not shown a very good agreement with the analytical solution. Although the exact agreement with the analytical solution is not determined, due to the explained approximation in the 1D equation, the validation can show that CHT results are close and parallel to the analytical approximations.

Based on the above explained error in the analytical solution (due to approximation) and the difficulty in finding an exact solution, a comparison to another commercial CHT solver was necessary. The validation of the code on parallel and counter flow HE cases was made in comparison to a commercial CHT solver (ANSYS CFX version 12.0). The results of the currently developed CHT solver on these test cases were of good

agreement with the results given by ANSYS, as shown in Figures 4.15 and 4.16, with maximum errors of about 1% in parallel flow and about 0.52% in counter flow.

The set up computer program for solving the Navier-Stokes equations integrated with the HC equation, replacing the adiabatic boundary, was validated in comparison to a real industrial case of gas-turbine cavity between two co-rotating discs. The test rig, built up at Thermo-Fluid Mechanics Research Centre (TFMRC) (Northrop 1984), was a complex geometry with so many details of unnecessary parts compared to modern experiments, such as wiring for thermo-couples and heating instruments coated by mat.

It is worth mentioning, for validation, that the geometry was simplified for meeting the structured mesh requirements as shown in Figures 5.1 and 5.2 of Chapter 5. The Rohacell insulation fill ($k = 0.05\ \mathrm{Wm^{-1}K^{-1}}$) was unnecessary in the numerical calculation, which was replaced with a perfectly adiabatic gap. Also, the five-stage heaters with the wiring and mat details were represented with a customized boundary condition of equally distributed estimated heat flux of $\sim 40\ \mathrm{kW\ m^{-2}}$. It is important to mention that Northrop's experiment was based on the assumption of a symmetrically heated rotating cavity. In reality, this is not the exact case where the inlet flow side is of lower temperature than the inlet opposite side. Hence, the cavity was not perfectly symmetric in terms of temperature distribution.

In Figures 5.3, 5.4 & 5.5, there is an increase in the difference of temperature values between numerical and experimental results starting from about 1.2% at $500\ rpm$ to about 3.08% at $1500\ rpm$. These data refer to some decrease in the accuracy of the proposed numerical CHT solution with the increase of Reynolds numbers when ($\mathrm{Re} \gg 10^5$). This is due to the fact that, in CHT solution, heat flux near the wall was

assumed as $q = -k_f \frac{\partial T}{\partial N}$. This HC equation is based on static fluid condition and becomes less accurate when the velocity very near to the wall is not zero, i.e. thermal convection takes larger effect near the wall when no-movement theory is not valid in turbulent flows with very high Reynolds' numbers.

6.2. Conclusions

In the current research study, fluid flow equations are solved numerically using SURF. A cell-vertex FVM is used in solving the 3D HC equation numerically by a FORTRAN based developed HC code. The use of FVM with cell-vertex scheme enhances the ability of HC to deal with unstructured meshes and solve problems of complex geometries. The use of FVM in HC code also allows a good integration of the CFD solution given by SURF.

In fluid side, Mesh refinement (near interface walls) is a vital issue in the currently developed CHT code. The HTC is based on the thermal conductivities of fluid and solid near their boundaries. The use of this strategy assumes no movement of fluid at the very near point to the wall. Unless a careful mesh refinement is made in the fluid side, the solution may diverge.

In the development of HC code, a previously proposed numerical solution to the heat transfer equation using Laplace's discretisation technique (Lyra et al. 2005) was initially implemented to solve the steady state HC equation. The tests on the initially proposed solution have proven failure to meet good agreement with the exact and other

commercial heat transfer solution (given by ANSYS) in 3D cases. This initial numerical solution was found to be of first order accuracy. It was therefore necessary to find a more accurate method for solving the HC equation.

A FVM was proposed using Gauss's theorem for solving the 3D HC equation in replacement with the initially implemented numerical solver, which is resulted in the development of an HC code. The tests over the HC code have proven high accuracy of the code in comparison to the available exact solution and other commercial numerical solver (ANSYS) for 1D, 2D and 3D HC cases.

The non-matching meshes at interface between two different (fluid/solid) domains were the main challenge in coupling the CFD and HC codes. The linear interpolation of mapped areas was tested in literature (Henshaw and Chand 2009) to overcome the problem with a straightforward implementation in the internally coupled codes (of SURF and HC). The tests on the proposed technique, of treating non-matching meshes, on 1D and 2D cases were found to be successful for investigating the capability of the coupled codes in developing and validating a CHT solver. Further tests were carried out on parallel and counter flow double-pipe HEs resulted in good agreements with the results given by another commercial CHT solver (ANSYS – CFX version 12.0), with errors of about 1% and 0.52%, respectively.

The CHT solver was tested on symmetrically heated two co-rotating discs with an axial inflow and radial outflow cavity. The typical case was chosen as a very common case in industry and because of the availability of the experimental results for validation. The results of the developed CHT solver were of good agreement with the experimental

results given by Northrop (1984) with minor errors of given explanation in the previous section (the discussion).

Finally, the main research objectives were achieved by the integration of the in-house CFD code (SURF) with the HC code. The HC code was examined with a grid independence check. Both codes, of HC and CHT (SURF-HC), were validated with different applications and various types of boundary conditions. The simulation, in comparisons to the available analytical solutions and other standard commercial numerical solvers, has proven the validation of the developed codes for a wide range of industrial applications.

BIBLIOGRAPHY

Abraham, J.P., Sparrow, E.M. and Tong, J.C.K. (2009) Heat Transfer in All Pipe Flow Regimes: Laminar, Transitional/Intermittent, and Turbulent. Int. J. H. & M. Trans. Vol. 52, 557–563.

Adams, J.C., Brainerd, W.S., Martin, J.T., Smith, B.T., Wagener, J.L. (1992) FORTRAN 90 Handbook: Complete ANSI/ ISO Reference. Mc-Graw Hill, NY, USA.

Albanakis, C. and Bouris, D. (2008) 3D Conjugate Heat Transfer with Thermal Radiation in a Hollow Cube Exposed to External Flow. Int. J. H. & M. Trans: Vol. 51, 6157–6168.

Al Qubeissi, M. (2012a) Proposing a Numerical Solution for the 3D Heat Conduction Equation. IEEE Proceedings of 6th Asia Int. Conf. Math./Analyt. Model. & Comp. Sim. (AMS2012).

Al Qubeissi, M. (2012b) Developing a Conjugate Heat Transfer Solver. Int. Conf. Fluid Mech., H.T. & Thermody. (ICFMHTT), Zurich, Switzerland.

Azimi, A., Hannani, S.K. and Farhanieh, B. (2008) Structured Multi-block Body-Fitted Grids Solution of Transient Inverse Heat Conduction Problems in an Arbitrary Geometry. J. Num H.T./ B, 54: 260–290.

Archambeau, F, Me'chitoua, N, Sakiz, M (2004) Code Saturne: A Finite Volume Code for the Computation of Turbulent Incompressible Flows-Industrial Applications. Int. J. on F.V./Feb: V1-1.

Asllanaj, F., Feldheim, V. and Lybaert, P. (2007) Solution of Radiative Heat Transfer in 2D Geometries by a Modified Finite-Volume Method based on a Cell Vertex Scheme using Unstructured Triangular Meshes. J. Num. H.T., B: Fundamentals, V 51, Issue 2, pages 97 – 119.

Barnett, A.R. and Balow, R.J. (1998) Computing for Scientists "Principles of Programming with FORTRAN 90 and C++". John Wiley and Sons Ltd, UK.

Bejan, A. and Kraus, A.D. (2003) Heat Transfer Handbook. John Wiley and Sons Ltd, New Jersey, USA.

Betchen, L., Straatman, A.G. and Thompson, B.E. (2006) A Non-Equilibrium Finite-Volume Model for Conjugate Fluid/ Porous/ Solid Domains. J. Num. H.T./ A: Vol. 49, 543–565.

Blažek, J. (2001) Computational Fluid Dynamics: Principles and Applications. Elsevier, ISBN: 008-0430090.

Brenner, C.B. and Scott, L.R. (2002) The Mathematical Theory of FEMs. Springer-Verlag, NY, USA.

Çengel, Y.A. and Turner, R.H. (2001) Fundamentals of Thermal-Fluid Sciences. McGraw-Hill (ISBN 0-07-239054-9), NY, USA.

Chapman, A.J. (1974) Heat Transfer. Collier Macmillan Publishing, London, UK.

Chénier, E., Eymard, R. & Herbin, R. (2009) A Collocated FV Scheme to Solve Free Convection for General Non-Conforming Grids. J. Comp. Phys.: 228, 2296–2311.

Chivers, I. and Sleightholme, J. (2000) Introducing Fortran 95. Springer-Verlag London Ltd., UK.

Comini, G., Nonino, C. and Savino, S. (2007) Modeling of Coupled Conduction and Convection in Moist Air Cooling. j/ Num. H.T., A: Applications, Vol. 51: 1,23-37.

Counihan, M. (1996) Fortran 95. UCL Press, UK.

Chung, T.J. (2002) Computational Fluid Dynamics. Cambridge Univ. Press, UK.

Daily, J.W and Nece, R.E. (1960) Chamber Dimension Effects on Induced Flow and Frictional Resistance of Enclosed Rotating Disks. J. Basic Eng., 82, 217-232.

Dalal, A, Eswaran, V. and Biswas, G. (2008) A Finite-Volume Method for Navier-Stokes Equations on Unstructured Meshes. J. Num. H.T., B, 54: 238–259.

De Boer, A., van Zuijlen, A.H., Bijl, H. (2008) Comparison of Conservative and Consistent Approaches for the Coupling of Non-Matching Meshes. Comp. Meth. Appl. Mech. Eng.: 197, 4284–4297.

Demko, J. A., and Chow, L. C. (1984) Heat Transfer Between Counter Flowing Fluids Separated by a Heat-Conducting Plate. AIAA J., 22(5), pp. 705–712.

Dettmer, W. G. and Perić, D. (2007) A Fully Implicit Computational Strategy for Strongly Coupled Fluid–Solid Interaction. Arch Comp. Meth Eng, Vol. 14, 3: 205-247.

Dorfman, L.A. (1963) Hydrodynamic Resistance and the Heat Loss of Rotating Solids. Oliver and Boyd, Edinburgh. Translated to English by Kemmer, N.

Ekman, V. W. (1905) On the influence of the Earth's rotation on ocean currents. Arch. Math. Astron. Phys., 2, 1-52.

Fletcher, C.A.J. (2000) Computational Techniques of Fluid Dynamics, Vol. 1: Fundamental of General Techniques. Springer-Verlag, NY, USA.

Fletcher, C.A.J. (2003) Computational Techniques of Fluid Dynamics, Vol. 2: Specific Techniques for Different Flow Categories. Springer-Verlag, NY, USA.

Frink, N.T. and Pirzadeh, S.Z. (1999) Tetrahedral Finite-Volume Solutions to the Navier–Stokes Equations on Complex Configurations. Int. J. Num. Meth. in F. 31: 175–187.

Gajic, Z. and Xuemin, S. (1993) Parallel Algorithms for Optional Control of Large Scale Linear Systems. Springer-Verlag, NY, USA.

Giles, M.B. (1997) Stability Analysis of Numerical Interface Conditions in Fluid-Structure Thermal Analysis. Int. J. Num. Meth. in Fluids: Vol. 25, 4/ 421-436.

George, P.L. (1991) Automatic Mesh Generation: Application to Finite Element Methods. John Wiley & Sons, Masson, France.

Hada, S., Tsukagoshi, K., Masada, J., Ito, E. (2012) Test Results of the World's First 1,600oC J-series Gas Turbine. Mitsubishi Heavy Industries Technical Review, 49, 1.

Ham, F., Mattsson, K. and Iaccarino, G. (2006) Accurate and Stable Finite Volume Operators for Unstructured Flow Solvers. Annual research briefs, Centre for Turbulence Research, Stanford University, CA.

Hatton, L. (1997) The T Experiments: Errors in Scientific Software. IEEE Comp. Sc. & Eng., Vol. 4, No. 2, 27-38.

He, L. and Oldfield, M.L.G. (2010) Unsteady Conjugate Heat Transfer Modeling. J. Turbomachinery: Vol. 133 / 031022-1.

Henshaw, W.D. and Chand, K.K. (2009) A Composite Grid Solver for Conjugate Heat Transfer in Fluid-Structure Systems. J. Com. Phys. 228-10 (3708-3741).

Hirsch, C. (1988) Numerical Computation of Internal and External Flows, Vol. 1: Fundamentals of Numerical Discretisation. John Wiley & Sons Ltd., UK.

Hoffmann, K.A., Chiang, S.T. (2000a) Computational Fluid Dynamics, Vol. 1. Engineering Education System, Kansas - USA.

Hoffmann, K.A., Chiang, S.T. (2000b) Computational Fluid Dynamics, Vol. 2. Engineering Education System, Kansas - USA.

Illingworth, J.B. (2006) Fluid-Solid Heat Transfer Coupling. DPhil thesis, School of Engineering, University of Sussex.

Incropera, F. P. and DeWitt, D. P. (1996) Introduction to Heat Transfer (3rd Ed.). John Wiley & Sons, ISBN: 0-471-30458-1.

Incropera, F. P. and DeWitt, D. P. (2002) Fundamentals of Heat and Mass Transfer (5th ed.). John Wiley, ISBN 0-471-38650-2.

Indinger, T. and Shevchuk, I.V. (2004) Transient Laminar Conjugate Heat Transfer of a Rotating Disk: Theory and Numerical Simulations. J. H. & M. Trans. Vol. 47, 3577-3581.

Karlekar, B.V. and Desmond, R.M. (1982) Heat Transfer. 2nd Ed., Wes Publishing Co.

Kármán, Th. Von (1921) Über laminare und turbulente Reibung. Zeitschrift für Angewandte Math. und Mech. 1/ 4, 233–252. Article re-published online: 17/11/2010. DOI: 10.1002/zamm.19210010401.

Kay, J.M. and Nedderman, R.M. (1979) An Introduction to Fluid Mechanics and Heat Transfer. 3rd Ed., Univ. Press, ISBN 0521205336.

Kassab, A., Divo, E., Heidmann, J., Steinthorsson, E., Rodriguez, F. (2003) BEM/FVM Conjugate Heat Transfer Analysis of a Three-Dimensional Fill Cooled Turbine Blade. Int. J. Num. Meth. For H. & F. flow. 13, 5/6.

Kelleher, M.D. and Yang, K-T. (1967) A Steady Conjugate Heat Transfer problem with Conduction and Free-Convection. Arch. of Com. Meths in Eng. Vol. 17, 4-5: 249-269.

Kim, H-G (2003) Interface element method: Treatment of non-matching nodes at the ends of interfaces between partitioned domains. Comt. Meths Appl. Mech. Eng.: 192, 1841–1858.

Kuznetsov, G.V. and Sheremet, M.A. (2006) Conjugate Heat Transfer in a Closed Domain with a locally Lumped Heat-Release Source: Free Convective Heat Exchange. J. Eng. Phys. and Therm-phys. Vol. 79, No. 1.

Leszczynski, J. and Pluta, S. (2002) The Efficient Generation of Un-Structured Control Volumes in 2-D and 3-D. Lecture Notes in Comp Sc. (LNCS), Springer-Verlag, 2328, pp. 682-689. http://arxiv.org: Accessed online on: July 21st 2009.

Lewis, R.W., Nithiarasu, P. and Seetharamu, K.N. (2004) Fundamentals of the Finite Element Method for Heat Transfer and Fluid Flow. John Wiley & Sons Ltd., UK.

Li, Y. and Kong, S.Ch. (2011) Coupling Conjugate Heat Transfer with in-Cylinder Combustion modelling for engine simulation. Int. J. H. & Mass Trans.

Long, C. (1999) Essential Heat Transfer. Pearson Education Ltd., UK.

Luo, J. and Razinsky, E.H. (2007) Conjugate Heat Transfer Analysis of a Cooled Turbine Vane Using the V2F Turbulence Model. J. Turbomach. Vol. 129/ 773-781.

Lyra, P. R. M. , de Lima, R. de C. F., de Carvalho, D. K. E. and da Silva, G. M. L. L. (2005) An Axisymmetric Finite Volume Formulation for the Solution of Heat Conduction Problems Using Unstructured Meshes. J. Braz. Soc. Mech. Sci. & Eng. vol.27 no.4 Oct/Dec. Rio de Janeiro – Brazil.

Mathews, R.N., Balaji, C. and Sundararajan, T. (2007) Computation of Conjugate Heat Transfer in the Turbulent Mixed Convection Regime in a Vertical Channel with Multiple Heat Sources. J. H.&M. Trans. Vol. 43,1063-1074.

Montenay, A., Pate, L. and Duboue, J. (2002) Conjugate Heat TransferAnalysis of an Engine Internal Cavity. ASME 2000-GT-282.

Northrop, A. (1984) Heat transfer in a cylindrical rotating cavity. DPhil thesis, Thermo-Fluid Mechanics research centre, University of Sussex.

Nouanegue, H., Muftuoglu, A., and Bilgen, E. (2008) Conjugate heat transfer by natural convection, conduction and radiation in open cavities. Int. J. H.&M. Trans. Vol. 51, July 2008, 6054 – 6062.

Nowak G. and Wróblewski W. (2011) Optimization of blade cooling system with use of conjugate heat transfer approach. Int. J. Therm. Scs. 50, 1770e1781.

Owen, J.M. (1971) The Reynlods Analogy Applied to Flow between a Rotating and a Stationary Disk. Int. H. & M. Trans. 14, 451.

Owen, J.M. and Rogers, R.H. (1989) Flow and Heat Transfer in Rotating-Disc Systems, Vol.1: Rotor-Stator Systems. Research Studies Press Ltd., UK.

Owen, J.M. and Rogers, R.H. (1995) Flow and Heat Transfer in Rotating-Disc Systems, Vol.2: Rotating Cavities. Research Studies Press Ltd., UK.

Ozisik, N. M. (1993) Heat Conduction. 2nd Ed. John Wiley and Sons, USA.

Patounas, D.S. (2007) Disc Heat Transfer in Gas Turbine H.P. Compressor Internal Air System. DPhil Thesis, Eng. Dept., Univ. Sussex.

Press, W.H., Flannery, B.P., Teukolsky, S.A. and Vetteling, W.T. (1990) Numerical Recipes: The Art of Scientific Computing (FORTRAN version). Cambridge University Press, UK.

Rahman, M.M., Lallave, J.C. and Kumar, A. (2008) Heat Transfer from a Spinning Disk during Semi-confined Axial Impingement from a Rotating Nozzle. Int. J. H. & M. Trans. Vol. 51, May 2008, 4400 – 4414.

Ranjan, R., Dalal, A., Biswas, G. (2008) A Numerical Study of Fluid Flow and Heat Transfer around a Square Cylinder at Incidence using Unstructured Grids. J. Num. H.T., A: Applications: Vol. 54: 9,890 - 913.

Rao, S. S. (1982) The Finite Element Method in Engineering. Pergamon Press Ltd., UK.

Rolls-Royce (2005) The Jet Engine. A document issued by Rolls-Royce plc, England. www.rolls-royce.com 1st May 2008.

Sayma, A.I., Vahdati, M., Sbardella, L. and Imregun, M. (2000) Modelling of Three-Dimensional Viscous Compressible Turbomachinery Flows Using Unstructured Hybrid Grids. J. AIAA, Vol. 38: 6.

Schlichting, H. and Gresten, K. (2000) Boundary Layer Theory, 8th Ed. Springer-Verlaf Berlin, ISBN 3-540-66270-7.

Shih, T.M. (1984) Numerical Heat Transfer. Hemisphere Publishing Corporation, USA.

Smith, G.D. (1978) Numerical Solution of Partial Differential Equations: Finite Difference Methods. Oxford university press, UK.

Spalart P. and Allmaras S. (1992) A one-equation turbulence model for aerodynamic flows. In 30th AIAA Aerospace Sciences Meeting, Reno, USA, AIAA 92-0439.

Toni, E. (2001) A Direct Discrete Formulation of Field Laws: The Cell Method. Computer Modelling in Engineering & Sciences (CMES), Vol. 2, No. 2, pp. 237-258.

Turner, I.W. and Ferguson, W.J. (1995) An unstructured mesh cell-centered control volume method for simulating heat and mass transfer in porous media: Application to softwood drying, part I: The isotropic model. J. App. Math. Mod. Vol. 19, Issue 11, November 1995, Pages 654-66.

Verdicchio, J.A. (2001) The validation and Coupling of Computational Fluid Dynamics and Finite Element Codes for Solving "Industrial Problems". DPhil thesis, School of Engineering, University of Sussex.

Versteeg, H.K. and Malalasekera, W. (1995) An Introduction to Computational Fluid Dynamics (The Finite Volume Method). Longman group Ltd, England.

Vujicic, M.R. (2006) Finite Element Solution of Transient Heat Conduction using Iterative Solvers. Material Research Centre, University of Swansea, UK.

Wegian, F.M., Yazdi, S.R. (2008) Symmetric Boundary Condition Technique in NASIR Galerkin Finite Volume Solver for 3D Temperature Field. J. Jordan Civil Eng. Vol. 2, 4.

White, F. M. (1984) Heat Transfer. Addison-Wesley Pub. Co.

Xia, G.H. , Zhao, Y. , Yeo, J.H. and Lv, X. (2007) A 3D Implicit Unstructured-Grid Finite Volume Method for Structural Dynamics. J. Com. Mech. 40:299–312.

Zhang, H. J., Zou, Z. P., Li, Y. and Ye, J. (2011) Preconditioned Density-Based Algorithm for Conjugate Porous/Fluid/Solid Domains. J. Num. H.T. (A), Applications: 60:2, 129-153.

APPENDICES (A TO H)

APPENDIX (A)

A.1. Gauss's Theorem

In Gauss's (the divergence) theorem of integration, derivatives in a control volume can be integrated (Hirsch 1988) as:

$$\iiint_{V} \nabla f \, dV = \oiint_{\partial V} f \, d\vec{S} \qquad (A.1)$$

Where,

$$\vec{\nabla} f = \left(\frac{\partial f}{\partial x}, \frac{\partial f}{\partial y}, \frac{\partial f}{\partial z}\right) \qquad (A.2)$$

A.2. Linear Interpolation

For: $G = inerpolation\ value\ of\ points\ (f)$,

$$G = \frac{\sum_{i=1}^{N} \frac{f_i}{l_i}}{\sum_{i=1}^{N} \frac{1}{l_i}} \qquad (A.3)$$

Where, i is the index of points, l is absolute distance between these points, f the known variables at each neighbour point and N is the number of points within mapped area. For example, when the interpolation is among three points, as shown in Figure A.1:

$$G = \frac{\left(\frac{f_1}{l_1} + \frac{f_2}{l_2} + \frac{f_3}{l_3}\right)}{\left(\frac{1}{l_1} + \frac{1}{l_2} + \frac{1}{l_3}\right)} \qquad (A.4)$$

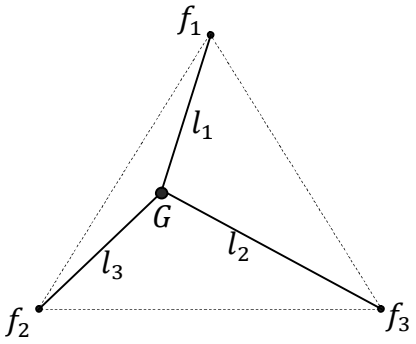

Figure A.1: An illustrative example of three points' linear interpolation

A.3. Holes Conversion to Groove

The 32 holes in the shroud, in the co-rotating discs, are converted to a one grove circumferential opening. The holes are assumed of the same size and the simple mathematical calculation is shown below.

$$A_g = 32\, A_h \tag{A5}$$

Where, A_g is the circumferential exit area and A_h is the round hole area. These can be described in the following relations:

$$A_h = \pi\, r^2 \tag{A6}$$

$$A_c = \pi D\, x \tag{A7}$$

Where, r is the radius of each hole, D is the cavity diameter and x is the width of the groove, as shown in Figure A.2. These lead to:

$$x = \frac{r^2}{D} \tag{A8}$$

The diagram of Figure A.3 further illustrates this operation.

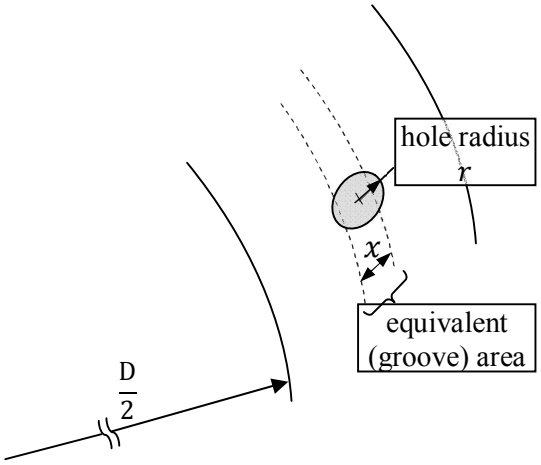

Figure A.2: Sketch of holes equivalent area in approximate dimensional scale

APPENDIX (B)

HEAT CONDUCTION RESULTS

B.1. 1D Test Case

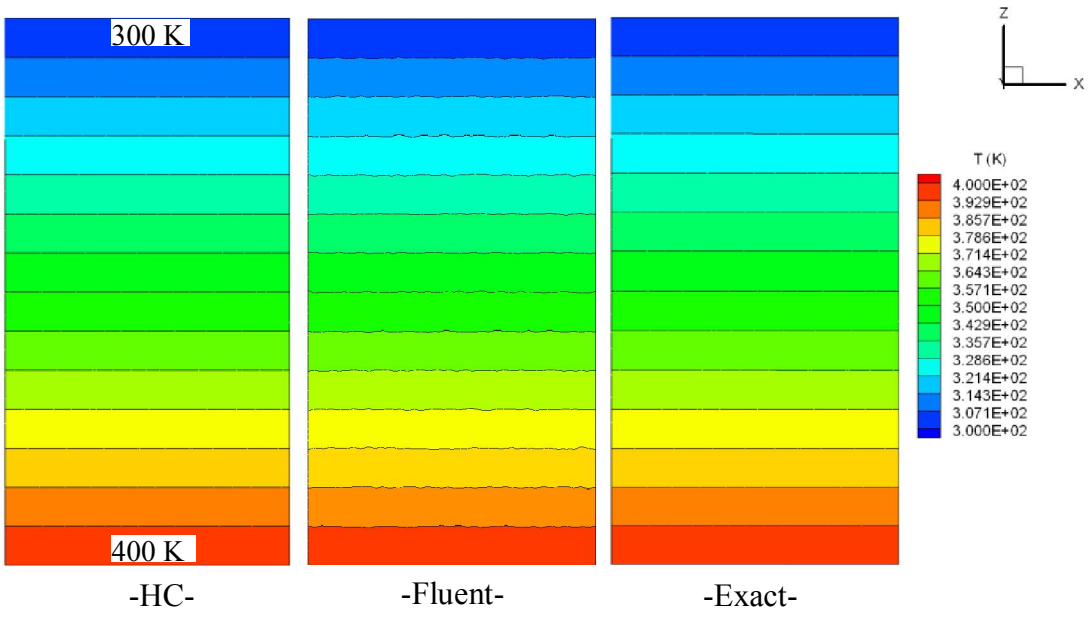

Figure B.1: 1D Temperature contours, at plane x=0.25 m, for HC vs. Fluent (ANSYS 12.0) & Analytical solutions

B.2. 2D Test Case

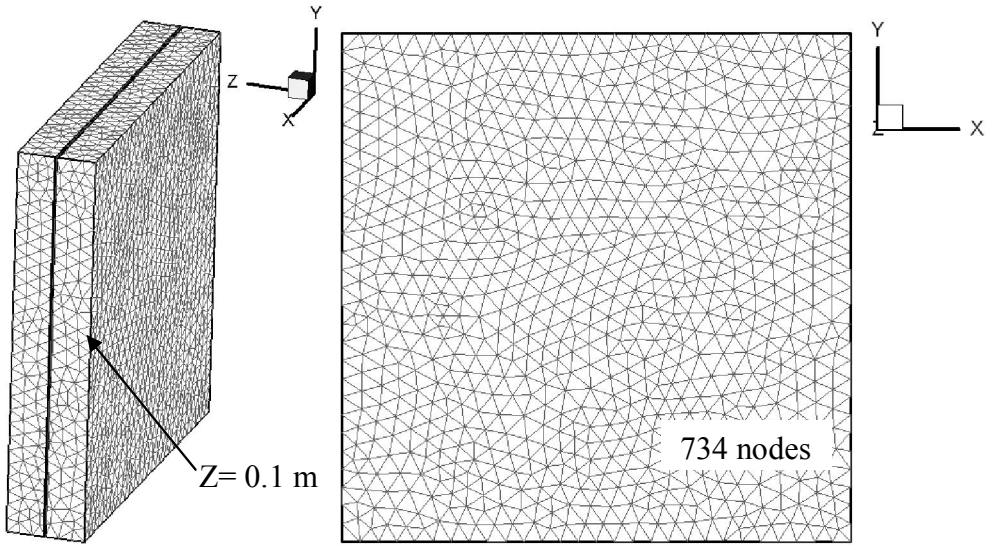

Figure B.2: 3D and 2D (at z=0.1) views of the tetrahedral mesh used for solving the 2D case

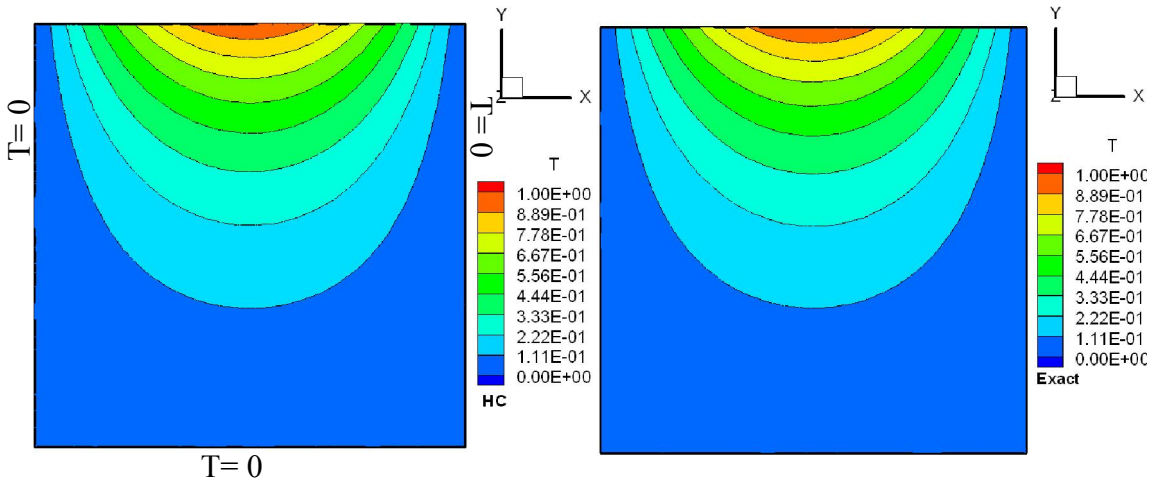

Figure B.3: 2D temperature profile at the section z=0.1 for a HC with a mesh density (at section z=0.1) of nodes in a comparison with the analytical solution

B.3. 3D Test Case

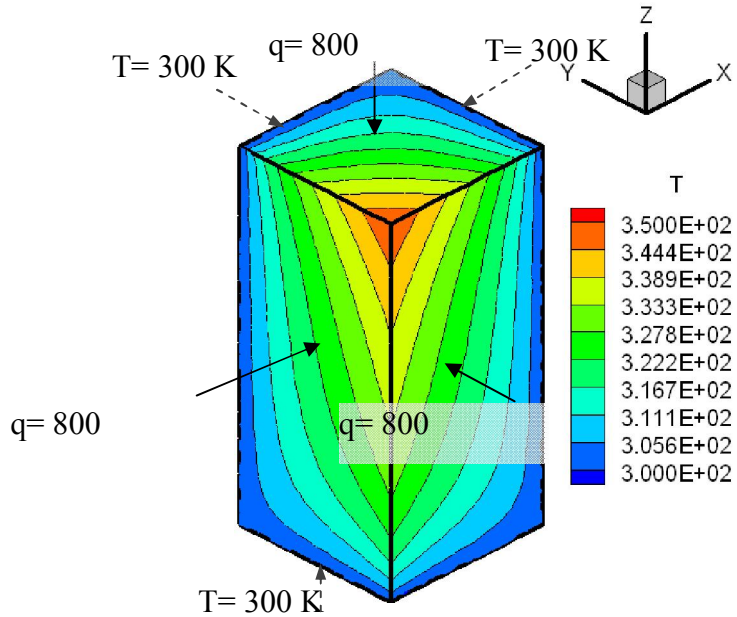

Figure B.4: 3D colour bands of HC temperature profile for a mesh of nodes

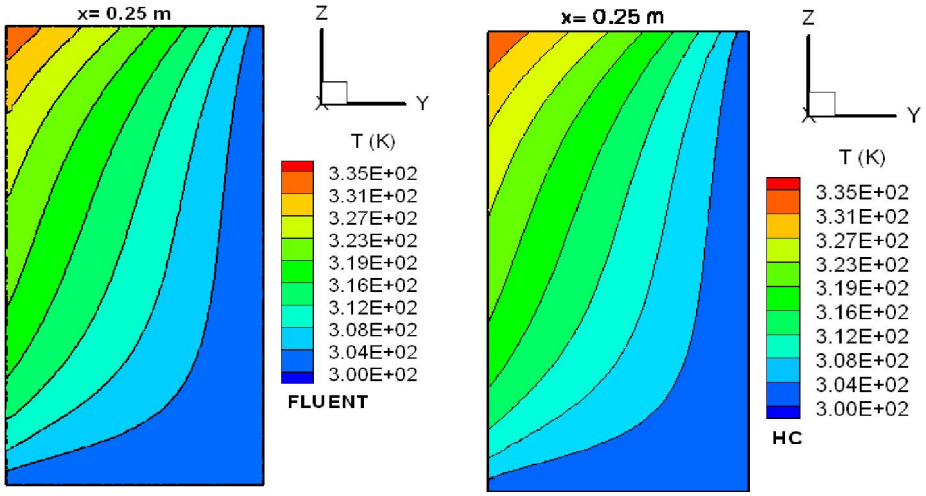

Figure B.5: HC and FLUENT (ANSYS 12.0) colour bands of temperature profile at section x=0.25

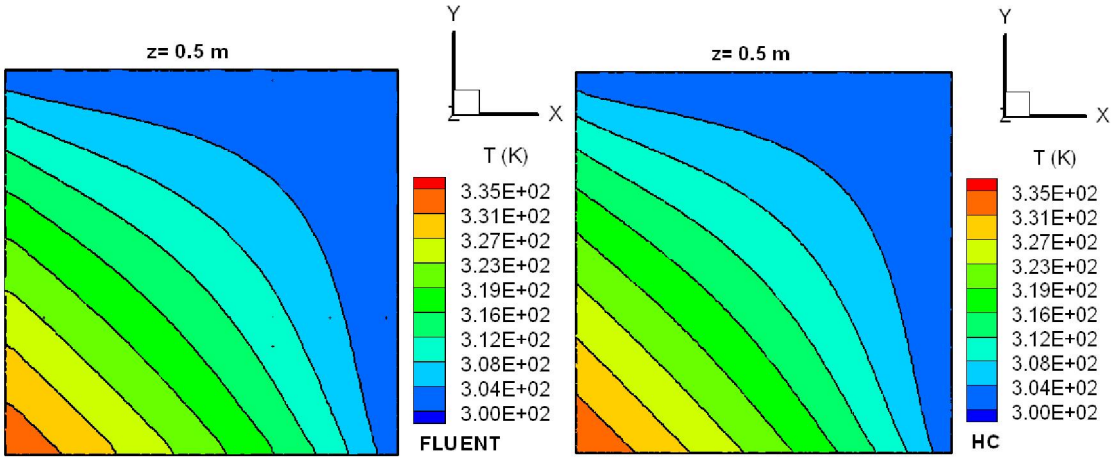

Figure B.6: HC and FLUENT (ANSYS 12.0) colour bands of temperature profile at section z=0.5

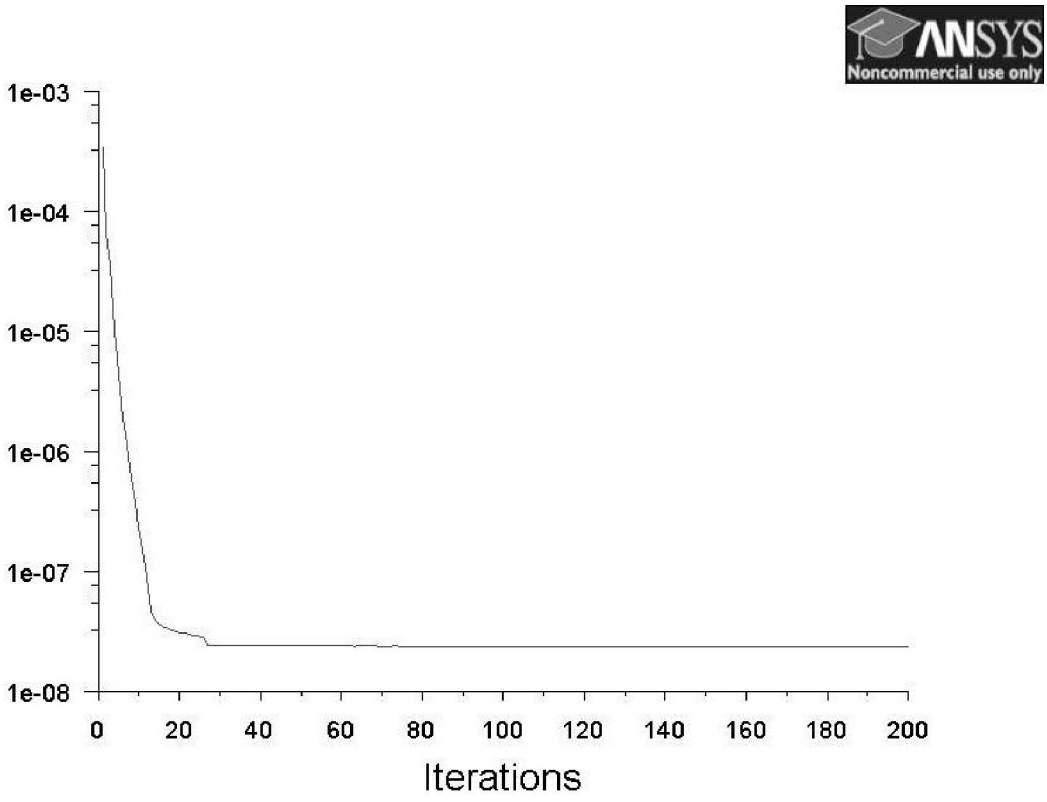

Figure B.7: Fluent residual history for the 3D case, with 91,000 nodes

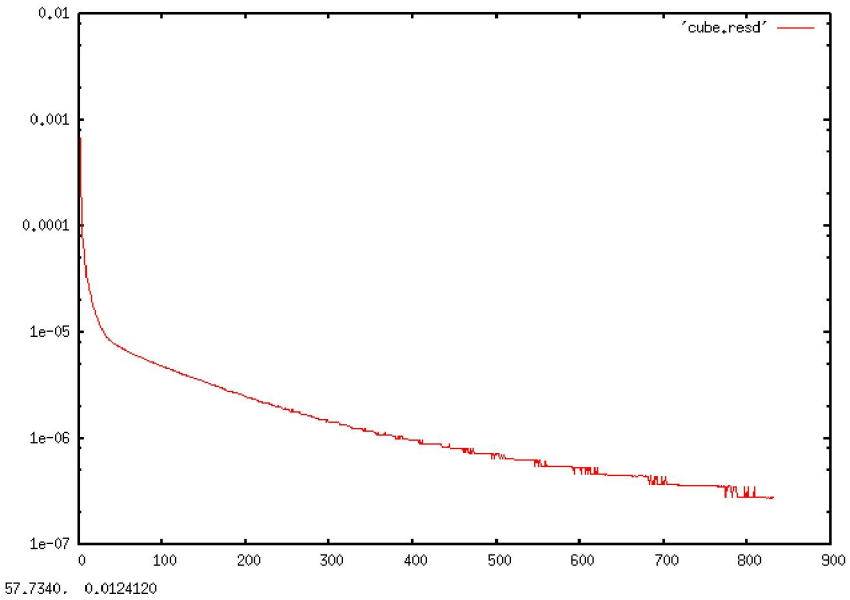

Figure B.8: HC residual history for the 3D case, with 91,000 nodes

B.3.1. Pipe (3D case)

In Figure B.9 (A and B) below, the outer and inner surfaces are insulated while one end is fixed at 1000 $^{\circ}$C and the other one at 0°C. The temperature gradients of both solvers are visually consistent.

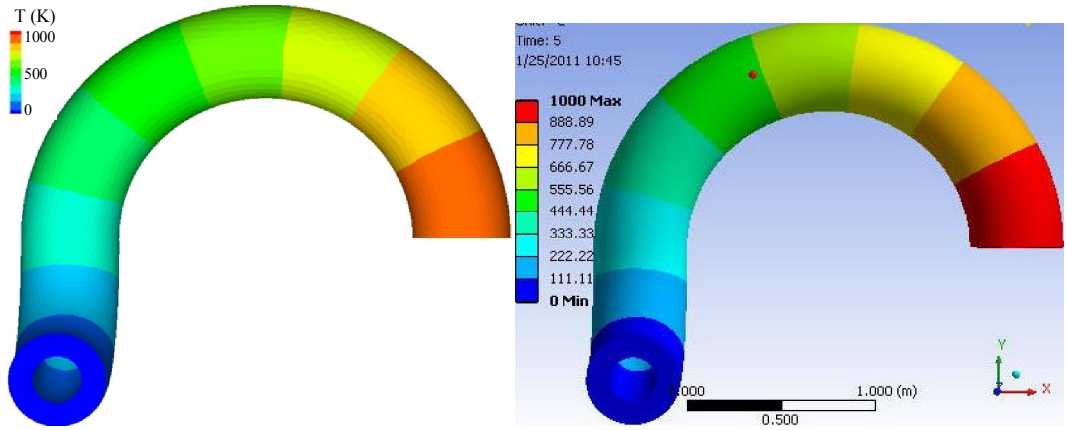

-A- **-B-**

Figure B.9: A comparison between ANSYS and HC code in temperature profile, (A) HC solver (B) ANSYS (12.0) solver, residuals $= 1^{-8}$ at ~1000 iterates

APPENDIX (C)

VALIDATION CASES OF THE FIRST ORDER ACCURATE SOLUTION (Not part of the CHT couple)

C.1. 1D Test Case

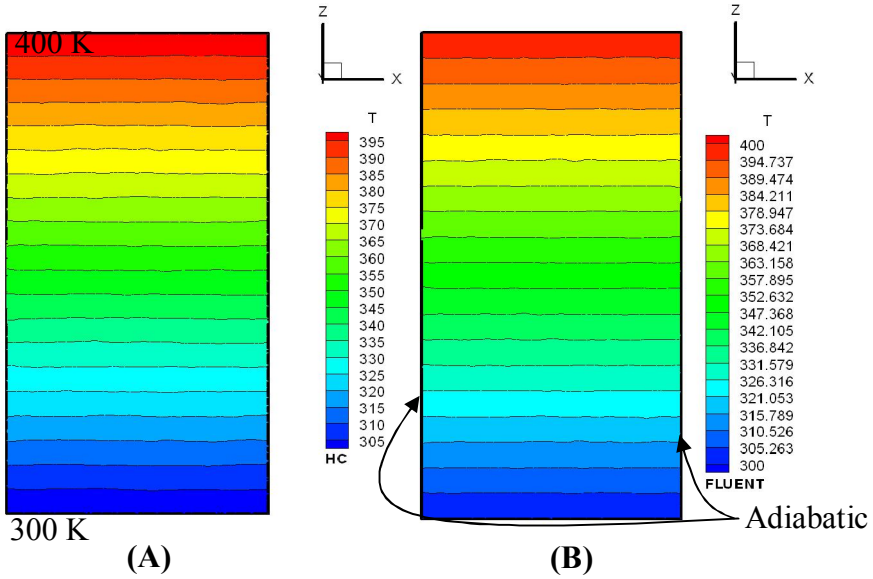

Figure C.1: colour bands of 1D temperature distribution as given by (A) HC and (B) FLUENT (ANSYS 12.0)

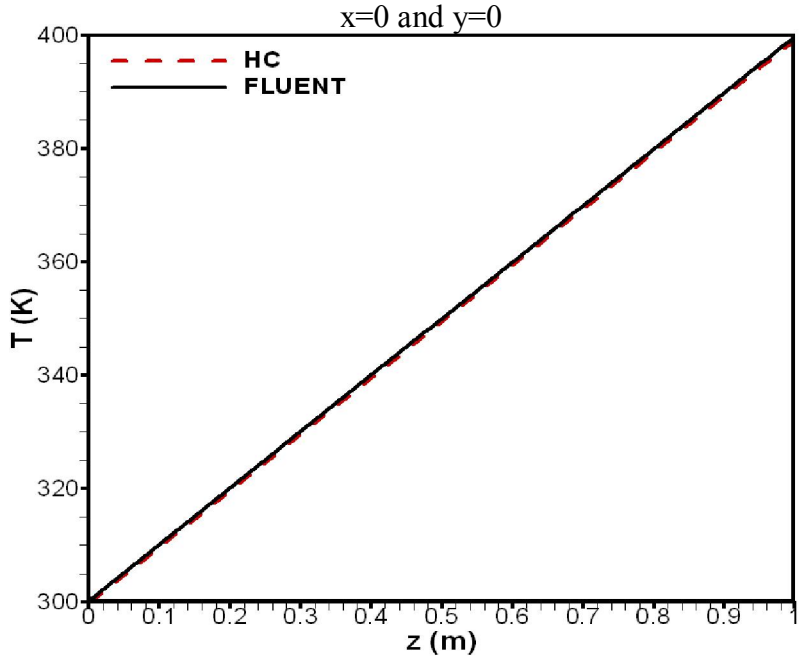

Figure C.2: Temperature distribution along z-direction at x=0 and y=0 of 1D case for HC vs. FLUENT (ANSYS 12.0)

C.2. 2D Test Case

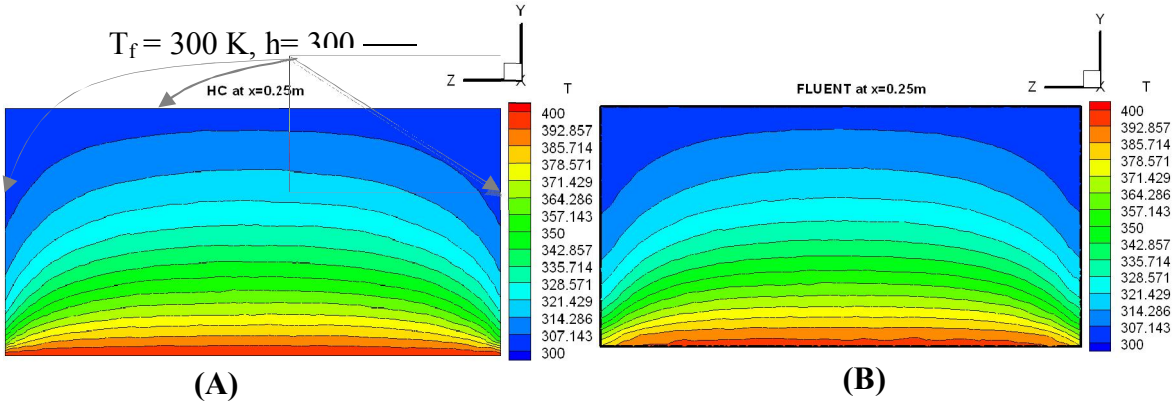

Figure C.3: Temperature colour bands in yz-plane at x=0.25m (A) HC and (B) Fluent

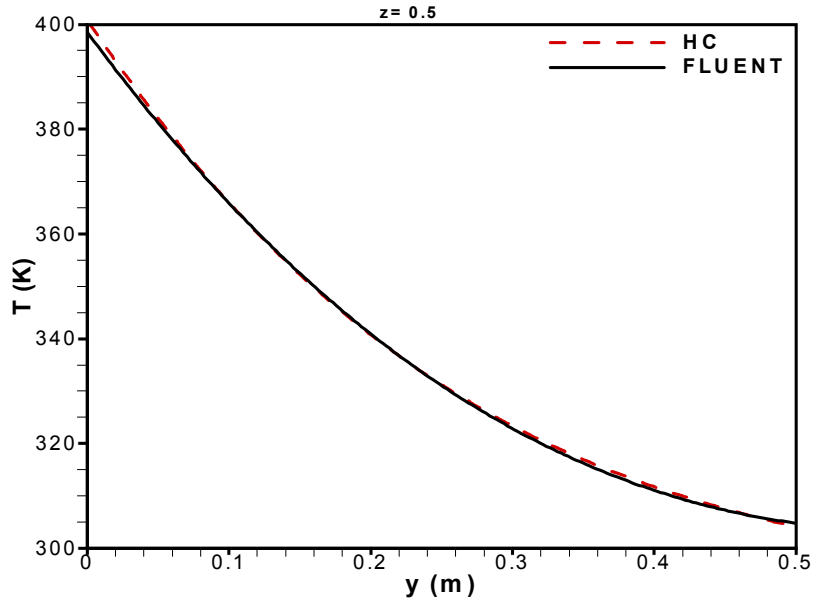

Figure C.4: HC vs. FLUENT temperature in y-direction at x = 0.25 & z=0.5m

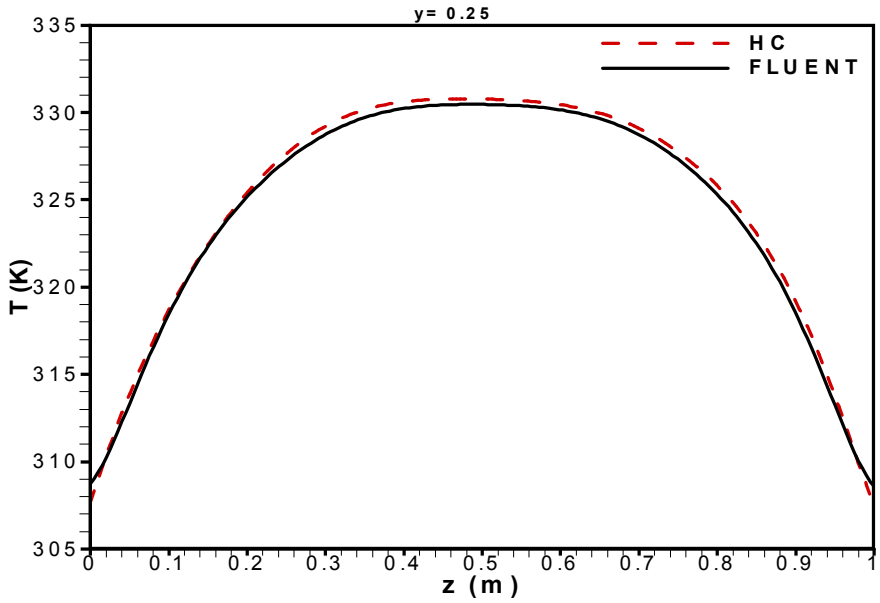

Figure C.5: HC vs. FLUENT (ANSYS 12.0) temperature distribution in z-direction at x=0.25 & y=0.25.

C.3. 3D Test Case

In 3D, 2 types of boundary conditions are applied on the six faces. The three faces sharing one corner are exposed to heat flux of 800 $\frac{W}{m^2}$. The opposite corner faces are fixed with temperature of 300 K, as shown in Figure C.6. The problem is physically applicable. Temperature contours of HC and Fluent in yz, xz and xy planes are shown in Figures C.7 throughout C.9, respectively; whereas Figures C.10 to C.12 show the temperature profiles in three directions.

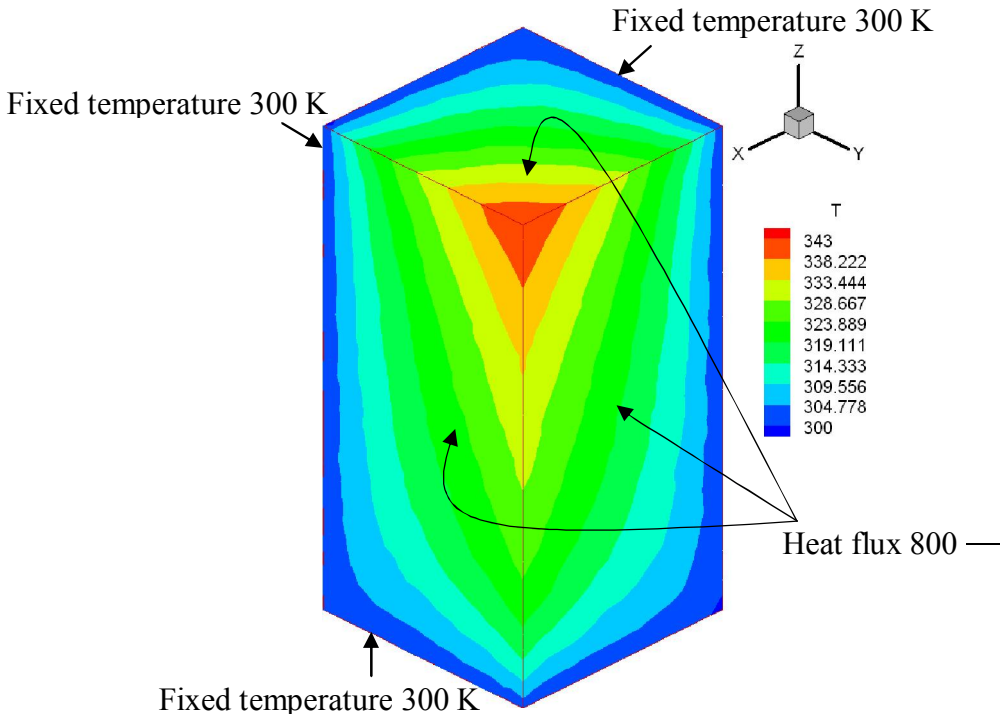

Figure C.6: Temperature colour bands in a 3D geometry with boundary conditions given by 1st order HC solver

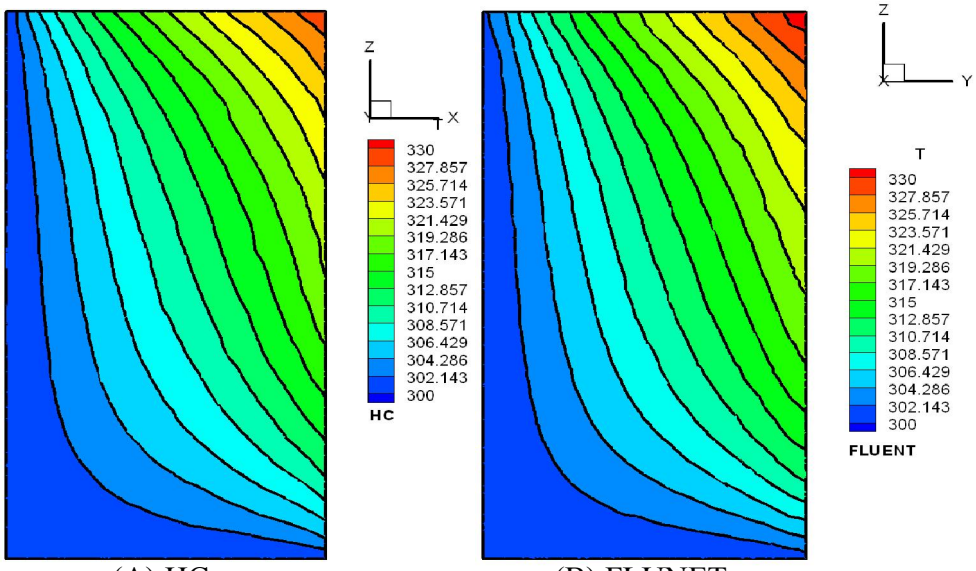

(A) HC (B) FLUNET

Figure C.7: Temperature profile in the yz-plane at section x= 0.25 m given by (A) 1st order HC and (B) 1st order FLUENT (ANSYS 12.0)

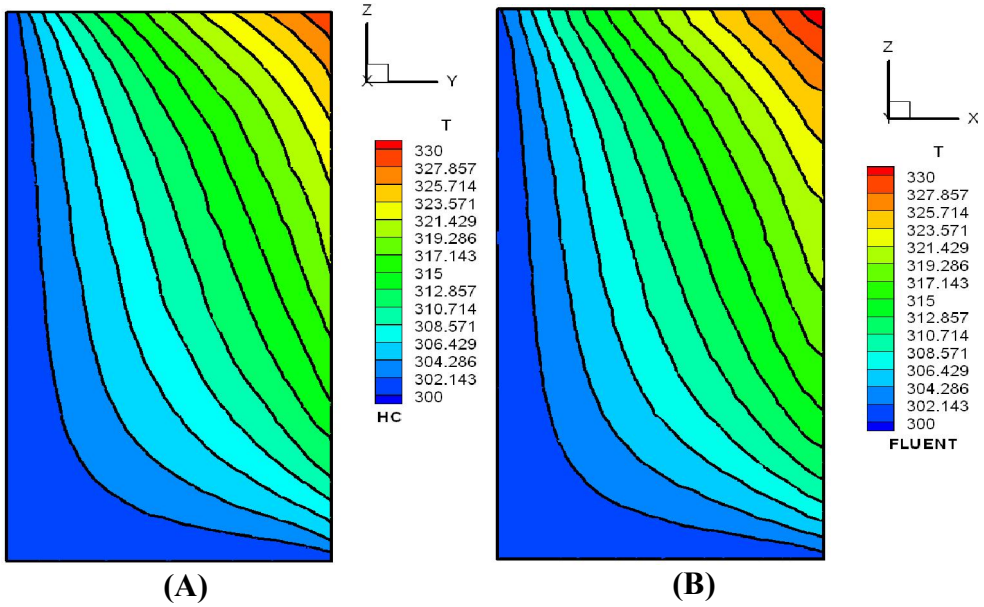

Figure C.8: Temperature profile in the xz-plane at section y= 0.25 m given by (A) 1st order HC and (B) 1st order FLUENT (ANSYS 12.0)

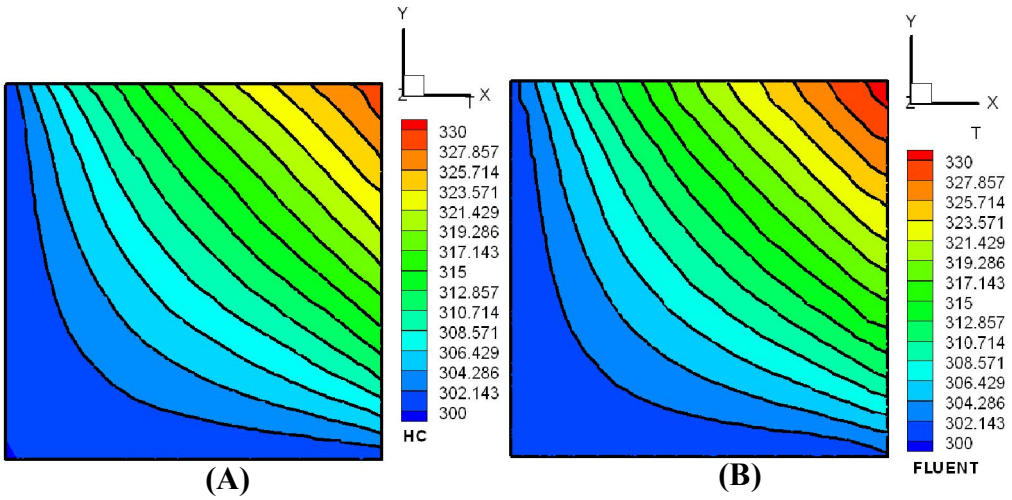

Figure C.9: Temperature profile in the xy-plane at section z= 0.5 m given by (A) 1st order HC and 1st order FLUENT (ANSYS 12.0)

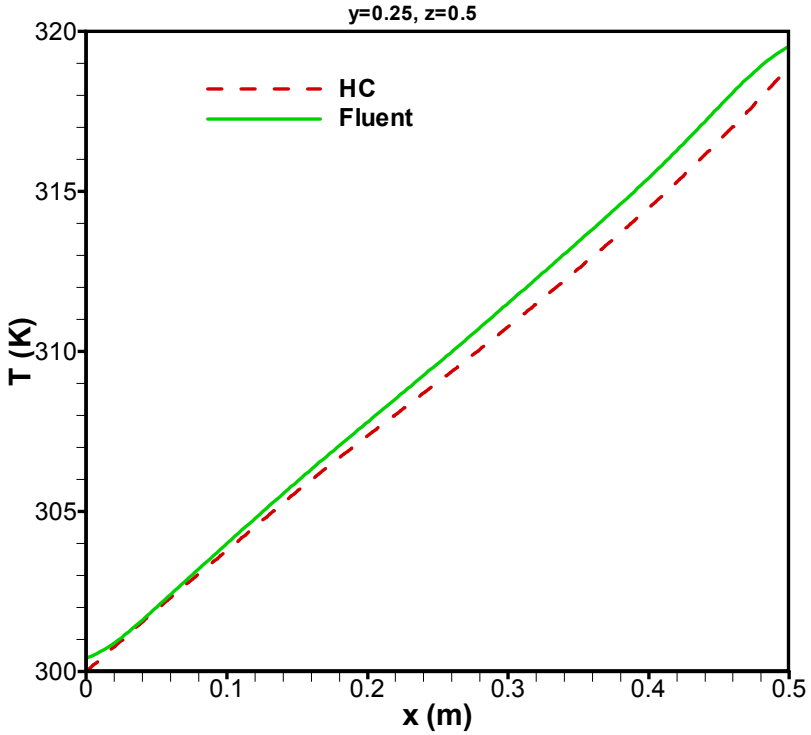

Figure C.10: 1st order solutions of HC vs. FLUENT temperature distributions in x-direction at v=0.25 m & z=0.5 m.

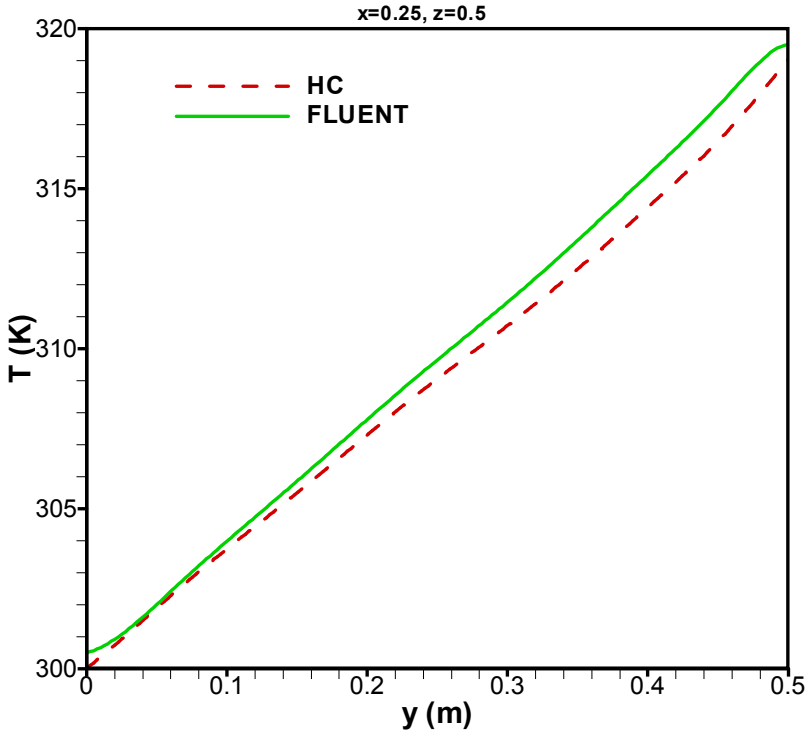

Figure C.11: 1st order solutions of HC vs. FLUENT temperature distributions in y-direction at x=0.25 m & z=0.5 m.

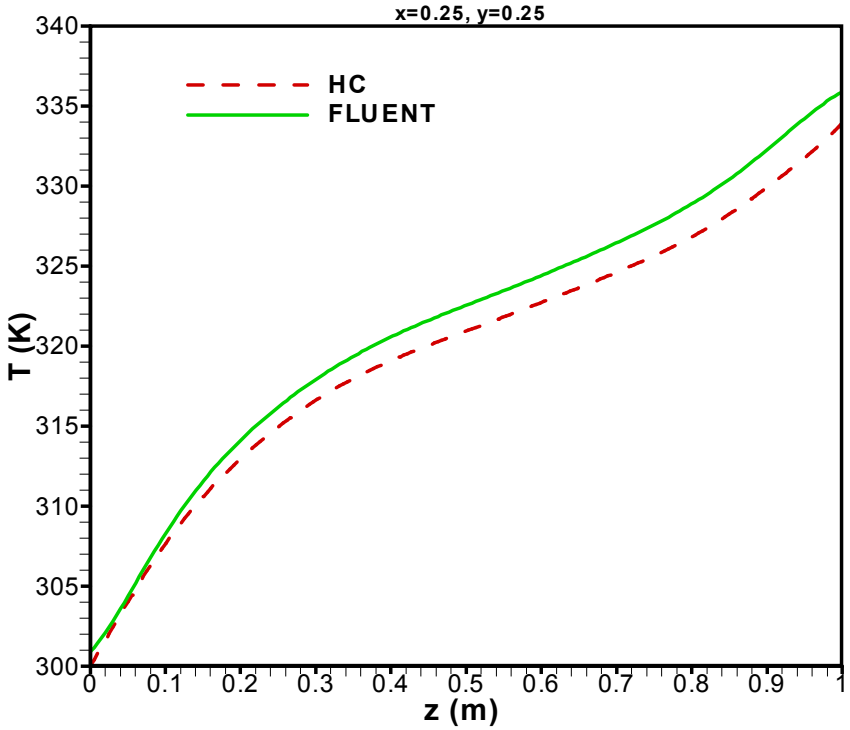

Figure C.12: HC vs. FLUENT Temp. distributions in z-direction at x=0.25 m & y=0.25 m

APPENDIX (D)

CHT COUPLING RESULTS

D.1. 1D & 2D CHT Test Cases

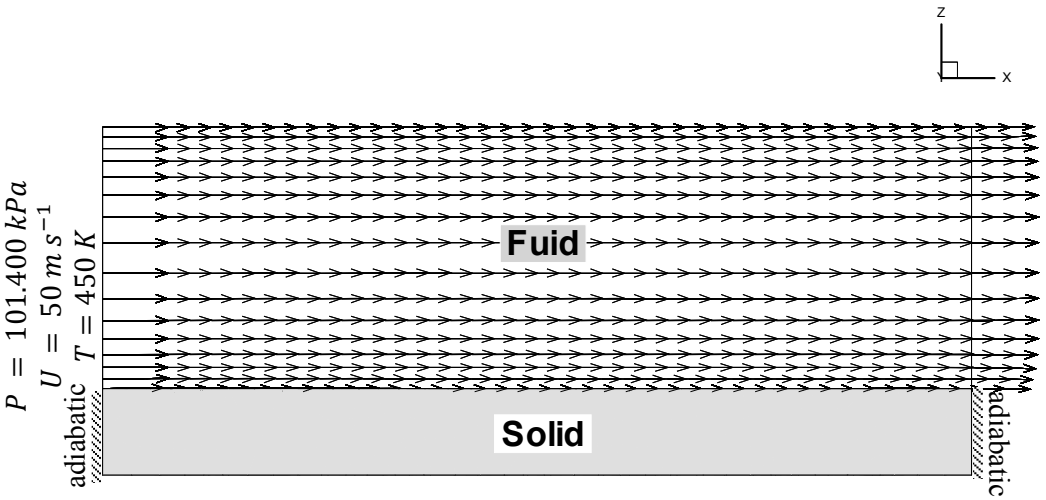

Figure D.1: Case specifications of the 1D conjugate heat transfer problem

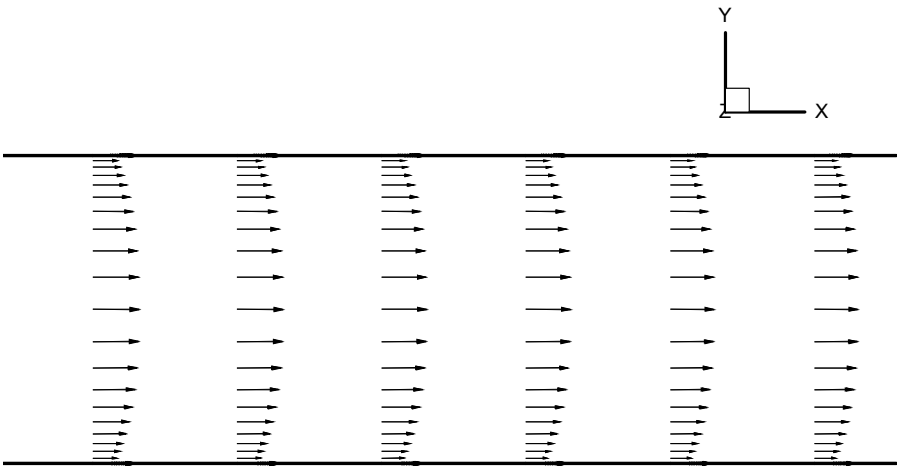

Figure D.2: Velocity vectors in the fully developed flow region of the 1D CHT problem

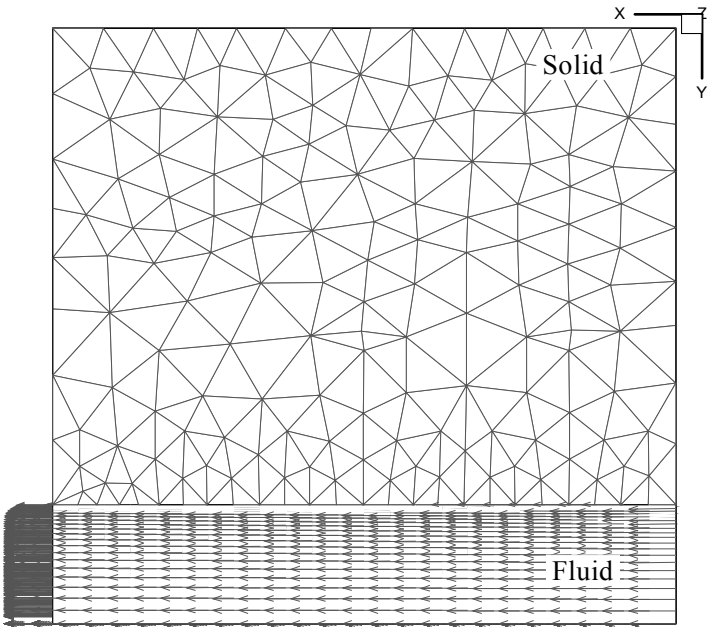

Figure D.3: Front view of the 2D case conjugate system showing the velocity vectors of the fluid flow and the coarse mesh of the solid domain

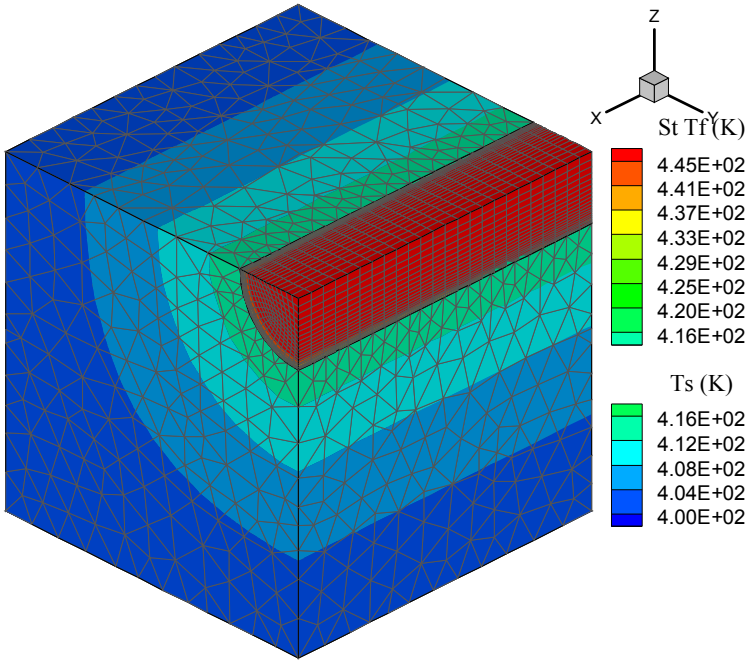

Figure D.4: 3D view of the 2D case conjugate system showing the meshes and the colour bands of temperature in both domains

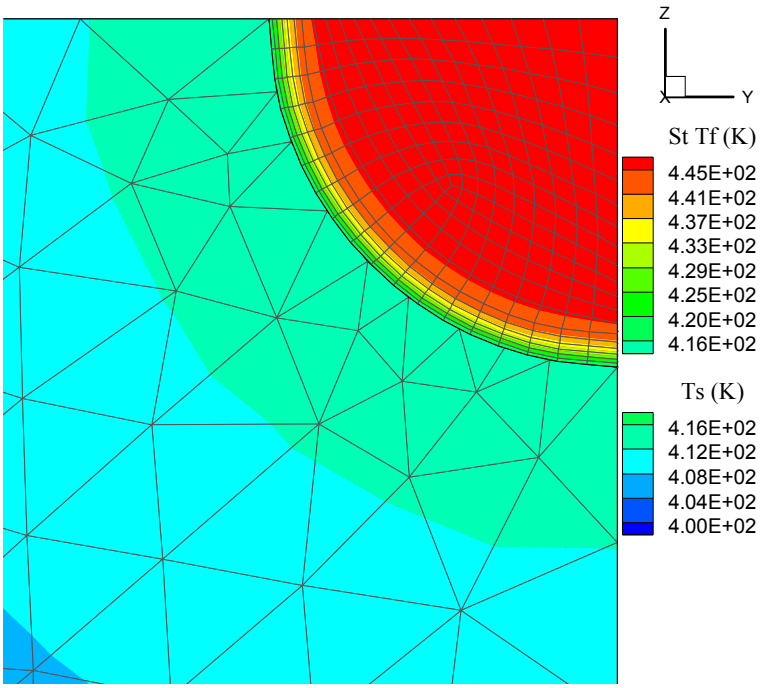

Figure D.5: Side (y-z) view of the 2D case conjugate system showing the meshes and the colour bands of temperature in both domains

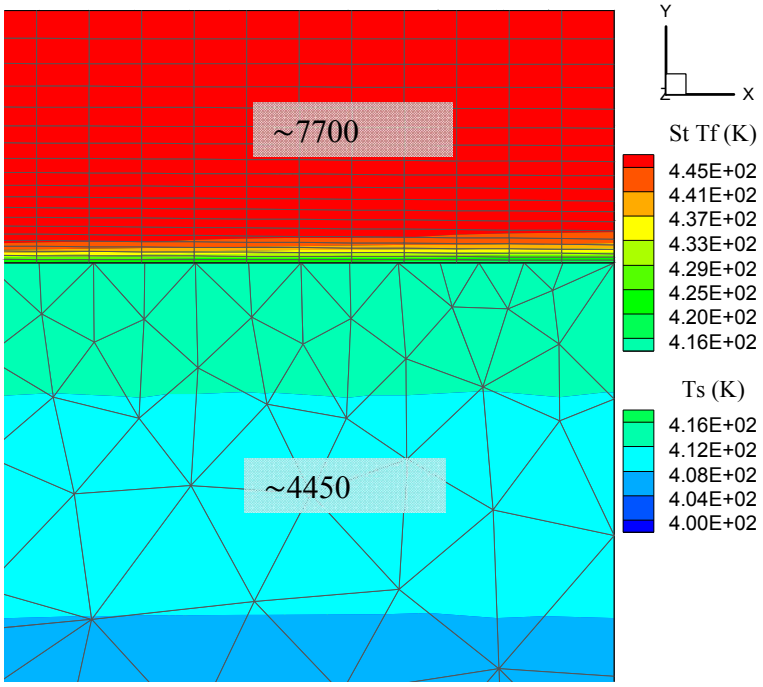

Figure D.6: Front (x-y) view of the 2D case conjugate system showing the meshes and the colour bands of temperature in both domains

D.2. Parallel Flow Double-Pipe HE

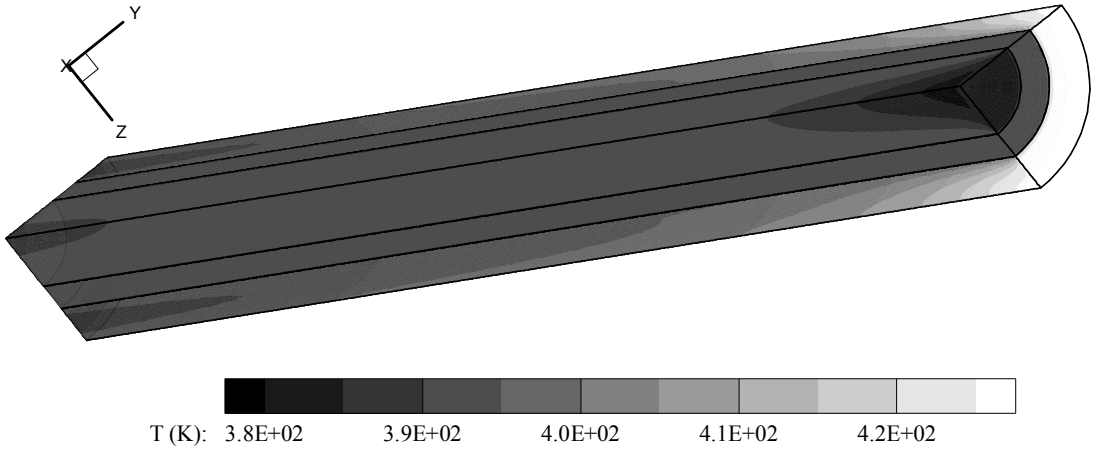

Figure D.7: A view of the double pipe showing the temperature distribution in the parallel flow type

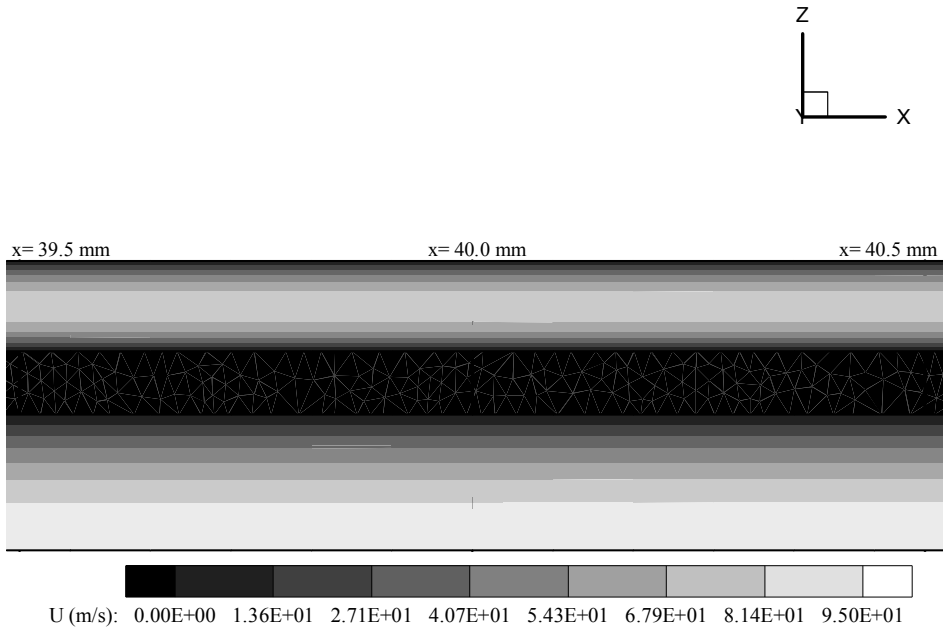

Figure D.8: Velocity contours in a test segment at the centre of the double-pipe

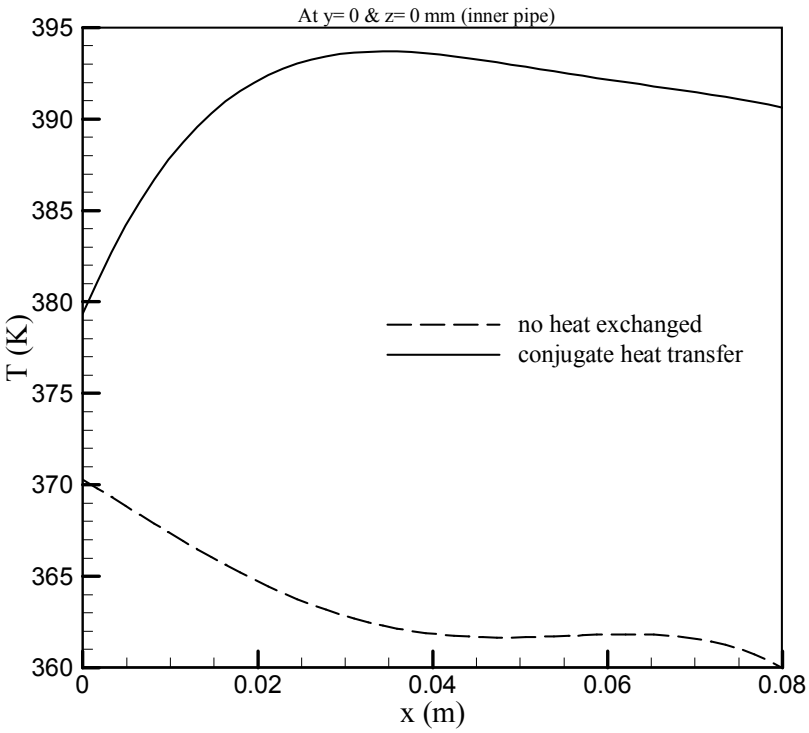

Figure D.9: Variation of Temperature along the centre of inner pipe in comparison between conjugate and adiabatic flow systems

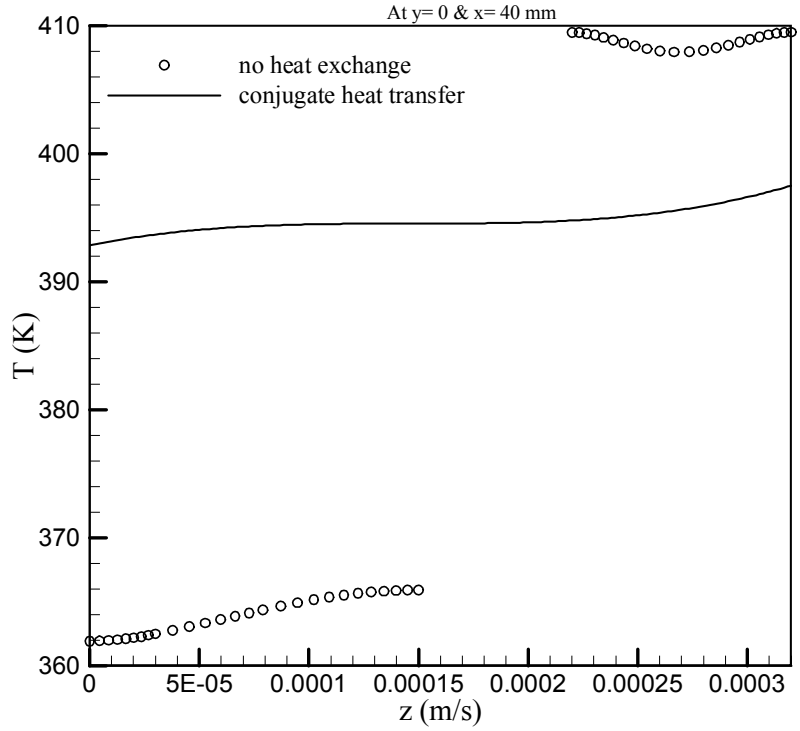

Figure D.10: The effect of integrating CFD solver with CHT on the temperature across the pipes (from the centre towards the outer surface)

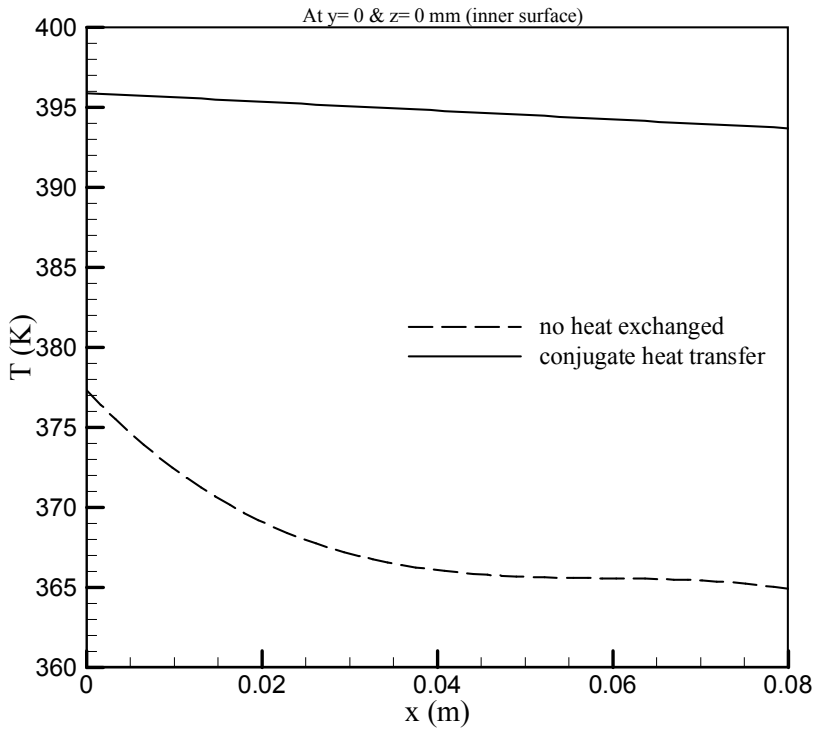

Figure D.11: The temperature profile along the inner surface in comparison between adiabatic and CHT flow systems

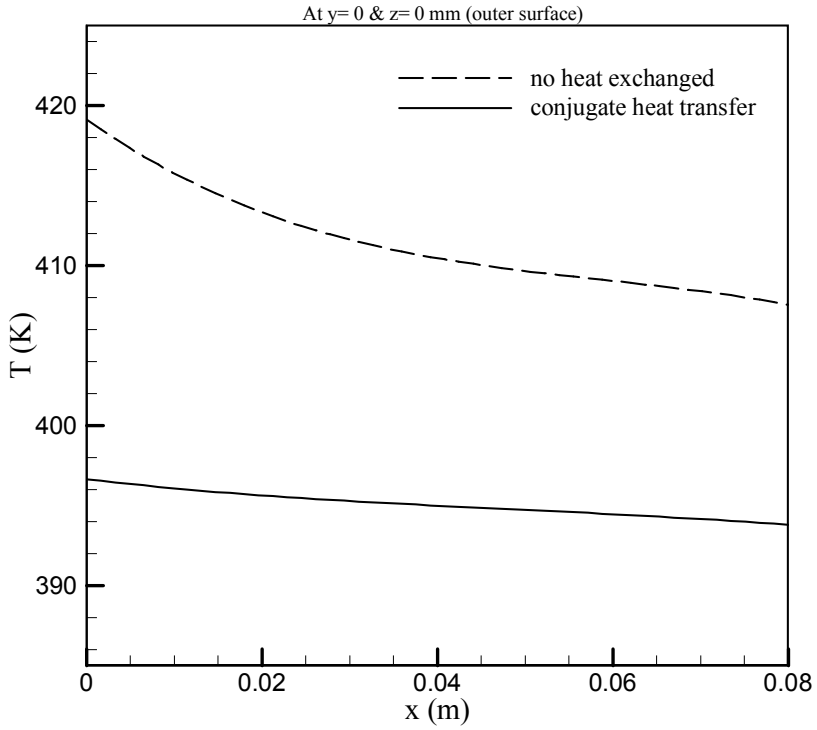

Figure D.12: The temperature profile along the pipe at the outer surface in comparison between adiabatic and CHT flow systems

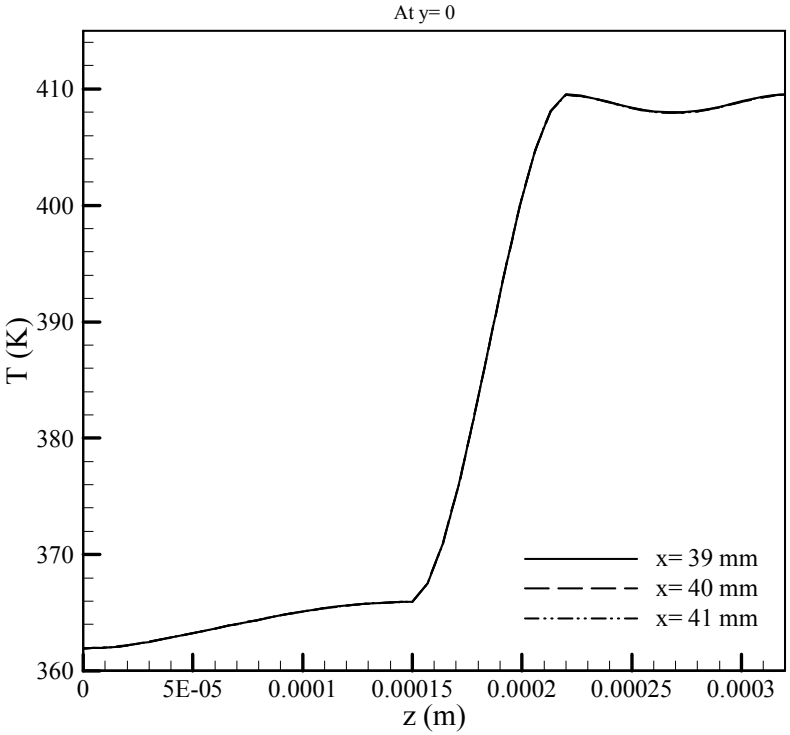

Figure D.13: The temperature profile across the double-pipe in three regions

D.3. Counter Flow Double-Pipe HE

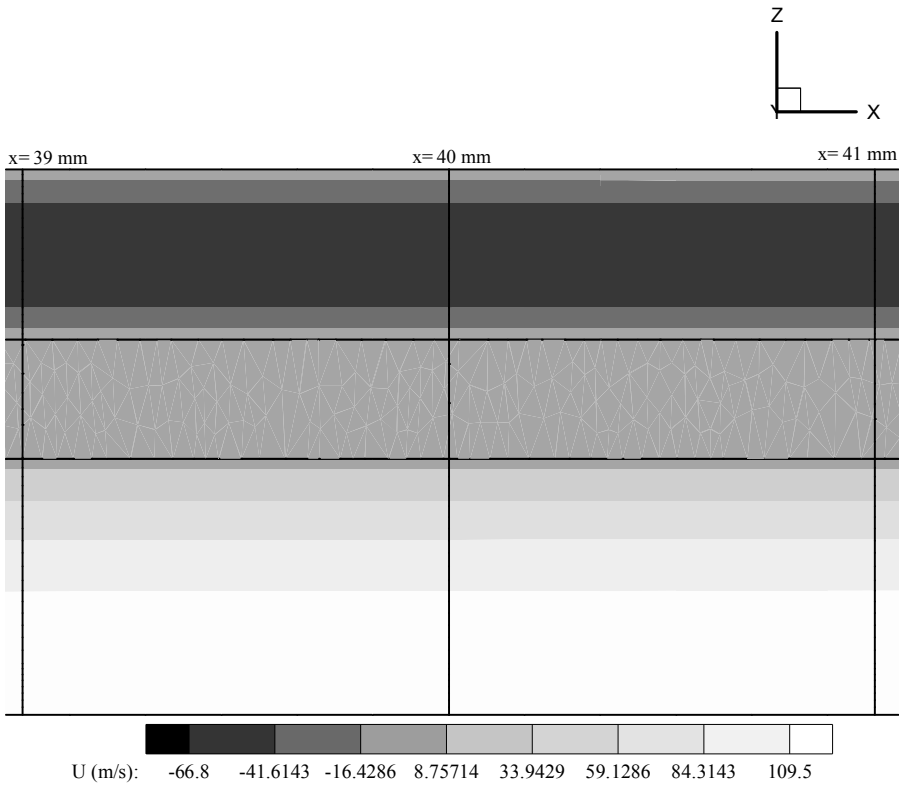

Figure D.14: Velocity contours for an element of the counter-flow CHT double-pipe system

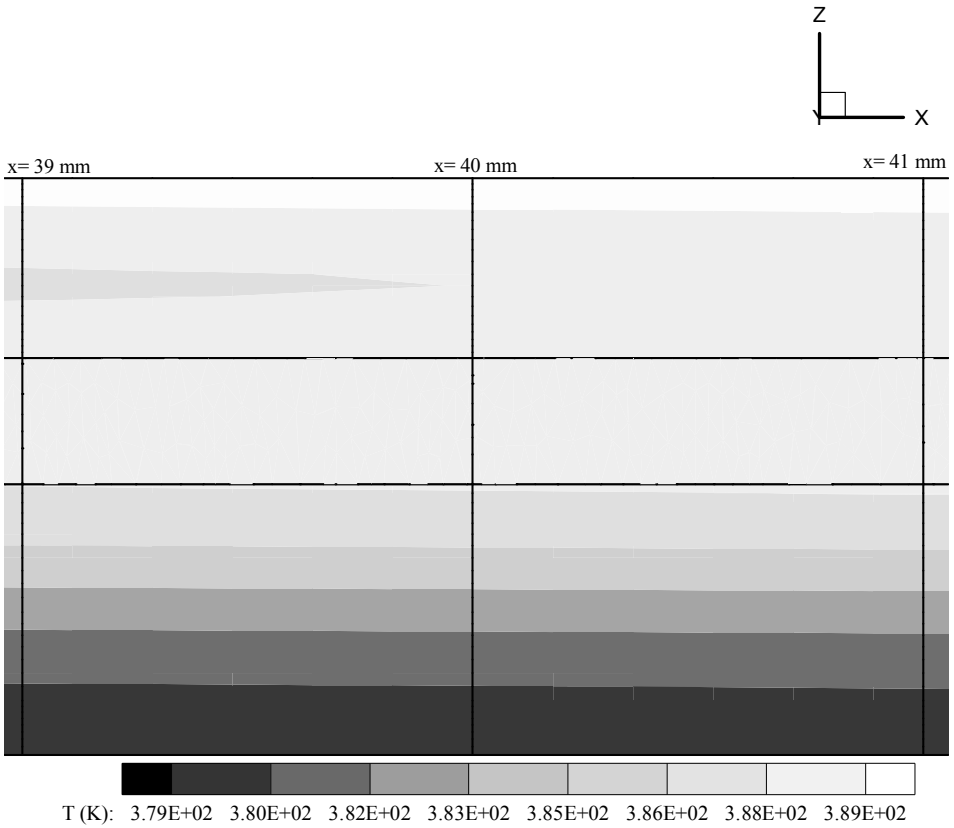

Figure D.15: Temperature contours for an element of the counter-flow CHT double-pipe

APPENDIX (E)

CAVITY AND CO-ROTATING DISCS

E.1. Experimental Data

The following tables are experimental results of temperature at the cavity-interface surfaces of the upstream and downstream co-rotating discs, given by Northrop (1984). Please note that ambient temperature and heat fluxes are not of the same values in all tests.

Table E.1: Temperature readings at rotational speed 500 $rev\ min^{-1}$, with following parameters ambient temperature 300.09 K, leading to an approximate outer face adiabatic temperature of 300.37 K, air inlet temperature 289.00 K and inner face mean heat flux $3188.16\ W\ m^{-2}$

Location No.	**radius** (mm)	**downstream disc** T (K)	**upstream disc** T (K)
1	138	344.55	363.73
2	177	353.80	369.71
3	208	359.88	372.71
4	235	363.87	374.39
5	259	366.95	375.68
6	282	369.75	377.06
7	302	372.52	378.72
8	321	375.17	380.50
9	340	377.55	382.23
10	357	379.59	383.83
11	373	381.22	385.20
12	389	382.35	386.23
13	404	382.49	386.28
14	419	381.04	384.59
15	433	377.53	380.58
16	447	371.59	373.75
17	460	362.90	363.73

Table E.2: Temperature readings at rotational speed $1000\ rev\ min^{-1}$, with following parameters ambient temperature 301.86 K, leading to an approximate outer face adiabatic temperature of 302.97 K, air inlet temperature 288.37 K and inner face mean heat flux $4269.74\ W\ m^{-2}$

Location No.	**radius** (mm)	**downstream disc** T (K)	**upstream disc** T (K)
1	138	343.70	354.21
2	177	354.11	361.42
3	208	361.14	365.76
4	235	366.21	368.92
5	259	370.54	371.99
6	282	374.76	375.50
7	302	379.12	379.60
8	321	383.36	383.87
9	340	387.24	387.97
10	357	390.60	391.64
11	373	393.32	394.72
12	389	395.24	396.99
13	404	395.62	397.65
14	419	393.56	395.77
15	433	388.35	390.61
16	447	379.43	381.59
17	460	366.34	368.23

Table E.3: Temperature readings at rotational speed $1499\ rev\ min^{-1}$, with the following parameters: ambient temperature 304.01 K, leading to an approximate outer face adiabatic temperature of 304.01 K, air inlet temperature 288.19 K and inner face mean heat flux $4619.27\ W\ m^{-2}$

Location No.	**radius** (mm)	**downstream disc** T (K)	**upstream disc** T (K)
1	138	337.54	340.09
2	177	344.09	346.97
3	208	349.68	351.8
4	235	355.22	355.85
5	259	360.86	360.10
6	282	366.68	365.02
7	302	372.60	370.69
8	321	378.29	376.54
9	340	383.45	382.11
10	357	387.88	387.08
11	373	391.44	391.20
12	389	393.94	394.22
13	404	394.58	395.33
14	419	392.39	393.55
15	433	386.57	388.14
16	447	376.53	378.49
17	460	361.76	364.11

E.2. Numerical Visualisation

This section illustrates the CFD prediction of temperature given by the CHT solver (SURF-HC) as in the following Figures E.1 to E.4.

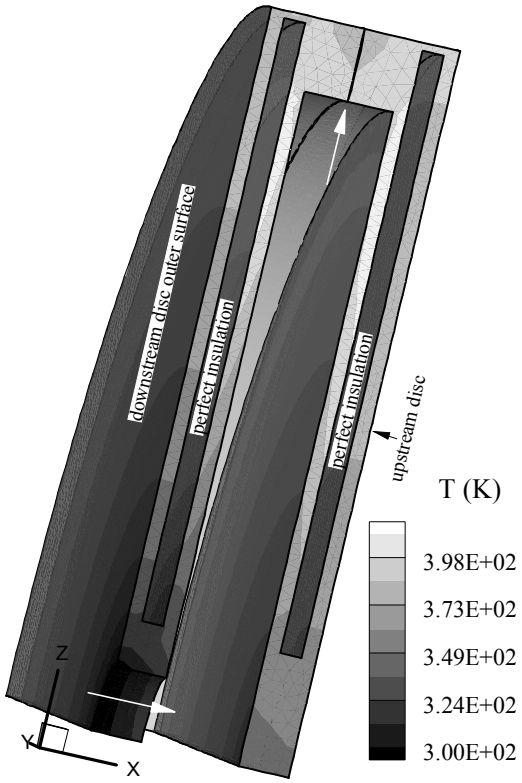

Figure E.1: 3D view of the temperature distribution contours in a segment of the co-rotating discs

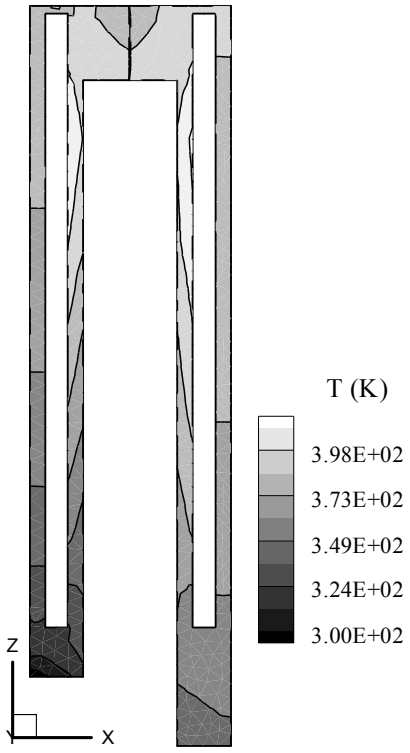

Figure E.2: View of the temperature distribution in xz-plane of the co-rotating discs

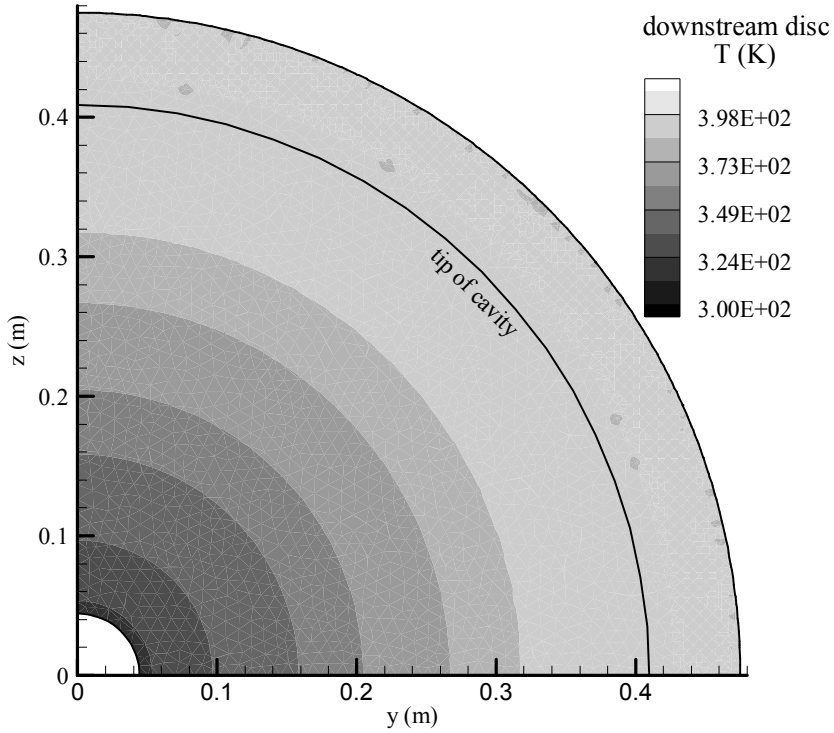

Figure E.3: View of the temperature distribution in yz-plane of the downstream disc

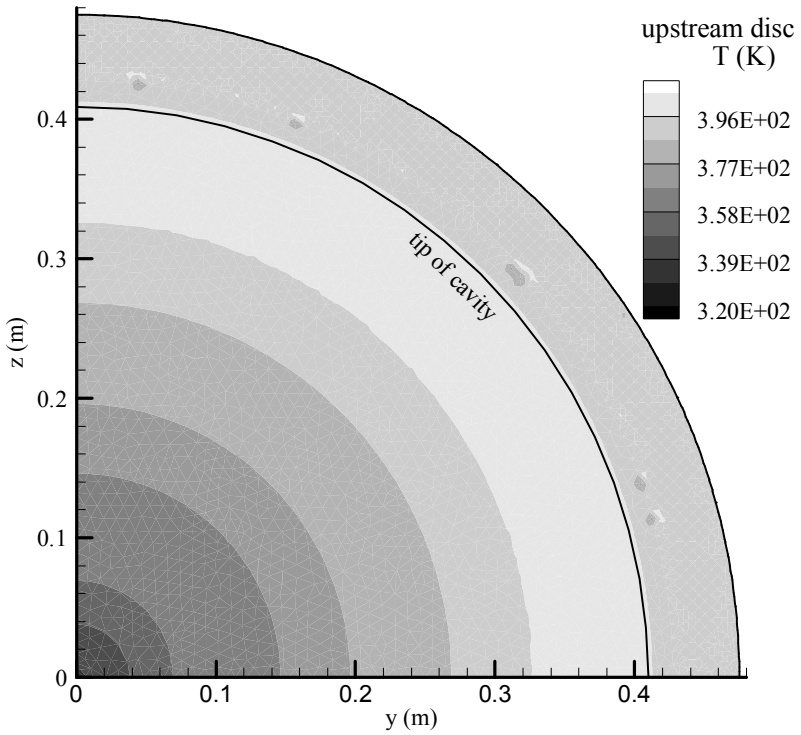

Figure E.4: View of the temperature distribution in yz-plane of the upstream disc

APPENDIX (F)

HC CODE FEATURES

The following appendices review the guidelines of using HC code and examples of how data are displayed.

F.1. Input (Boundary Conditions) File

The entrance of specified boundary conditions is made in a separate file of format *case.bou*. The boundary details are given according to the boundary type (not the boundary surface). This strategy saves time and memory when numerous surfaces are of same boundary types. Table F.1 shows the inputs inside *case.bou* file.

Table F.1: The boundary condition (case.bou) file is set up in this work as the input file of HC code

N1	N2				
N3					
Group number (N4)	Boundary type (N5)	Heat flux (q_b)	Heat convection coefficient (h)	Temperature of fluid (T_f)	Temperature at the surface (T_b)
Case name (or any text)	Number of modelled bodies (N6), not important				
Body number (N7)	Thermal conductivity (k)	Internal heat generation rate (q_{in})	Initial temperature (T_{in})		

The definition of each character is as follows:

N1： an integer, which is 0, 1 or 2. (0) is set for initial calculations, (1) for reading from old data of matching non-conforming meshes only and (3) for building from all old data including previous solution.

N2: scale conversion factor, which is set to [1] when no value is entered.

N3: number of boundary type groups. Each group of faces has specific type of boundary.

N4: group number, which can contain more than on face of the geometry.

N5: type of boundary. The types of boundaries (N5) are recognised by the code according to their integer values, as: (1) Dirichlet type of boundary condition, i.e. fixed temperature, (2) given fluid temperature and convection coefficient, i.e. Neumann boundary condition, (3) fixed heat flux, including adiabatic wall when heat flux is set to zero, this type is of Neumann boundary condition, (4) solid-to-solid interface, i.e. there is another solid domain with different specifications, and (5) solid-to-fluid interface, i.e. coupling with SURF is occurring through this surface (or group of surfaces). When some inputs do not apply to the type of boundary condition, these inputs are given as zero. For example, if a Dirichlet boundary condition applies, only surface temperature is read by the code and the rest are considered zero.

N6: number of modelled bodies. If there is more than one volume is read as solid domains, it is recommended to insert the number. However, the code will search the number of volumes from the mesh file.

N7: body number, if there is more than one volume to be read. Otherwise, it must be [1].

An example of the input file created for a typical rotating disc case is shown in Table F.2.

Table F.2: Typical example of boundary file created in HC code, representing Northrop co-rotating discs

```
0 1
5
1       1       0.      0.0     0.0     320.0
2       1       0.      0.      0.      300.
3       3       0.      0.      0.      0.
4       3       400.    0.      0.      0.
5       3       0.      0.      0.      0.
internal        1       0.0
1       10      0.0     310.0
```

F.3. Customized Boundary by HC Code

Boundary conditions in HC code can be customized either by internal modification, for complicated types of BCs, or by the boundary condition file. An example of a customized boundary condition is given in Figure F.1.

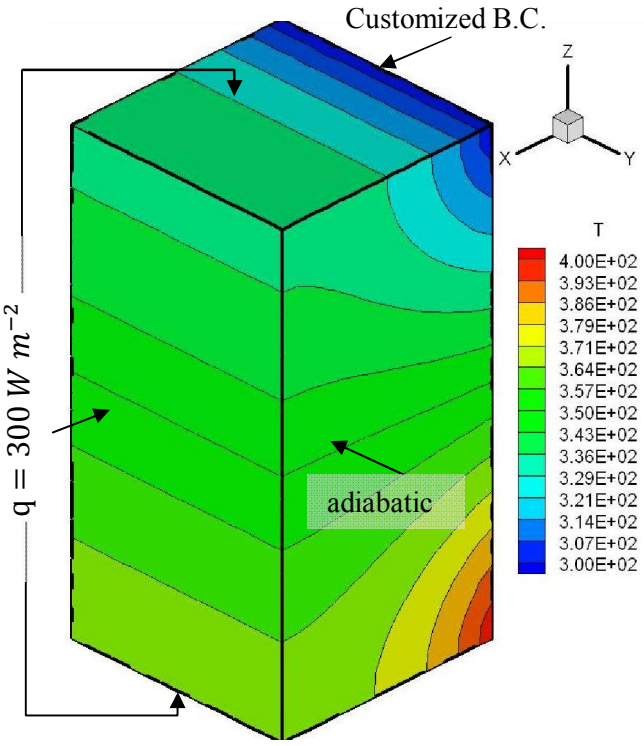

Figure F.1: Temperature contours in a rectangular geometry showing a user (defined) customized boundary type by HC code

Example of reading a group of boundary data with their specified boundary types is shown below:

```
-----------------------------------
B.C. of surface number (34)
& assigned boundary No ( 4) is read..
-----------------------------------


-----------------------------------
B.C. of surface number (35)
& assigned boundary No ( 5) is read..
-----------------------------------




Data of internal elements, Body No. ( 1) are read..


Number of modelled bodies =( 1)
Fixed Temp surfaces       =(22)
Convected surfaces        =( 0)
Insulated surfaces        =(12)
Exposed to Heat flux      =( 1)
Solid-interface surfaces  =( 0)
=============================================

Total volume              :  0.8854E+07
```

F.4. HC Outputs

The iterations and residuals until the end of the simulations are displayed on the screen then the results, which contain coordinates (x, y, & z axes) and temperature, are saved in the temperature file. Iterations given by HC code for a typical example of co-rotating discs, with internal surfaces of fixed temperatures 355 K and external ones exposed to fluid flow with temperature 340 K, is displayed below. A typical example of residuals history is given in Figure F.2.

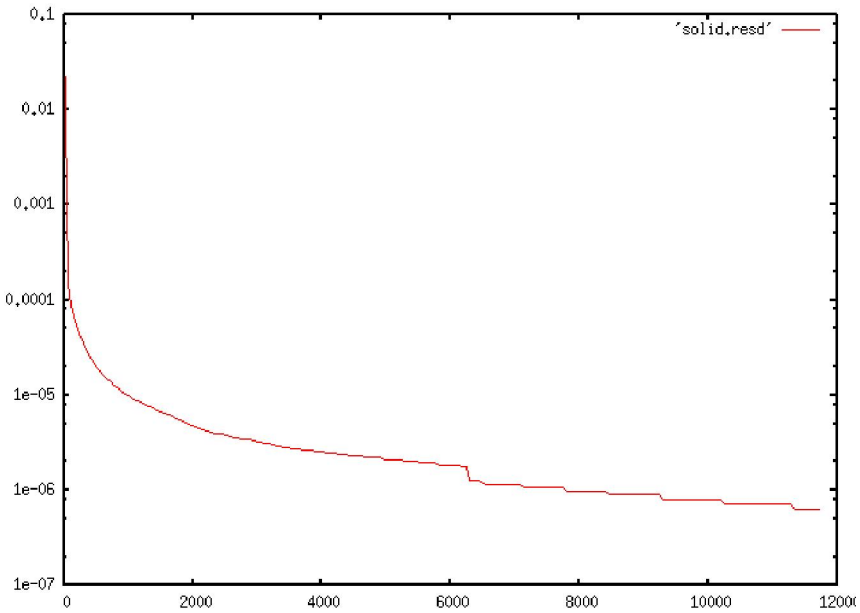

Figure F.2: Residuals history given by HC code for a typical example of co-rotating discs

```
- - - - - - - - - - - - - - - - - - - -
Number of iterations =        1328
Initial residual     =   0.3800278529524803E-02
Residuals approached =   0.8845675125712660E-07
- - - - - - - - - - - - - - - - - - - -
- - - - - - - - - - - - - - - - - - - -
Number of iterations =        1329
Initial residual     =   0.3800278529524803E-02
Residuals approached =   0.8845675125712660E-07
- - - - - - - - - - - - - - - - - - - -
- - - - - - - - - - - - - - - - - - - -
Number of iterations =        1330
Initial residual     =   0.3800278529524803E-02
Residuals approached =   0.8845675125712660E-07
- - - - - - - - - - - - - - - - - - - -
- - - - - - - - - - - - - - - - - - - -
Number of iterations =        1331
Initial residual     =   0.3800278529524803E-02
Residuals approached =   0.8845675125712660E-07
- - - - - - - - - - - - - - - - - - - -
- - - - - - - - - - - - - - - - - - - -
Number of iterations =        1332
Initial residual     =   0.3800278529524803E-02
Residuals approached =   0.8845675125712660E-07
- - - - - - - - - - - - - - - - - - - -
- - - - - - - - - - - - - - - - - - - -
Number of iterations =        1333
Initial residual     =   0.3800278529524803E-02
Residuals approached =   0.8845675125712660E-07
- - - - - - - - - - - - - - - - - - - -
- - - - - - - - - - - - - - - - - - - -
Number of iterations =        1334
Initial residual     =   0.3800278529524803E-02
Residuals approached =   0.8845675125712660E-07
- - - - - - - - - - - - - - - - - - - -


Max Temp    354.904113769531
Min Temp    343.291809082031
```

APPENDIX (G)

SURF-HC CODE FEATURES

This appendix clarifies the guidelines of using SURF-HC. SURF-HC is an integration of the CFD code (SURF) with the numerical heat conduction code (HC). For more information about how to use SURF, the reader is refered to SURF users guide issued by SURF Flow Solutions Ltd.

G.1. Input Files

In the original SURF code, there are three main input files one for pre-processing, so called case.flag file and two solving files, namely case.top and case.bou. In flag (or case.flag) file of SURF code, the adiabatic wall is assigned with the maker 1-800. When dealing with CHT problem, the interface wall is no longer adiabatic. Hence, the interface wall is assigned in SURF-HC code within the markers 11-20. The boundary file entries should remain in the same format of SURF. However, the boundary file values need to be consistent with the CHT system requirements.

In top (or case.top) file, the thermal conductivity of the static-fluid near the wall is defined as fcon and need to be given, otherwise this will be assumed as 0.0285 $W\,m^{-2}\,K^{-1}$. Example of thermal conductivity entry is shown below in table G.1 of a typical HE case, lmmf80.top file.

Table G.1: A typical example of top file entries in SURF-HC code.

```
&top
 ivisc      = 1,
 omg        = 0.001,
 ntime      = 100000,
 iold       = 2,
 csfin      = 30,
 csini      = 30,
 csinc      = 0.5,
 fcon       = 0.04,
&end
```

G.2. Output Files

In a similar way to SURF solving procedure, the output data are displayed on the screen and can be plotted in form of residual history using plotting software, as shown in Figure G.1 The output data can be transferred into the unknown file and saved for plotting the results.

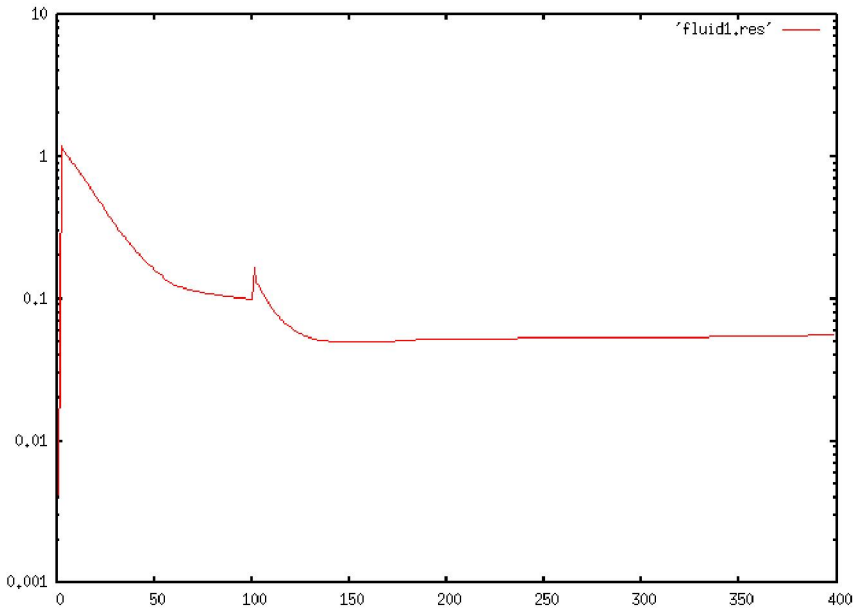

Figure G.1: A typical residual history for the rotating cavity

In Figure G.1, the residuals go up at certain points and start converging again. This shape refers to the iteration levels where IDIs start again.

APPENDIX (H)

Properties of Air

Table H.1: Thermal Properties of dry air at atmospheric pressure (Incropera and DeWitt 2002)

Temperature - t - (^oC)	Density - ρ - (kg/m^3)	Specific heat capacity - c_p - ($kJ/kg\ K$)	Thermal conductivity - λ - ($W/m\ K$)	Kinematic viscosity - ν - (m^2/s) $x\ 10^{-6}$	Expansion coefficient - β - ($1/K$) $x\ 10^{-3}$	Prandtl's number - P_r -
-150	2.793	1.026	0.0116	3.08	8.21	0.76
-100	1.980	1.009	0.0160	5.95	5.82	0.74
-50	1.534	1.005	0.0204	9.55	4.51	0.725
0	1.293	1.005	0.0243	13.30	3.67	0.715
20	1.205	1.005	0.0257	15.11	3.43	0.713
40	1.127	1.005	0.0271	16.97	3.20	0.711
60	1.067	1.009	0.0285	18.90	3.00	0.709
80	1.000	1.009	0.0299	20.94	2.83	0.708
100	0.946	1.009	0.0314	23.06	2.68	0.703
120	0.898	1.013	0.0328	25.23	2.55	0.70
140	0.854	1.013	0.0343	27.55	2.43	0.695
160	0.815	1.017	0.0358	29.85	2.32	0.69
180	0.779	1.022	0.0372	32.29	2.21	0.69
200	0.746	1.026	0.0386	34.63	2.11	0.685
250	0.675	1.034	0.0421	41.17	1.91	0.68
300	0.616	1.047	0.0454	47.85	1.75	0.68
350	0.566	1.055	0.0485	55.05	1.61	0.68
400	0.524	1.068	0.0515	62.53	1.49	0.68